Journal Pre-proof

Next-generation graphene oxide additives composite membranes for emerging organic micropollutants removal: Separation, adsorption and degradation

Beenish Mustafa, Tariq Mehmood, Zhiyuan Wang, Abdoulmohammad Gholamzadeh Chofreh, Andy Shen, Bing Yang, Jun Yuan, Chang Wu, Yangbowen Liu, Wengang Lu, Weiwei Hu, Lei Wang, Geliang Yu

PII: S0045-6535(22)02826-0

DOI: https://doi.org/10.1016/j.chemosphere.2022.136333

Reference: CHEM 136333

To appear in: *ECSN*

Received Date: 3 July 2022

Revised Date: 19 August 2022

Accepted Date: 1 September 2022

Please cite this article as: Mustafa, B., Mehmood, T., Wang, Z., Chofreh, A.G., Shen, A., Yang, B., Yuan, J., Wu, C., Liu, Y., Lu, W., Hu, W., Wang, L., Yu, G., Next-generation graphene oxide additives composite membranes for emerging organic micropollutants removal: Separation, adsorption and degradation, *Chemosphere* (2022), doi: https://doi.org/10.1016/j.chemosphere.2022.136333.

Credit Author Statement

Next-Generation graphene oxide additives composite membranes for emerging organic micropollutants removal: Separation, adsorption and advanced oxidation process.

All persons who meet authorship criteria are listed as authors, and all authors certify that they have participated sufficiently in the work to take public responsibility for the content, including participation in the concept, design, analysis, writing, or revision of the manuscript. Furthermore, each author certifies that this material or similar material has not been and will not be submitted to or published in any other publication before its appearance in the Chemosphere.

Authorship contributions

Conceptualization: B. Mustafa, T. Mehmood and G. Yu; ***Data curation:*** B. Mustafa; ***Formal analysis:*** B. Mustafa, G. Yu, Lei Wang; ***Funding acquisition:*** G. Yu; ***Investigation:*** B. Mustafa, T. Mehmood, A. G. Chofreh, W. Lu and Z. Wang; ***Methodology:*** B. Mustafa, W. Lu, Z. Wang, A. Shen , B. Yang, J. Yuan, C. Wu and Y. Liu; ***Project administration:*** G. Yu; ***Resources:*** G. Yu and L. Wang; ***Software:*** B. Mustafa and T. Mehmood; ***Supervision:*** G. Yu and L. Wang; ***Validation:*** B. Mustafa, T. Mehmood, A. G. Chofreh, G. Yu, Lei Wang and W. Hu; ***Visualization:*** B. Mustafa, Z. Wang and W. Lu; ***Roles/Writing – original draft:*** B. Mustafa; ***Writing – review & editing:*** B. Mustafa, T. Mehmood, A. G. Chofreh, G. Yu, Lei Wang and W. Hu.

All authors have approved the manuscript and agree with its submission to Chemosphere.

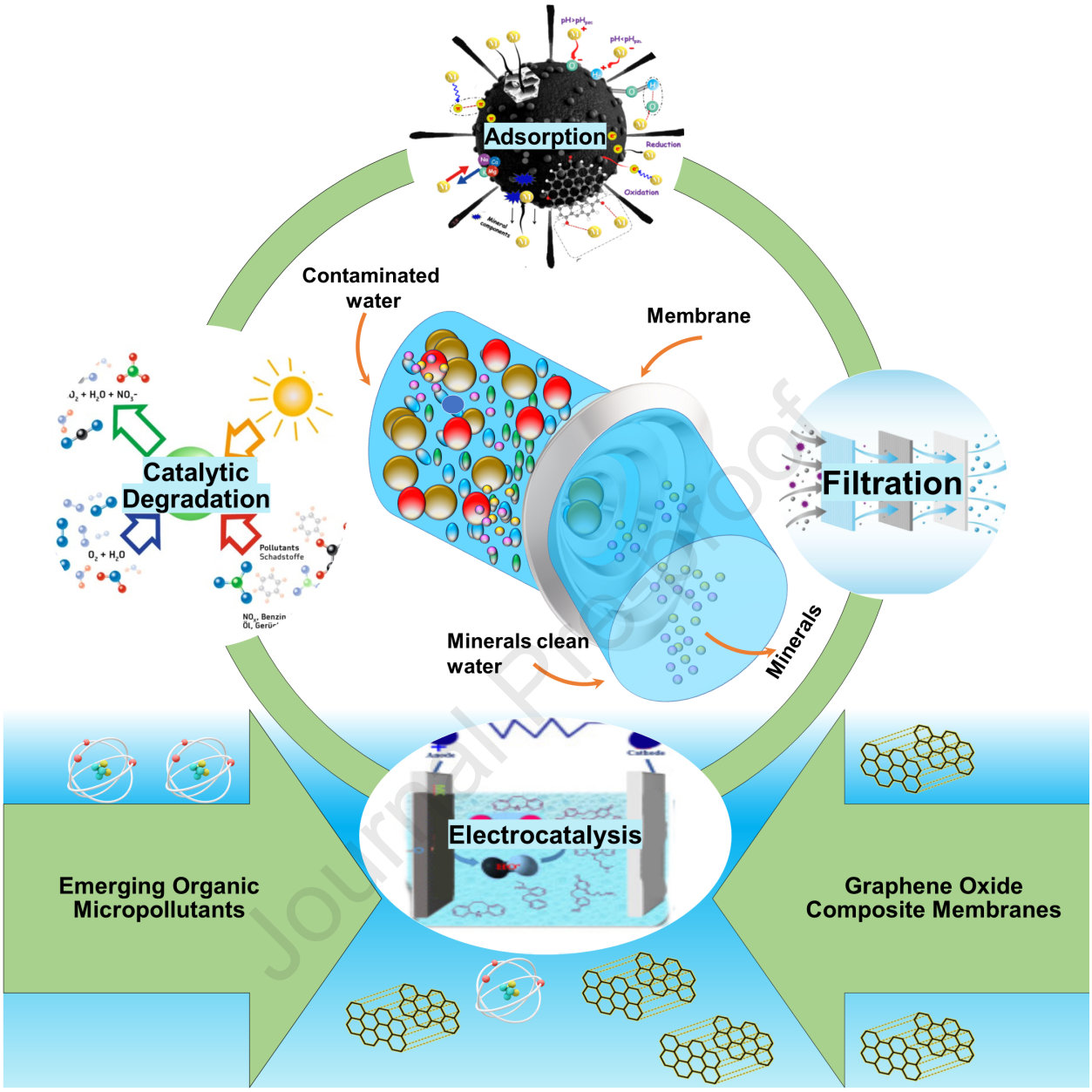

Next-Generation graphene oxide additives composite membranes for emerging organic micropollutants removal: Separation, adsorption and degradation

Beenish Mustafa[1], Tariq Mehmood[2], Zhiyuan Wang[1], Abdoulmohammad Gholamzadeh Chofreh[3], Andy Shen[4], Bing Yang[4], Jun Yuan[4], Chang Wu[4], Yangbowen Liu[4], Wengang Lu[1], Weiwei Hu[5], Lei Wang[1,6]*, and Geliang Yu[1,6]*

1 *National Laboratory of Solid State Microstructures, School of Physics, Nanjing University, Nanjing 210093, China*

2 *College of Ecology and Environment, Hainan University, Haikou, Hainan Province, P.R. China 570228*

3 *Sustainable Process Integration Laboratory, SPIL, NETME Centre, Faculty of Mechanical Engineering, Brno University of Technology, VUT Brno, Technická 2896/2, 616 00, Brno, Czech Republic*

4 *Hubei Jiufengshan Laboratory, Wuhan 430206, China*

5 *Jiangsu Industrial Technology Research Institute, Nanjing 210093, China*

6 *Collaborative Innovation Centre of Advanced Microsctructures, Nanjing University, Nanjing 210093, China*

*Corresponding authors:

Geliang Yu, yugeliang@nju.edu.cn;

Lei Wang, leiwang@nju.edu.cn

Abstract

In the past two decades, membrane technology has attracted considerable interest as a viable and promising method for water purification. Emerging organic micropollutants (EOMPs) in wastewater

have trace, persistent, highly variable quantities and types, develop hazardous intermediates and are diffusible. These primary issues affect EOMPs polluted wastewater on an industrial scale differently than in a lab, challenging membranes-based EOMP removal. Graphene oxide (GO) promises state-of-the-art membrane synthesis technologies and use in EOMPs removal systems due to its superior physicochemical, mechanical, and electrical qualities and high oxygen content. This critical review highlights the recent advancements in the synthesis of next-generation GO membranes with diverse membrane substrates such as ceramic, polyethersulfone (PES), and polyvinylidene fluoride (PVDF). The EOMPs removal efficiencies of GO membranes in filtration, adsorption (incorporated with metal, nanomaterial in biodegradable polymer and biomimetic membranes), and degradation (in catalytic, photo-Fenton, photocatalytic and electrocatalytic membranes) and corresponding removal mechanisms of different EOMPs are also depicted. GO-assisted water treatment strategies were further assessed by various influencing factors, including applied water flow mode and membrane properties (e.g., permeability, hydrophily, mechanical stability, and fouling). GO additive membranes showed better permeability, hydrophilicity, high water flux, and fouling resistance than pristine membranes. Likewise, degradation combined with filtration is two times more effective than alone, while crossflow mode improves the photocatalytic degradation performance of the system. GO integration in polymer membranes enhances their stability, facilitates photocatalytic processes, and gravity-driven GO membranes enable filtration of pollutants at low pressure, making membrane filtration more inexpensive. However, simultaneous removal of multiple contaminants with contrasting characteristics and variable efficiencies in different systems demands further optimization in GO-mediated membranes. This review concludes with identifying future critical research directions to promote research for determining the GO-assisted OMPs removal membrane technology nexus and maximizing this technique for industrial application.

Keywords:

Composite membranes, Graphene oxide, Membrane technology, Micropollutants, Wastewater

1. Introduction

Organic micropollutants (OMPs) in water have gained significant attention due to their implication for water security, human health, and environmental safety (Silvestro et al., 2021). These pollutants include

a wide range of chemicals: Pharmaceuticals and personal care products (PPCPs), Pharmaceutically active compounds (PhACs), hormones/ endocrine-disrupting chemicals (EDCs), pesticides and other industrial chemicals. The small molecular weights but long persistence and high diffusivity trace quantities of OMPs from industrial effluents and daily wastewater remain untreated due to low concentrations. The concentration of OMPs may be varied from ng L^{-1} to mg L^{-1} (Zheng et al., 2022), and if present below parts per million (ppm), they are known as emerging organic pollutants (EOMPs) (Lapworth et al., 2012).

Although EOMPs are always present in trace concentrations, they significantly impact human health (Han et al., 2018). Only endocrine-disrupting chemicals (EDCs) cause considerable financial costs, such as217 billion(1.28% of gross domestic product, GDP) in Europe (Trasande et al., 2015) and 340 billion (2.33% of GDP) in the United States (Attina et al., 2016). On the other hand, human-usable water resources are becoming increasingly scarce over time, necessitating the effective treatment of OMPs contaminated water. Since wastewater treatment plants (WWTPs) units are not logged to treat OMPs and treatment standards and guidelines for OMPs are yet to be defined, these contaminants remain unchecked in wastewater treatment processes and are frequently discharged into the environment (Zheng et al., 2022).

Incessantly, the scientific community seeks satisfactory enhancements to conventional cleanup procedures or novel alternatives. However, understanding OMPs, including EOMPs and related efficient treatment technologies, is still in infancy (Kanaujiya et al., 2019). Integration of membrane filtration technology with conventional WWTPs has proven to improve EOMPs removal performance in the system. To date, considerable research has been done on membrane separation performance for gas (Mubashir et al., 2015), dyes (Dadvar et al., 2017), and other environmental remediations (Ali et al., 2022).

Membrane systems, including reverse osmosis (RO), nanofiltration (NF), ultrafiltration (UF), and microfiltration (MF) are pollutants specific and have specific operating requirements, pollutants removal efficiencies, advantages, and limitations. For instance, due to high transmembrane pressures requirement, fouling, and membrane concentrate management, NF and RO spectacularly increase operational expenses (Luo et al., 2014b). Therefore, these membranes require additional assistance from different supporting technologies. On the other hand, advanced membrane bioreactors are well established in treating refractory organic pollutants, nutrients, and organic matter (e.g., humic acid (HA)) but are ineffective for nonbiodegradable EOMPs and often face severe membrane biofouling, need modern

water treatment strategies (Ding et al., 2021). Advanced oxidation processes (AOPs) disintegrate persistent MOPs into simpler minerals. In paired cleaning procedures, these AOPs reckon on various oxidants that can totally mineralize EOMPs or increase their biodegradability for later bioremediation (Li et al., 2022a). Fenton oxidation is a common and eminent AOPs method. Fenton oxidation and ozone/UV oxidation process has excellent removal efficiency, rapid functions, and broad use range (Yu et al., 2020).

Nonetheless, some organic substances are resistant to oxidation by ozone or UV-based processes, and partial mineralization of molecules can produce even more harmful byproducts. Besides, activated carbon is merely a separation procedure that requires additional post-filtration (Ma et al., 2022). Electrochemical advanced oxidation process (EAOP), a simple automated in situ executable system, compact and modular reactor architecture, and absence of chemical storage or handling, is efficiently used to treat aqueous OMP waste streams but is ineffective when used EOMPs contents are low.

To meet the challenges of these membrane coherent advance treatment processes, the development of robust, multi-functional, resilient, and economical composite membranes for treating domestic and industrial effluents containing EOMPs is progressing. However, some parameters that should be considered while considering advanced composite membrane are physical strength and stability against chemicals, selectivity, high flux, permeability, high rejection rate, type of pollutants, and removal mechanisms (Yuan et al., 2020; Wang et al., 2021). These features are directly related to the material characteristics of the composite membrane (Shen et al., 2017). Popular two-dimensional (2D) materials with outstanding selectivity and permeability, such as MXenes, graphene, 2D covalent-organic and metal-organic frameworks, and Molybdenum disulfide (MoS_2), are increasingly used in membrane production for water purification. As evidenced by the vast amount of research conducted in this field, graphene oxides have been widely utilized in numerous membrane systems to remove various OMPs from contaminated water. GO membranes are emerging as additive materials that improve antifouling behavior, selectivity, and flux performance of membranes (Liu et al., 2020c; Wu et al., 2020) due to high mechanical strength, high thermal stability, huge surface area, hydrophilicity, and efficient electron transformation.

It has been proven various membrane substrates showed contrasting characteristics while in conjugation with GO. Once GO is incorporated, it alters the membrane physiochemical characteristics, impacting EOMPs removal pathways and corresponding efficiencies (Zhu et al., 2017b; Ye et al., 2021b).

Importantly membrane filtration studies denoting water purification have been applied in various systems such as UF, NF, MF, and RO (Table S1). These membrane systems are operated under various flux dynamics, e.g., cross-flow (CF), surface-flow (SF), and flow-through (FT) , as well as in different treatment systems (MBR, hybrid DMBR). Consequently, efficiencies and EOMPs removal mechanisms substantially varied with operating system changes. Likewise, treatment cost and environmental implications regarding membrane reusability, stability, and the desorption and leaching of supporting material are also changed (Nguyen et al., 2021; Ma et al., 2022). Only biofouling can increase 50% the cost of filtration operation (Fortunato, 2017). Such disparities limit their applications in multi-contaminated wastewater treatment. Although some lab-scale studies showed appreciable performance in this context, a field scale is still challenging (Li et al., 2021a; Wei et al., 2021; Ye et al., 2021b).

Based on the current literature, the following limitations can be concluded: (i) reviews discussed the single type of membranes based on removal mechanisms (Thakre et al., 2021; İlyasoglu et al., 2022), (ii) GO membranes removal performance partially reviewed or discussed along other 2D materials (Bodzek et al., 2020; İlyasoglu et al., 2022) (iii) Membrane performance for organic contaminated water treatment has been reviewed, but a detailed review on EOMPs removal by different GO membranes is still elusive (Khanzada et al., 2020; Jia et al., 2022), (iv) a detailed insight assessment of purely GO-based membranes and a critical comparison of GO functions in different removal mechanisms are not available, (v) and due to complex nature of EOMPs, limitations in conventional membrane filtration systems and increasing interest of researchers for GO membranes, a review on adsorption, degradation, and filtration of EOMPs by GO modified membranes is warranted.

To curb these gaps, the main objectives of this review are to (1) evaluate GO additive membranes in various types of filtration systems (e.g., microfiltration, ultrafiltration, nanofiltration, reverse osmosis) and delineate the synergism of adsorption, degradation, and electro-photocatalytic strategies in the removal of EOMPs, (2) probe the integration of GO with diverse membrane substrates (e.g., ceramic, polyethersulfone (PES), polyvinylidene fluoride (PVDF)) to remediate OMPs, (3) to compare the removal mechanisms of various EOMPs by GO-assisted membranes, and (4) elucidate the main factor affecting GO integration with different substrates and corresponding physicochemical changes in GO-modified membranes compared to the pristine membrane.

We are convinced that reviewing simple to most advanced GO additive membranes will advance our understanding of pollutants-specific, economic, and more stable membrane synthesis, which is essential for next-generation membranes development and advanced industrial applications.

2. Literature search methodology

For this study, the Scopus database (updated on July 1, 2022) was searched by entering the following keywords into the titles of publications: (("Graphene Oxide" or "GO"), ("membranes"), ("water treatment"), (emerging pollutants), and (organic micropollutants) yielded a total of 74 results. In a separate search, the keyword in the title: (("Graphene Oxide" or "GO"), ("membranes"), ("water treatment"), and (emerging pollutants) produced 333 articles. We selected all SCOPUS database indexes articles published between 2004 and 2022, with an emphasis on the last five years of study. This search approach is commonly employed in Scopus bibliometric studies (Palansooriya et al., 2020; Mehmood et al., 2021). Because this search resulted in many unrelated publications, the articles were initially filtered by reading the article titles based on GO's usage in removing EOMPs from water. The shortlisted articles were then read to decide which ones were relevant. All these investigations are summarized in Tables 1 through 3.

3. Emerging Organic Micropollutants in Environment

Organic micropollutants are a broad chemical category that includes PAHs, endocrine disruptors, antibiotics (Silvestro et al., 2021), plasticizers, and flame-retardants. These pollutants are a global issue, and their trace amount (ng L^{-1} to g L^{-1}) carries substantial adverse impacts on the environment and public health (Zheng et al., 2022). Other OMPs like personal care items, medications, insecticides, additives, and hormones in water and wastewater are found in fewer than parts per million (ppm), collectively called emerging contaminants (ECs), and if they are organic pollutants ascribed as EOMPs. These chemicals have adverse environmental implications but have untracked sources and remained formerly unregulated or unchecked in environmental samples but have suddenly become a public health issue (Yang et al., 2016).

EOMPs are classified as (i) PPCPs, (ii) EDCs, (iii) Per- and polyfluoroalkyl substances (PFASs)/industrial chemicals, and (iv) organic wastewater-related compounds based on their sources and properties (Rahman et al., 2009). EOMPs can be located in various settings, including industry, agriculture, healthcare, and everyday life. Wastewater treatment facilities (WWTPs) effluent, landfill

debris/leachate, septic/drainage tank leakage, and agricultural runoff comprise a major fraction of EOMPs in surface and groundwater. Likewise, household garbage, hospitals, and other industrial applications are the most common sources of EOMPs pollutants (Rahman et al., 2009; Zheng et al., 2022). A detailed description of EOMPs and an overview regarding the performance of membrane separation technology in the treatment of EOMPS contaminated water has been provided in the supplementary information.

4. Scope of GO for membrane separation

Graphene is a potential adsorbent material for membrane separation due to its unusual p-electronic configuration and greater specific surface area. This material has recently been outlined for its perks in a spectrum of uses, particularly in photocatalysis (Chen et al., 2017; Zhu et al., 2017a; Heu et al., 2020), superlattices formation (Yu et al., 2014) and MST (Shen et al., 2017; Wu et al., 2021a). Of the best graphene derivatives is its oxidized form, known as "graphene oxide (GO; formerly known as graphitic oxide)," which has caught the interest of researchers worldwide. Brodie was the first to synthesize GO by oxidizing graphite with a potassium chlorate solution and fuming nitric acid in 1859. Previously, in 1958, Hummers and Offeman described "The Hummers' Method," which included KMnO4, $NaNO_3$, and H_2SO_4 (Fig. 1 a-c). Various modified Hummer methods have been described in the literature (Khorramshokouh et al., 2022; Yin et al., 2022). GO is also synthesized by pyrolysis with the complete carbonization of carbon-enriched waste materials (e.g., sugarcane Bagasse) (Somanathan et al., 2015) and carboxyl-based compounds (e.g., citric acid) (Dong et al., 2012), as presented in **Fig. 1**.

Fig. 1 about here

As shown in Fig. 1d, the oxidation of graphite and the exfoliation of graphite oxide are two main steps in preparing GO from graphene. 2D honeycomb-like crystalline lattice structure of GO contains numerous water channels. Analogous to graphene, sheets of GO are asymmetrically attributed to specific basal and edges holding oxygen-containing functional groups. On the other side, GO is a single atomic-layered thick nanosheet with a hexagonal carbon composition that, unlike graphene, has a number of unique properties, including being the stronger but lightest sheet, having exceptional thermal conductivity (approximately 5000 W m^{-1} K^{-1}), contains the meager electrical resistivity (106 U cm), and a massive theoretical specific surface area (SSA) (2630 m^2 g^{-1}) when referred to similar materials. It also features a hexagonal structure with more active functional groups on the surface, such as hydroxyl (–OH), alkoxy (C–O–C), carboxyl (–COOH), and other oxygen enriched functional groups (Wang et al.,

2021). Oxygen-rich functional groups enable the production of nanocomposite materials with prominent chemical permanency, excellent hydrophilicity, and remarkable antifouling properties by providing a varied variety of reaction sites for chemical reactions (Ye et al., 2021b; Ye et al., 2021c; Xu et al., 2022).

Due to its unique structural features, it has been increasingly applied to various MSTs as a novel type of additive in recent years. However, the GO bases membrane has many problems, which are exacerbated by several techniques. For example, such oxygen-bearing groups reduced the electrostatic stability of nanosheets in water, which is another limitation of GO (Nebol'sin et al., 2020). However, hydroxyl, epoxide, carbonyl, and carboxyl groups can be introduced to the basal planes of GO to facilitate dispersion in aqueous conditions in the absence of any stabilizer (Wang et al., 2021). The small layer spacing also impacts the water flux of GO nanosheets (Wu et al., 2014). Hence widening the layer spacing is a promising area of study. Water can travel through GO sheets if provided nanopores but other ionic substances cannot (Foller et al., 2022).

Membrane surface reconfiguration is a technique for adjusting membrane hydrophilicity, surface charge, porous structure, and roughness. Due to its particular qualities for separation efficiency, the GO has been commonly applied for surface modification. Several methods for assembling GO nanosheets into laminar membranes have been described in the literature (Fig. 2), like filtration (pressure-, vacuum-, and evaporation-assisted) (Baskoro et al., 2018), layer-by-layer (Nair et al., 2012b), dip-coating (Li et al., 2022b) and immersive method (Rashidian et al., 2021), spin coating (Nair et al., 2012b) and drop-casting (Rollings et al., 2016), and spray-coating (Guan et al., 2017). Hu et al. (Ayyaru and Ahn, 2017) used a layer-by-layer technique to segregate water from the dye mixture to build a coupled GO membrane. As an additive material in membrane production, GO offers many applications.

The most often used approaches include the incorporation of GO in polymer matrix by conventional blending (Ayyaru and Ahn, 2017) and/or coating via dip coating (Surana et al., 2015) and sol–gel methods (Luo et al., 2014a). However, due to the nanomaterials' restricted homogenous scattering in the polymer, these techniques lacked uniformity and repeatability for permeation and selective removal purposes. Essential characteristics for forthcoming surface alteration techniques are the uniform distribution and adjustable GO thickness on a membrane's active layer (Kong et al., 2021). Atomic layer deposition (ALD) and electrospinning are two novel methods for immobilizing functional GO and its uniform dispersion on membrane surfaces with a customizable thickness (Lee et al., 2020).

Fig. 2 about here

GO's smooth surface and hydrophilicity make it promising as a membrane additive as it demonstrates great changes, including anti-fouling/biofouling and selectivity behavior in membranes by altering pore size and surface charges while also amplifying the permeate and water fluxes of the membrane (Liu et al., 2020c; Wu et al., 2021a). These GO-based membranes can be classified into three categories: (i) porous GO layers, (ii) GO laminates, and (iii) GO composites (Shen et al., 2017; Wu et al., 2020). Nair et al. (2012a) showed that water could pass freely via helium-tight, submicrometer-thick membranes. Wei et al. (2021) developed a polyamide GO nanofiltration membrane (GO/PA) for purifying water with a high flux (44.2 L m^{-2} h^{-1}). Organic dyes preserved a high percentage (>99 percent), whereas ion salts retained a low rate (5%). About 20%–60% of total removal was attributed to GO due to its adsorption capacity for pollutants in water solution. For instance, Li et al. (2021a) used GO with a Europium-metal organic framework; the membrane showed 100% removal of organic phosphine and increased the flux from 0.76 to 5.01 L m^{-2} h^{-1}.

Jin et al. (2015) demonstrated that magnetically reduced GO has an analogous mechanism for the adsorption of BPA and 4-n-nonylphenol. Aside from the fact that GO has been used in diverse ways to aid membrane pattern and surface changes, the following section relies on GO-based membranes and their suitability for micropollutant contaminated water treatment systems, owing to their widespread use and promising applications for improving membrane processes (Chu et al., 2017; Shen et al., 2017). In both pressure- and temperature-driven membrane processes, the introduction of GO materials has been widely exploited to increase permeability, selectivity, and fouling control (Ma et al., 2020; Li et al., 2021a; Zhang et al., 2022).

5. GO-based separation/filtration membranes

Numerous studies have demonstrated that incorporating GO into membranes either as a bulk component or as a surface graft improves the antifouling function of the membrane by improving hydrophilicity and lowering the surface roughness (Mahlangu et al., 2017; Zhang et al., 2018). Many GO additives membranes are eminent by underlying removal mechanism, proficiency, stability, and environmental implications. The next section provides a detailed overview of several GO-mediated next-generation approaches for EOMPs cleaning, emphasizing their efficiency, perks, and shortcomings (Section 4.1-4.4, Table 1).

Table 1 about here

5.1. Mixing of GO with other 2D materials

The oxygen-bearing groups on the basal boundary of GO nanosheets improve GO dispersion in water, which is beneficial for boosting interactions with transport species (water molecules and ions) during water purification (Li et al., 2019b; Wang et al., 2021). The repulsive forces between GO-linked functional groups and water molecules as well as within GO nanosheets are the major factor that causes GO dispersion in water, separation of EOMPs, and also cause instability and destroying its permeability (Nair et al., 2012a; Wang et al., 2021). Therefore, managing the balance between selectivity and permeability is challenging when simply employing GO membranes. However, utilization of ionic cross-linking ligands and functional materials and the decrease of oxygen-containing groups in GO are common approaches adopted to cope with this situation (Kang et al., 2017). Likewise, combining GO with other two-dimensional materials in membrane production showed encouraging elimination of EOMPs from water (Kang et al., 2017; Liu et al., 2020b).

MXene(Ti_3C_2Tx) is getting prominence due to its outstanding characteristics, which include high electrical conductivity, mechanical strength, extensibility, and wettability (Lu et al., 2022). MXene membranes with a laminar configuration and high hydrophilicity, for instance, promoted quick and targeted water molecule transport with a desirable permeability flux in water filtration (Liu et al., 2020b). Assuming that the 2D lamellar heterogeneous form of the GO/MXene composite membrane, compared to individual GO or MXene membranes, may have offered synergistic benefits, leading to an optimal trade-off between selectivity and permeability.

Ding et al. (2017) demonstrated a considerably higher interlayer gap and flow than a GO membrane was by two-dimensional lamellar MXene membrane. They addressed the absence of oxygen-containing functional groups, and larger interlayer spacing are the main reasons for the GO/MXene composite membrane's improved flow, as discussed later. The lamellar construction with an uneven thickness of 0.7 nm (GO) and 1.5 nm (MXene) promotes water flow transit by preventing the creation of lamellar nanosheets, allowing multistage micropores to be produced, and maximizing the production of multistage micropores the number of microchannels. Likewise, by carefully adjusting the surface functional group makeup of GO/MXene composite membranes, a high rejection frequency for EOMPs, such as common pigments and representative forms of natural organic matter found in raw waters, may be preserved (Liu et al., 2020b).

GO and MXene membranes laminated onto porous support successfully removed methyl red (68%), rose Bengal (93.5%), methylene blue (99.5%), and brilliant blue (100%) from water (Kang et al., 2017). At the same time, using GO/MXene intercalants membrane, Liu et al. (2020b) demonstrated 95% removal of organic dyes from raw water while rejecting 100% natural organic components (sodium alginate (SA), bovine serum albumin (BSA) and HA). Notably, the introduction of 2D material resulted in a potential improvement in the membrane separation process attributable to GO membranes. MXene comprises a vast family of 2D materials; however, only MXene has been coupled with GO and investigated in the EOMPs membrane removal method to date. This should be explored further in the context of forthcoming research.

5.2. GO integrated ceramic membranes

Ceramic membranes outperform polymeric membranes in harsh environments owing to corresponding chemical, mechanical, and thermal resistance. They are also easier to clean and have higher flux stability (Zielińska and Galik, 2017). However, the performance of ceramic membranes to remove low molecular ionic chemical retentions in nanofiltration is not much higher, which can be substantially improved by incorporating GO (Hu et al., 2016). Although the deformity of the GO layer in an aqueous environment widens interlayer gaps and resuspends the GO, which declines the membrane removal performance (Lou et al., 2020), but the interlayer space of GO can be modulated using layer-by-layer assembly (LbL) method, which produces more stable GO layer spaces (Nair et al., 2012b).

Shen et al. (2017) developed SG@GO composite membrane using pyrene derivative solvent green (SG) molecules and GO owing to π-π-stacking interactions. As a result, they achieved a membrane with a desirable spacing arrangement (Fig. 3h). Previously, Liu et al. (2012) found the wide flat aromatic structure of SG molecules can bind with GO sheets' hydrophobic surface by π-π – interactions. The π-π -stacking interactions is analogous to that of covalent bonding, which improves the stability of the GO composites in aqueous media. Additionally, the π-π stacking alteration does not affect the GO sheet pairing, which preserves graphene's characteristics (Liu et al., 2012).

Fig. 3 about here

Shen et al. (2017) demonstrated that the incorporation of SG enhanced electronegativity, reduced contact angle, and improved hydrophilicity. A direct relationship between the interlayer spacing of GO laminate and SG concentration was attributable to a rise in sulfonate ($-SO_3$) concentration, which enhances the electrostatic repulsive forces between the SG@GO sheets by increasing the negative surface

zeta potential (SZP) (Fig. 3g). Consequently, when the electrostatic repulsive forces between the GO layers increased, the nanochannels for water molecules grew larger. GO membrane thickness rose from 2.2 to 2.7 nm in SG@GO sheets by increased static repulsion force, whilst the inter-layer gaps of GO sheets in pristine GO laminates (7.70Å) were increased to 8.29Å and 8.41Å in SG@GO laminates at SG concentrations of 1.2 and 1.6 g/L, respectively.

GO laminates by immersion method of depositing SG@GO nanocomposites onto PDA-amended hollow ceramic substrates demonstrated a significant increase in pores numbers and enhanced surface roughness (Fig. 3a-f) (Shen et al., 2017). Although GO improved removal but it hinders water flux too. In comparison, SG contains huge planar aromatic compounds that engage via π-π stacking interactions with GO sheets, hence enhancing the mass transfer routes and electrostatic repulsive force, resulting in increased flows but decreased retention (Fig. 3i). However, a thicker and denser separation layer of SG@GO enhanced the rejection efficiency from 94.2 to 98.0% at moderately higher flux rate. The SG@GO hybrid membrane performed excellent electronegativity EBT molecules removal from water due to the Donnan effect and molecular filtering. However, advanced materials and fabrication procedures are necessary to improve ceramic membrane nanofiltration performance and more straightforward preparation.

Lee et al. (2015) addressed that an excellent cationic polyelectrolyte with a high positive charge density Polyethylenimine (PEI), can link GO to form electrostatic LbL arrangements. However, Yang et al. (2018) identified owing to wider pores of the substrate, only addition of PEI addition is void while co-deposition with GO could cover all pores, and they recommended a combination of metal-organic frameworks (MOFs) (Fig. 4a-e). The authors demonstrated 99% removal of organic solvent by co-depositing PEI and Zeolitic Imidazolate Framework (ZIF-8) nanoparticles additive GO on a tubular ceramic substrate via a vacuum-assisted process approach. Using GO sheets or ZIF-8 nanoparticles, they prevented PEI from entering the substrate's pores, resulting in a thin film composite membrane (Fig. 4g). Agglomeration occurred only when ZIF-8 particles were mixed with PEI, resulting in an extremely rough surface. ZIF-8@GO laminates aid in the construction of a regular separation layer structure while preventing the aggregation of ZIF-8 particles and the wrinkle formation of GO nanosheets in ZIF-8@GO composite nanosheets.

The improvement of ceramic membrane nanofiltration needs further assessment for other EOMPs (Yang et al., 2018). Cha et al. (2022) recently used LbL methods and incorporated PEI-GO assembly in

the ceramic membrane for semiconductor wastewater purification in NF. Three GO-PEI bilayers GO-ceramic eliminated 8.4 and 3.2 times as much ammonium as the pure ceramic NF substrate. However, the use of these strategies is still limited in literature, particularly for EMOPs removal studies.

Fig. 4 about here

5.3. GO in PES membrane

Although PES membranes are one of the most extensively used polymeric UF membranes, efficiency needs to be enhanced (Zhang et al., 2021). Metal oxides were found to be useful in increasing PES membranes' performance and stability when incorporated into GO. For example, during concurrent filtration and disinfection of a UF system, Jiang et al. (2016b) discovered that a GO-TiO_2 modified PES membrane under UV irradiation displayed excellent self-maintenance and increased antibacterial activity during extended operation intervals. Likewise, in a 72-hour long-term trace organics rejection experiment, Mahlangu et al. (2017) treat trace organic compounds (TOrCs) and examine the influence of temporal solute adsorption on rejection using 5 g/L carbamazepine as the model solute. They discovered that although PES membranes without GO-ZnO had a significant drop in carbamazepine rejection (30%), those treated with nanohybrid GO-ZnO showed a less severe drop (less than 20%).

PES membranes impregnated with nanohybrid graphene oxide-zinc oxide (GO-ZnO) showed considerable improvements in hydrophilicity, pharmaceutical rejection (by lowering membrane-solute hydrophobic interactions), organic fouling resistance, and photodegradation. The specific alteration in GO could also improve its permeability, for instance, the use of HGO at 0.08 g/m^2 doubled the permeability of the PES membrane. A 0.04 g/m^2 level of HGO coated PES membranes showed improved (55% to 92%) rejection for NOM (e.g., BSA, SA, and HA). Increasing HGO loading also slowed the transition from pore blockage to the cake layer HA-based fouling and irreversible fouling of PES resistance lessened from 3.45 to 1.73 and from 62.86%–95.83% with HGO coating (Ding et al., 2021). HGO outperformed GO in terms of performance and NOM rejection, suggesting that membrane fouling in water supply, wastewater treatment, and reuse can be adjusted using modifying GO synthesis methods. It also notices that managing the HGO pore size, setting appropriate working conditions, and assuring the stability of the HGO composite membrane are all important considerations.

Lemos et al. (2021) demonstrated that GO-integrated membrane showed a 13% lower decline in flux than PES membrane. For both membranes, the permeate flux was less affected during the filtration of HA solution than the BSA one. The PES-GO membrane performed remarkably well regarding HA

solution, showing a minimal flux decay of only 2% after a permeate recovery rate of 80%. Irreversible fouling decreases significantly with GO due to the more negative surface charge flux recovery ratio (recoverable + irrecoverable) increased from 72% for the control PES membrane to 85% for the PES-GO high rejection and antifouling properties for HA and BSA in model solutions. After prolonged exposure to sodium hypochlorite solution, PES-GO exhibited loss of hydrophilicity and presented a significant indication of pitting-like damage on the active chlorine layer. However, GO strengthening with co-depositing PEI and Zeolitic Imidazolate Framework (ZIF-8) nanoparticles successfully removed up to 99% of organic pollutants.

5.3.1. GO-PES membranes antifouling functions in membrane MBRs

Ultrafiltration (UF) is a modern, cost-effective, and environmentally friendly technique used in membrane bioreactors (MBRs) (Zhang et al., 2018), and it is commonly supported by PES membrane, which is hydrophobic by nature (Zhang et al., 2021). However, over time the membrane could be ineffective for organic and microbial biomass deposition (Zhang et al., 2018).

Since GO is poisonous to bacteria, the GO composites membrane could prevent microorganism growth in MBRs. Unlike many other antimicrobial nanoparticles, GO nanosheets' antibacterial activity is triggered by direct contact with bacterial cells (Thambirajoo et al., 2021). Two major mechanisms by which GO disrupted the integrity of bacteria cells were (i) the penetration of GO's atomically sharp edges into the bacterial cell (Lu et al., 2017) and (ii) the oxidation reactivity with the GO nanosheets linked to cell membrane (Nanda et al., 2016; Zhang et al., 2021). Other organic fouling and early bacterial deposition inhibition methods include (i) antibacterial material coating, zwitterion polymers alteration (Zhang et al., 2018), and catalytic oxidation attributed elimination are all viable methods for decreasing (Zhang et al., 2021).

Zhang et al. (2018) developed a zwitterion polyampholyte hydrogel-imbedded PES membrane surface (p-PES membrane) for loading onto GO nanosheets (GO-p-PES composite membrane) (Fig. 5). BSA's adsorption potential was reduced by 70% due to the synergistic impacts of both. The composite membrane killed over 80% of E. coli colonies after 12 hours and showed a 25% reduction in flux compared to a 65% reduction in the pristine PES membrane. Furthermore, the biofilm layers on the GO-p-PES (9 m) and p-PES (8 m) membranes surfaces were lower than 19 m on the unmodified PES membrane. GO-p-PES and p-PES exhibited a similar organic fouling tendency in static biodegradable CA ultrafiltration membrane separation and dynamic filtration. Over 98% of the GO was still present on

the membrane surface after seven days, which shows very low leaching. Zwitterion polymers effectively lessen early bacterial adhesion and organic fouling, which in turn slows the development of biofilm. These results indicate that the GO-functionalized polyampholyte hydrogel membrane has effective anti-biofouling characteristics.

Fig. 5 about here

5.4. GO added PVDF membranes

PVDF membranes are the most broadly used membranes in MST because of their inexpensive flexibility, mechanical strength, and chemical and thermal resistance. The improved membrane was predicted to show potential in practical applications based on its exceptional performance in water science. On the other hand, the high hydrophobicity of PVDF prevents their application in water purification. According to Wu et al. (2020), grafting polyvinylpyrrolidone additive GO (PVP-GO) onto PVDF membranes resulted in a negative charge and improved hydrophilicity, resulting in solid repulsive forces between biopolymer and membrane, boosting antifouling performance (Fig. 6c). Advanced treatment (tertiary treatment) may be required for organic residues resistant to ordinary treatment (Oller et al., 2011).

Since soluble microbial products and self-polymerized organic molecules have a high molecular weight, they can be separated from salts and water (Yang and Yen, 2013). Earlier studies indicated that specific preparation procedures could enable GO membranes to fix the challenges of concentrated waste containing organics, inorganic ions, and chemical or energy consumption (Han et al., 2018; Yang et al., 2019). However, just a few research looked into the production of GO membranes for enhanced treatment of refractory toxics from wastewater (Yu et al., 2020). Han et al. (2018) created a GO membrane that can separate organic and inorganic salts, reducing the problem of mixed concentrate waste and boosting resource recovery from inorganic concentrate waste generated during membrane filtration (Fig. 6a). The modified GO membrane rejects COD at 76% and salt at 14% in a typical secondary effluent of recalcitrant effluents. Additionally, a greater assembly pressure (~10 bar) helped develop a membrane with a better exclusion rate and lesser roughness. The results of this study established an innovative application for GO membranes in wastewater treatment enhancement (Fig. 6b). Removal of inorganic and organic salts and the fabrication and application of GO membranes are currently understudied. Likewise, the impact of the supporting membrane surface characteristics (pore size, roughness), synthesis pressure (Tsou et al., 2015), and GO layers levels (Lou et al., 2020) on different salts, dyes, and OMPs separation performance and other GO membrane parameters are still unknown.

Fig. 6 about here

Recently, Wu et al.(2021a) demonstrated that grafting PVP-GO composites on the PVDF hollow fiber membrane surface and coating $Ag2CO_3$ significantly reduced the formation of bio-cake layers by (i) limiting microalgae growth on membranes, (ii) increasing hydrophilicity, (iii) decreasing protein binding, (iv) preventing the formation of bacterial aggregate and biopolymers, and (v) expelling large clusters from the membrane. The PVDF membrane has a maximum FDR of 83.1%. Following membrane-provided hydrophilic alteration, the A 83% FDR of PVDF (83%) was reduced and reached 67% (PVDF/GO) and 37.7% (PVDF/GO/Ag_2CO_3), showing remarked anti-pollution properties of the modified membrane. This is because the high hydrophilicity of the membrane prevents the binding of hydrophobic BSA (Mansourpanah et al., 2015). In practical applications, the modified membrane is remarkably successful at enhancing the antifouling characteristics and permeability of PVDF UF membranes.

5.4.1. GO-PVDF membranes antifouling performance in bioreactor (MBR)

GO additives are commonly used in membrane bioreactors (MBR) for treating industrial and domestic wastewater due to their minor trail, good water quality, and ease of usage (Mukherjee et al., 2018; Qin et al., 2018). Nevertheless, significant membrane fouling is always seen as the main impediment to MBRs being used in industry (Wu et al., 2020; Zhang et al., 2021). The main foulants in MBRs, extracellular polymeric substances (EPS), cause membrane biofouling (Zhang et al., 2018; Zhang et al., 2021). Protein and polysaccharides are the two most important components, accounting for 70–80% of total EPS (Wu et al., 2020).

In PVP-GO modified membrane, the distinct hydrophilic ligands on PVP chains act as planar combs, inhibiting Chlorella bindings with the membrane surface. For example, Wu et al. (2020) developed PVP-GO/PVDF membranes in algae MPBR (solids retention times: 30 d; hydraulic retention times:24 h) that successfully removed 97.8% and 76.9% of influent COD and NO_3-N, respectively, which was higher than the pristine membranes' removal of 93.0% and 70.6%. Moreover, the concentration of NH_4-N^+ in the influent declined below 7 mg L^{-1}, ranging from 68.4 to 71.9 mg L^{-1}. The results showed that farmed *Chlorella pyrenoidosa* biomass was more effective at removing ammonia nitrogen. To create microalgae *pyrenoidosa*, they obtained 96.8% removal in PVP-GO/PVDF composite membrane. Likewise, the protein content of loosely tied LB-EPS, EPS on the surface of PVP-GO/PVDF, and pristine PVDF composite membrane was (7.07 mg g^{-1} versus 55.24 mg g^{-1}), i.e., 1/8 of the latter. The protein percent of

tightly bound EPS and TB-EPS was (27.11 mg g^{-1} versus 72.55 mg g^{-1}), i.e., below half of the unchanged membrane surface (Fig. 6e). Overall, after 16 days, the biomass content was sustained at approximately 780 mg $L^{-1,}$ and the mean biomass generation rate approached 45 mg L^{-1} d (Wu et al., 2020).

5.4.2. GO-PVDF additive molecularly imprinted polymers membranes

Tetracycline (TC) is a macrolide antibiotic with a wide range of applications in agriculture and human health (Liu et al., 2014; Wu et al., 2021b). Significant separation fluxes and sensitive molecular selectivity coexist in aquatic habitats, making TC removal problematic. Graphene oxide is a low-cost adsorbent for removing PhACs from wastewater, but its limited selectivity prevents it from being used for a wide range of pollutants (Yang et al., 2016; Zhang et al., 2018). The Molecular Imprinting Technology (MIT) based membrane showed excellent pollutants selectively water purification system (Ghasemi and Nematollahzadeh, 2018; Ma et al., 2022).

Ma et al. (2022) demonstrated κ-carrageenan-altered GO nanosheets-double-layer-imprinted mixed matrix membranes, TC-imprinted activated carbon (AC) and SiO_2 GO@SiO_2/AC-based filter layers could be used with other PhACs or environmental contaminants than other MIMs. First and second-TC-imprinted layers created in DI-MMMs using PDA-based MIT and thermal-initiated radical imprinting polymerization resulted in improved-selectivity TC-imprinted spots with dual identifying function. Moreover, 50% of the porosity of composite membranes could be achieved for all prepared membranes in three operating cycles. Membrane showed excellent selectivity and removed 3.60, 3.33, and 3.51 for CEX/ TC, βSMZ/TC, and βOTC/TC.

Wu et al. (2021b) presented the manufacture of dual-imprinted GO/SiO_2 membranes (GS-DIMs) with excellent reabsorption capability for selective choice separation and elimination of TC via pressure filtering of TC-imprinted GO/SiO_2 nanocomposite sheets by two-stage polydopamine (PDA) imprinting (Fig. 7a). These PDA-based MIPs were able to create stable complexation with identical sites that were complementary in size and shape to TC molecules, allowing them to form chelates with TC molecules. The membrane/GO/SiO_2 contact would be more adherent with the PDA-modified supports. The amount of TC adsorption sites on GS-DIMs increased their ability to rebind considerably (more than 3.5). The TC-permeation efficacy (β value) of the GS-DIMs was 4.27, 3.88, and 4.11, indicating that the GS-DIMs were highly selective. One GS-DIM retained a good rebinding efficiency for the TC molecule after ten cycles of adsorption/desorption, losing just 8.9% of its maximum rebinding capability. They have recently designed dual-imprinted mixed matrix membranes loaded with GO/TiO_2 (Wu et al., 2022). The

GT-DIMs' dual-imprinted approach enabled high permselectivity (5.0) of TC in complexation rejection systems and synthetic wastewater samples and better rebinding (70.63 mg/g) at a 30-minute adsorption equilibrium rate (Fig. 7b).

Fig. 7 about here

These findings suggested that porous dual-imprinted PDA membranes supported by GO and functional nanomaterials-loaded nanocomposite structures could be useful for a range of other selective separation applications, including practical wastewater samples and industrial-scale applications.

5.4.3. GO-Biopolymer mediated membranes

Researchers have recently focused on developing a high-efficiency, low-cost biopolymer membrane for wastewater treatment. Bio-based polymers have the ability to link diverse molecules and are renewable, plentiful, and cost-effective (Tian et al., 2011; Silvestro et al., 2021). Some bio-based polymers that could be used in matrix membranes to improve their hydrophilic characteristics and permeability include cellulose acetate (CA), chitosan (CS), sodium alginate, and carboxymethyl cellulose (Mondal and Purkait, 2018; Lou et al., 2020).

According to Tian et al. (2011), CA (a bio-based polymer) is also used as a polymer matrix membrane because of its superior film forming ability, biocompatibility, environmental friendliness, and potential affinity for water penetration and metal ion rejection properties. Due to its poor mechanical and thermal qualities, CA, on the other hand, is inappropriate for NF (Sabir et al., 2015). CA is combined with GO to advance membranes' chemical and mechanical characteristics (Silvestro et al., 2021; Wang et al., 2021).

Wang et al. (2021) used an electrostatic self-assembly method to modify GO layers by injecting Co-Al LDH. They efficiently deposited on cellulose acetate (CA) membranes in various ratios (Fig. 8). They found that the Co-Al LDH contents are proportionate to the water affinity of GO/Co-Al LDH. The increase in flow was linked to the rise in Co-Al LDH, which widens the interlayer gap among GO, resulting in more outstanding water networks that allow easy movement of water molecules. The composite membrane has a high rejection rate (>90%) for n-hexane, Congo red (CR), rhodamine b (RhB), petroleum ether, methylene blue (MB), and mesitylene in vacuum filtration (VF). Other composite membranes have a rejection efficiency and flux of 87.16 percent, whereas 10 ppm MB has a rejection efficacy and flux of 97.19 percent. At a greater level of MB (80 ppm MB), it indicated 93.75%, which was still higher. Figure 8e shows that GO/Co-Al-2 has a high rejection efficiency (98%) for three

oils in water suspensions such as mesitylene suspension, n-hexane emulsion, and petroleum ether suspension, with corresponding membrane fluxes of 47.47, 83.28, and 57.35 Lm^{-2} h^{-1} bar^{-1}., indicating about complete separation of these emulsions. Creating polymeric networks can generally prevent polymeric materials from breaking down and improve their mechanical properties.

Fig. 8 about here

Like CA, chitosan has attracted substantial attention as a sorbent material, but its hydrophilic nature may interfere with nonpolar or hydrophobic pesticide interactions (Sanchez-Martin et al., 2006). Although the strong hydrophilicity of amine groups made CS less stable in an acid medium, however, amine groups of CS are known to be excellent reactive sites for network development and are promising for polymeric networks to prevent dissolution and improve mechanical characteristics. Achieving physical linkages with anionic crosslinkers (genipin, epichlorohydrin, glutaraldehyde) or physical crosslinking with anionic crosslinkers (sulfosuccinic acid, sodium citrate, oxalic acid, and sodium tripolyphosphate) has permitted the use of CS in a broader range of applications (Berger et al., 2004; Silvestro et al., 2021).

Silvestro (2021) discovered that a high GO content could successfully control the CS adsorption dynamics, favoring contacts with water repellent pollutants and decreasing exchanges with water-loving pollutants, using a glutaraldehyde crosslinker to assist chitosan in biopolymers-GO composite membranes. The pollutant recovery capacity (R percent) shows that the membrane water resistance influenced the yields. Pollutants that carry the octanol/water partition coefficient (log Kow) values (0.8 to 2) showed a small R% when CS or CS-GO with a low GO concentration (1-5%) was used. This may be addressed by the composite membranes' more excellent hydrophilic character, which allowed for more robust interaction with contaminants yet impaired the extraction phase. The incorporation of both hydrophilic groups (COOH and OH groups in GO and NH2 and OH groups in CS) and hydrophobic regions, on the other hand, allowed for a beneficial interface between the low log Kow pesticides and compound membranes. Similar results were obtained when log Kow 2 and 3 were used, but when log Kow 3 and 6 were utilized, the highest R percent was obtained. Increasing the matrix's hydrophobicity did not influence the reclamation of more water-repellent pollutants, which improved in lockstep with the rise in GO percentage (Fig. 8f).

The 20% GO chitosan/polyacrylamide/graphene oxide nanocomposites (CAGs) can achieve maximal adsorption of methylene blue. On the other hand, the magnetic CS-GO nanocomposites

removed rifampicin with a removal efficiency of over 95% (Silvestro et al., 2021). This behavior demonstrated that creating hydrophobic association (π-stacking) and hydrogen linkages may be regulated via changing the GO concentration in the CS integrated membranes, resulting in better pollutant extraction.

6. GO assisted adsorptive membranes

6.1. GO nanoparticles as adsorption material in membranes

Diverse kinds of membrane filtering apparatus have been implemented for water purification, such as MF, NF, UF and RO filtration (Fig. 9a). The exceptional purity of effluents from NF/RO treatment supports their use in post-treatment in wastewater/sewage treatment plants (Ma et al., 2022). Understanding the underlying mechanisms (size omission, hydrophobic bonding, and electrostatic interaction) is essential for NF/RO processes to remove EOMPs with varying physicochemical characteristics (size, hydrophobicity, hydrophobicity, solubility charge, and diffusivity) (Fig. 9b) (Ojajuni et al., 2015; Khanzada et al., 2020). Hydrophobicity has recently been found to significantly correlate with molecular weight (MW) by (Licona et al., 2018; Pollitt et al., 2019), indicating that size exclusion and adsorption are the most important removal processes.

Fig. 9 about here

Bisphenol A can be removed effectively using RO and NF membranes. For example, Bolong et al. (2010) combined a negative charge polymer with polyethersulfone nanofiltration membranes and discovered that at a pH of 14-8.0, the retention rate of BPA can surpass 90%. Kim et al. (2008) reported removing more than 95% of BPA from polyamide NF membranes by surface grafting using ethylenediamine, methacrylic acid and succinic acid. Commercial polysulfone ultrafiltration membranes have a capacity of just 16.6 mg m^2 for BPA adsorption (Wu et al., 2010). Regardless of how effectively BPA is retained by RO and NF membranes which are limited in application by small permeability and more operating pressure (Schrotter and Bozkaya-Schrotter, 2010). While the permeability of the affinity membrane may be adequate, one of the most important measures is its adsorption capacity. Although Heo et al. (2012) used carbon nanotubes and a polyethersulfone UF membrane system to study BPA adsorption, the most effective rates and capabilities are likely to be larger than 90% and 60 mg m^2, respectively.

For industrial applications, higher adsorption capacity is still desired. Chen et al. (2020) created graphene oxide (GO) nanosheets modified with -cyclodextrin (β-CD) to eliminate BPA (CDGO). The

grafted β-CD molecules provide adsorption spots on the surface of 2D nanochannel-containing CDGO membranes. Through host-guest recognition, β-CD, as a molecular chelator, may create serpentine complexes with BPA molecules (Alsbaiee et al., 2016). While GO nanosheets were chosen, (i) GO-associated functional groups are easy to modify with β-CD molecules, and (ii) because they are single atomic layer materials with a lot of specific surface area for adsorption (Wang et al., 2014).

The researchers claimed that ethanol washing could renew the CDGO composite membranes, and 100% restoration efficiency can be achieved after many cycles in the BPA exclusion process. Moreover, in comparison to standard GO, NF, or RO membranes, CDGO may have high flux and remarked adsorption performance for efficient BPA retention due to (i) plentiful adsorption positions on the surface of newly formed nanochannel and (ii) surface decorating of GO nanosheets with β-CD molecules, where the CDGO nanosheets may be crumpled with the fixing of β-CD molecules which compact the dimensions of 2D nanochannels in CDGO membranes (Chen et al., 2020).

Table 2 about here

To summarize, manufacturing high-permeability membranes with high adsorption capacity for efficient BPA removal remains challenging. Several studies have shown a number of advantages and limitations regarding GO-mediated adsorptive membranes (Table 2). During a four-hour treatment, Zambianchi et al. (2017) removed 90% of a variety of OMPs, including PhACs, pigments, PPCPs, and surfactants. Cho et al. (2019) demonstrated the use of GO nanoribbons (GONRs) to build composite membranes results in rapid water permeation and precise molecule separation >95 percent for OMPs with a larger hydration radius of 5 Å. Fryczkowska et al. (2020) created composite membranes that retained a significant protein (85 percent). When covalently coupled to GO, NF membranes maintain 85.03% of rhodamine B, and 95.43 percent when covalently linked to GO/polyacrylamide (Cheng et al., 2019).

According to Nguyen et al. (2021), the most critical factor impacting adsorption efficacy appears to be outer surface adsorption. Owing to colloidal instability, the structure, surface charge, shape, and conformation of nanoparticles in an aqueous solution might affect the contact of surface area. They found removal processes comprise (i) adsorption by hydrophobic contacts and electrostatic linkages between charged species (a part of van der Waals) (Dugyala et al., 2016); start at long distance (up to 10 nm), (ii) adsorption via π/π stacking (Ghosh et al., 2019), XH / π (X = C, O) contacts (Yaya et al., 2019), van der

Waals attractions (Thierfelder et al., 2011), and O⋯H hydrogen bonding (Jin et al., 2015); at comparatively low ranges (0.2–0.5 nm) (Fig. 10a).

Fig. 10 about here

Nonetheless, developing a single plausible explanation for the observed molecule adsorption tendencies in all carbon-based materials is challenging. In contrast to aromatic interactions, GO-based desorption is controlled by linkages between basal plane groups such as epoxy, -COOH C=O, and -OH. This could be because there are fewer π-rings than functional groups. Furthermore, adsorption is a complicated process governed by quite a few adsorbate parameters, including size, branching extent, and solvent polarizability, which are hard to quantify (Bunmahotama et al., 2020). Nevertheless, carbon nanotubes and GO are generally interesting for composite membrane integration, shorter residence periods, and substantial adsorption (Nguyen et al., 2021).

6.2. Metal/nanomaterial incorporated GO integrated biodegradable polymer membranes

Membrane separation is suited for phenol removal because of its high surface area, microporous structure, superior adsorption capacity, purity, and simplicity of access. Nevertheless, low removal rates with various filter technologies and high operating pressure are frequently constraints (Nguyen et al., 2021). The NF and RO both demand higher pressures, which raises operating expenses (Luo et al., 2014b). However, UF is ineffective for specific contaminants like hormones (Li et al., 2021b). Li et al. (2017) hypothesized that a nano-augmented membrane (i.e., NPs incorporated membrane) could efficiently remove organic contaminants utilizing ultrafiltration.

Recently, Nguyen et al. (2021) looked into six different types of carbon-based nanoparticles, including graphene oxide, graphene in two grades, multi- and single-walled CNTs, and fullerene C60. Graphene and CNPs demonstrated substantial uptake capacity for hormones that couldn't be quantified in isotherm investigations (more than 10 mg g^{-1}), and all NPs had swift kinetics. Moreover, based on the linear relationship between supernatant concentration and adsorbed mass, GO enhanced membrane had > 10 mg g^{-1} adsorption efficiency, which was significantly more than that of GP-AO2 (6.59 mg g^{-1}) and C60 (1.78 mg g^{-1}). Moreover, GO nonaugmented membranes had many times the Langmuir-based E2 adsorption capacity (150 mg g^{-1}) elsewhere, even though cellulose acetate (CA) membrane filters contributed significantly to adsorption (up to 80%) (Jiang et al., 2016a).

Recently, Li et al. (2021b) coated and grafted tannic acid(TA)-aminopropyltriethoxysilane (TAAPTES) on the membrane ferric ions (Fe^{3+}) to create a GO membrane with (interlayer gap and

transverse defects) (Fig. 10a). The GO membrane is first prepared using Fe^{3+}-mediated GO nanosheets. Then, the surface of the prepared membrane was coated with TA-APTES, which has a high affinity for Fe^{3+}; thicker TA-APTES was used to repair Fe^{3+} attributed to larger membrane defects. This "speckled" TA-APTES coating improved the antifouling capabilities while nanochannels in the GO membrane were regulated. However, it was unclear whether the presence of Fe^{3+} caused the selective placement of TA-APTES complex on GO membrane defects and or whether the pore size distribution was constrained. The results showed that TA-APTES modification of the GO-Fe-coated membrane increased the rejection of the endocrine disruptor BPA (BPA, 228 Da) from 26 to 81%, with minor porousness damage following BPA separation.

In contrast, the permeability cost of the GO-Fe membrane was over 36% after filtering 50 mL BPA solution. However, TA-APTES coating compromised BPA retention/in the GO-Fe membrane owing to a considerable rise in antifouling properties. The substantial BPA removal of the GO-Fe-containing membrane can be related to enhancing size segregation. Neutral OMP size segregation and adsorption are thought to be the main rejection processes in NF (Chen et al., 2020; Yuan et al., 2020)

6.3. GO in biomimetic membrane (BM)

Specific contaminants, like hormones, are resistant to ultrafiltration (Nguyen et al., 2021; Zhang et al., 2022). A carbon-coated nanofiltration membrane can efficiently remove phenol at pressures up to 8 bar (Cetinkaya and Ozdemir, 2018). However, a high-pressure membrane is not cost-effective. At 3 bar pressure, a carbon-coated UF membrane removed 93% of EOMPs, yet UF rarely rejected micropollutants, and the reactive membrane's removal efficacy was proportional to membrane flow (Zhang et al., 2022).

Increased water flux means less membrane contact time with EOMPs, which necessitates a faster oxidation rate. Coatings of cobalt carbon, for example, can eliminate 95 percent of EOMPs while producing more significant fluxes (>120 L/m2 h) because of the weak oxidation rates of micropollutants compared to UF flux. Laccase immobilized membranes had a lower water flux (50 L/m2 h) but a higher phenol and other EOMPs clearance ratio (82–96%) (Zhu et al., 2020a; Zhu et al., 2020b). They can, however, increase clearance at higher flux rates when paired with metal NPs and laccase. GO mediated gravity-driven biomimetic membrane (GDBM) showed 84.32% removal with 25~70 mg L^{-1} BPA removal rate and showed prominent stability (LMH: 27~42 and BPA removal: 55~70%) during 30 days' operation (Zhu et al., 2020b).

Biomimetic membranes with co-immobilized laccase and adsorption transporter on the membrane have recently been lauded as a "green" and long-lasting membrane technology (Zhu et al., 2020a). On-membrane enzymes help break down EOMPs and reduce foulants, extending the life of biocatalytic membranes (Zhu et al., 2020a; Bourassi et al., 2021). The enzyme-fouling layers generated as a result of enzyme immobilization, on the other hand, significantly improve filtration resistance, but regeneration is complex (Zhang et al., 2021).

According to Soroush et al. (2016), in situ generations of silver nanoparticles (AgNPs) using graphene oxide nanosheets greatly boosted bacterial inactivation (98%) in forward osmosis (FO), thin-film composite (TFC) membranes. Ag nanoparticles were successfully regenerated on Go-Ag modified membranes. Likewise, while carbon nanotube coating and chemical immobilization effectively prevent biofouling by isolating enzymes, the crosslinking agents used in coating and chemical immobilization alter permeability (Vanherck et al., 2013). To overcome this problem, Zhu et al.(2020a) employed GO as carriers and "coated" them with enzymes (laccase) that were physically adsorbed on the "dynamic" carrier layer on the BDM surface (Fig. 10b). The results showed that when CNT/GO concentrations (20–45 g m2) increased, the CNT/GO&Laccase@UF membrane's EOMPs removal rate increased proportionally to the biocatalytic membrane's adsorption capacity. Mixed-filtration BDM performed better than stepwise-filtration BDM.

Laccase activity was higher on GO than CNT. Flux and removal rate fluctuated significantly with certain laccase dosages. Enhancing GO or CNT level increased rejection efficiency but decreased flux, and after 5 cycles, removal rate and flux reduced by 10–15%. At 65 g m^{-2}, the elimination rate for GO-BDM increased to 98 percent and for CNT-BDM to 87 percent. Increased CNT/GO dosage increased removal rate but decreased fluxes. In contrast, increased laccase dosage changed both flux rates and removal rates, implying that a thicker CNT/GO layer results in a smaller pore size and a longer membrane penetration channel. At the optimal laccase dosage of 50 g m^2, the 25 g m^2 CNT/GO dose with ideal laccase action (3.97 and 3.24 U cm^2 for GO-BDM and CNT-BDM, respectively) maintained fluxes above 100 L m^{-2} h^{-1} and a clearance rate greater than 65 percent, demonstrating that laccase growth and catalytic strength did not become effective by additional CNT/GO. Overall, the most efficient production process for BDM for water/wastewater treatment was CNT/GO&Lac@UF (a combination of laccase filtration and CNT/GO on UF).

Biomimetic membrane (BM) can effectively remove a variety of MOPs, including dyes, and endocrine hormones, and antibiotics, in a closed membrane apparatus system while maintaining a low membrane fouling rate and a permeability greater than 20 L m^{-2} h^{-1} (LMH)/bar, allowing BM to attain a "high-pressure membrane effect" with "low-pressure membrane operation." However, these membranes are only useful in open natural therapy circumstances due to the lack of a filtering driving force. In open natural water systems, gravity-driven membranes (GDMs) have recently emerged as promising water filtration alternatives (Zhu et al., 2020b). Due to its independence from an outer accelerating force, high level of stability, cheap cost of energy, positive financial value, and simplicity of use and servicing, GDMs with GO showed soy sauce polluted natural water treatment (Pronk et al., 2019).

Zhu et al. (2020b) used to GO, CNT (carbon nanotubes), and activated carbon (AC) in GDBM and found that GO-GDBM had a greater permeate flow (40.33 LMH) than CNT-GDBM (30.95 LMH) or AC-GDBM (12.52 LMH). Furthermore, GO-GDBM was found to be much more effective at removing micropollutants due to its enzymatic efficiency and adsorption capacity (exceeding 60 percent). Overall, after 8 hours, GO-GDBM is stable and feasible, with >75 percent phenol elimination and >15 LMH fluxes. Laccase enrichment and accumulation are facilitated by the homogeneous mixing of GO and laccase. The GO is required to catalyze laccase's second copper ion binding T2/T3 active site. In contrast, azide ions bound the T2/T3 trinuclear copper group stabilized the native intermediate of oxidized laccase, bolstering GO and laccase's ability to remove micropollutants.

6.3.1. GO assisted PES membrane in EMOPs removal

Zhang et al. (2021) demonstrated the catalytic oxidation removal of endocrine disruptor chemicals in a PES membrane employing an enzyme-like ligand, Iron (III)- tetra-amido macrocyclic ligand (Fe(III)-TAML). Fe(III)-TAML is activated by H_2O_2 to produce high valence Fe. The bulk of EOMPs was efficiently removed using ultrafiltration with a TAML/GO-PEI/PES membrane. Porosity and hydrophilicity were increased with GO-PEI addition in the PES membrane. The complementary nature of GO and TAML was identified; TAML's improved oxidation performance improves the UF membrane's micropollutant removal at a high flux (Fig. 11).

Fig. 11 about here

The degradation routes suggested that the owning to C–C bond cessation, BPA (P1) breakdown into degraded phenol (P5) and 4-isopropylphenol (P2), and the P2 would again oxidize to hydroquinone (P4). On the other hand, the GO additive membrane's dense pore structure offered a superior substrate for

TAML loading. The membrane's tiny pore size promoted micropollutant contact with the TAML, which was beneficial for oxidation. Furthermore, 1 mmol L^{-1} H_2O_2 showed sufficient removal (100%) of 10 g/L BPA from the feed water maintained at the high flux of 192 $L^{-1}m^2$ h. The re-adsorption of the adsorbed Fe(III)-TAML on the GO-PEI membrane was simple, and the BPA flux and removal efficiency remained consistent during five cycles. The marketability of immobilized UF with an enzyme-like ligand highlights the scope of enzyme-like ligand catalytic oxidation in combination with UF to remove EOMPs at an excellent flux and ensure drinking water safety.

7. Enzymatic modified polyethersulfone (PES) membranes

Niebergall and colleagues (2014) used a wet-phase inversion method to introduce nanospheres with absorbency features into PES matrices (Xu et al., 2017). The produced nanocomposite membrane absorbent was then employed to remove BPA since it possessed an adsorption capacity of 7.7 mg m^{-2} at a pH of 3.5 (Niedergall et al., 2014). Wu and colleagues discovered that their membrane absorbers were 99.8% effective at removing endotoxins (Wu et al., 2017). However, adsorption saturation and pollutant leaks occur during regeneration, resulting in considerable secondary contamination.

Biocatalytic membranes can directly eliminate micropollutants, avoiding the "adsorption saturation" limit (Zhang et al., 2019). Immobilized laccase on (1) nano-copper integrated electrospun fibers showed a 95.4 percent removal efficiency of 2,4,6-trichlorophenol (Xu et al., 2017), and (2) 4-methoxyphenol was efficiently removed from functionalized CNTs/polysulfone (Costa et al., 2019). Despite this, the selection ability of membranes is compromised owing to the usual dipping contact manner application approach.

Laccase solution filtration by reverse filtration followed by dopamine (DA) coating layer enable its application for rejection, sorting, or catalysis (Cao et al., 2016). In an alkaline environment, numerous substrates can be covered with a durable polydopamine (PDA) coating layer that maintains enzymes within the membrane subnetwork by various processes (Cao et al., 2016). However, this biocatalytic membrane has poor solubility and is susceptible to enzymatic leakage and product accumulation, leading to membrane clogging and product interference (Cao et al., 2018).

The development of almost unhindered 2D nanochannels with a powerful rejection capability has resulted in a greater permeability for GO-based membranes (Han et al., 2018). Authors also offer excellent transport qualities, low manufacturing costs, elasticity, and chemical tolerance (Chen et al., 2018a; Chen et al., 2018b; Wang et al., 2018). A sulfonated GO altered PVDF membrane could improve

water flux by 146.6% (Ayyaru and Ahn, 2017), and a binding enzyme to GO nanosheets can generate a significant theoretical SSA (2630 m^2 g^{-1}) with better adsorption potential for EMOPS (Phatthanakittiphong and Seo, 2016), and a holding enzyme to GO nanosheets can give enhanced stability and activity (Vanherck et al., 2013; Zhu et al., 2020a; Zhang et al., 2021). The Hanes-Woolf method was used to measure Laccase's Vmax and Km values, which indicated a 47% increase following immobility on Go, outperforming other immobilized approaches. The Km values for GO-Zn-E and GO-NH2-E were lower than that for GO-E, implying a lower negatively charged controlled conditions could boost substrate attraction. Positive groups like Zn^{2+} and $–NH_2$ may alter the direction of contacts between GO derivates and enzymes, resulting in increased affinity and more active laccase sites exposed to substrate. GO-E and GO-Zn-E demonstrated enhanced durability and continued capacity to remove BPA after 72 hours.

GOZn-E also had a better removal efficiency than GO-E, which is most likely due to its increased stability. BPA oxidation derivates carrying a positive charge may also bind to GO via hydrophobic and electrostatic adsorption (Lee et al., 2013; Chu et al., 2017). Laccase restriction was reduced in the positive charge groups Zn^{2+} on GO-Zn, limiting the electrostatic bonding of derivates, while GO and GO-Zn-based laccase boosted enzyme action and stability relative to soluble laccase. These observations also validated the inconsistent results. Consequently, GO-Zn and GO were added to boost the biocatalytic membrane's functionality. The permeable membrane obtained by reverse filtering GO into NF270 improved by 14.8 % to the pristine membrane. Because the PDA layer increased the membrane's hydrophilicity (Luo et al., 2014b), the PDA coating restored some of the lost permeability. The enzyme filling of NF-E, reNF-E/GO and reNF-E/GO-Zn was nearly identical, reaching 60%. Reverse filtration and co-deposition can generate GO-based biocatalytic membranes. Higher permeate flow ought to accelerate permeate clearance and enhance biocatalytic membrane re-utilization, but it did not appear in greater BPA rejection by the membrane or adequate interacting time between BPA and laccase through GO adsorption. BPA may be detected semi-quantitatively using GO-based membranes with increased storage durability. These findings reveal the involvement of GO and its derivatives in laccase immobilization and biocatalytic membrane production, which can be used for EOMPs detection and elimination.

8. GO assisted membrane in EOMPs degradation studies

Wastewater influents are typically treated for pathogens and suspended or flocculated debris, but EOMPs like PhACs remain untreated due to their trace level (Mladenov et al., 2022). Effective ways for removing PhACs from wastewater include adsorption, advanced oxidation, and membrane filtration. Combining of more than one strategy is promising and could accelerate the performance of the water treatment system. Particularly, membrane filtration facilitates the degradation process and can increase 2.15 times degradation efficiency of the system (Gao et al., 2020). However, GO-based membranes are still not much efficient for organic contaminated water filtering due to (i) limited catalytic activity, (ii) the substantial tailoring necessary for intercalated materials, (iii) and delayed catalytic kinetics.

Previous studies as shown in table 3, claim the desirable removal capacity of GO for atenolol, propranolol, caffeine, carbamazepine, diclofenac, acetaminophen, acetylsalicylic acid and ketoprofen when integrated with catalytic membranes (Xu et al., 2019; Bhatia et al., 2021).

Table 3 about here

8.1. Catalytic Membranes

In EOMPs contaminated water treatment, sulfate radical-mediated advanced oxidation processes (SR-AOPs) is a modern research hotspot due to the formation of reactive oxygen species (ROS) via peroxymonosulfate (PMS) stimulation (Ye et al., 2021a). Catalyst performance and practical application are two essential variables in PMS activation in wastewater treatment (PMS). Ye et al. (2021b) formed a composite membrane supported by GO (Fig. 12a). Firstly, they formed a 1D/2D nitrogen-doped carbon array with controlled FexOy by in-situ transmutation of ZIF@MILs-20. Then, this dual metal-organic framework was intercalated into adjacent GO. The 1D/2D associative porous ZIF@MILs-20 structures supported by restricted FexOy and increased oxygen vacancies were beneficial for removing NX via a collaborative "trap-and-zap" approach for PMS stimulation. The ZIF@MILs-20/PMS system eliminated 99.4% of NX after 40 minutes. However, the degradation process generates several intermediate including hydroxyprolyl-tryptophan, oglufanide, mitiromycin despropylene gatifloxacin, oxonorfloxacin, desethylene norfloxacin hydrochloride, 5-ethyl-5-(4-fluorophenyl)-1,3-diazinane-2,4,6-trione, flumequine and n-feruloylglycinate. When comparing the removal efficiencies of many persistent organic pollutants, such as perfluorooctanoic acid (PFOA), CBZ, and BPA catalytic membranes were shown to achieve ultra-high removal efficiencies (89.3, 95.7, and 100%, respectively) than powder catalyst (43.5, and 76.3 and 94.3%, respectively). Additionally, after five cycles, the ZIF@MILs-20/GO

membrane retained over 90% SMX degradation efficiencies, verifying catalytic membrane (ZIF@MILs-20/GO) with high stability and reusability.

Fig. 12 about here

With a capacity of 165.3 mg g^{-1}, the ZIF/MILs-20/GO membrane had the best capacity for NX adsorption, demonstrating that the GO increased catalyst wettability by lowering the reaction space of ROS and active sites (Zhu et al., 2018). The ZIF@MILs-20/GO framework exhibited simultaneous catalytic oxidation and separation of organics with a constant flow of 156.3 $Lm^{-2}h^{-1}bar^{-1}$, considerably overcoming membrane fouling. Furthermore, singlet oxygen ($^1O_2$) has been shown to play an important role in the breakdown of NX. In a nutshell, using catalytic membranes to treat wastewater is a novel concept.

The proposed mechanisms showed Fe^0 peak vanished completely at first, whereas the Fe^{2+} peak shifted slightly, indicating that Fe^0 countered with electrons to free Fe^{2+}, as provided in Eqs. 1 and 2. In particular, Fe^0 can reutilize Fe^{3+} by replacing Fe^{2+}, as shown in Eqs. 3–5. Furthermore, Fe^{2+} regeneration may occur by electron transport at N species and transition metal NPs interface, boosting catalytic activity even more (Eq. 6) (Luo et al., 2011). Alongside, sp^2 hybridization of pyridinic N can generate a -system by connecting two carbon atoms or donating one p electron (Liu et al., 2020a). Furthermore, as demonstrated in Eqs. 7 and 8, free electrons will combine with the lone-pair electrons of the N dopant, accelerating PMS activation. Additionally, it has been established that SO_4^- interacts with H2O to yield OH (Eq. 9).

The synthesis of $SO_5^{\cdot -}$ was aided by the presence of hydroxyl groups on the catalyst surfaces, which aided in the breakdown of PMS molecules (Eqs. 10 and 11). In contrast, the reaction between H_2O and $SO_5^{\cdot -}$ aided in forming $^1O_2$ and accelerated PMS degradation (Eqs. 12 and 13) (Wang et al., 2019). Because the redox potential of $O_2^{\cdot -}$ acquired since the catalytic process for pollutant removal was weak, it was changed to $^1O_2$ (Eqs. 14–17) (Hu et al., 2020). Some $^1O_2$ can be made by reacting H_2O with OH (Eq. 18). While Eq. 19 shows the $^1O_2$ formation from oxygen vacancies and PMS molecules (Zeng et al., 2020). Finally, Eq. 20 shows that a mix of radicals and non-radicals increased NX breakdown, resulting in totally mineralized NX molecules converted to CO_2 and H_2O.

$$Fe^0 + 2HSO_5^{\cdot -} \rightarrow Fe^{2+} + 2SO_4^{\cdot -} + 2^{\cdot}OH \quad (1)$$

$$Fe^{2+} + HSO_5^{\cdot -} \rightarrow Fe^{3+} - OH + SO4^{\cdot -} \quad (2)$$

$$Fe^{2+} + HSO_5^{\cdot -} \rightarrow Fe^{3+} + SO_4^{2-} + {}^{\cdot}OH \quad (3)$$

$Fe^{3+} + HSO_5^{\cdot -} \rightarrow Fe^{2+} + H^+ + SO_5^{\cdot -}$ (4)

$Fe^0 + 2Fe^{3+} \rightarrow 3Fe^{2+}$ (5)

$Fe^{3+} + e^- \rightarrow Fe^{2+}$ (6)

$HSO_5^{\cdot -} + e^- \rightarrow SO_4^{\cdot -} + OH^-$ (7)

$C\text{-}\pi^{\cdot} + HSO_5^{\cdot -} \rightarrow C\text{-}\pi + OH^- + SO_4^{\cdot -}$ (8)

$SO_4^{\cdot -} + H_2O \rightarrow SO_4^{2-} + {}^{\cdot}OH + H^+$ (9)

$Fe^{3+}\text{-}OH + HSO_5^{\cdot -} \rightarrow Fe^{3+}\text{-}HSO_5^{\cdot -} + OH^-$ (10)

$Fe^{3+} + HSO_5^{\cdot -} + H_2O \rightarrow Fe^{2+}\ {}^{-}OH + SO_5^{\cdot -} + 2H^+$ (11)

$2SO5^{\cdot -} + H2O \rightarrow 2HSO_4^- + 1.5\,{}^1O_2$ (12)

$HSO_5^{\cdot -} + SO_5^{2-} \rightarrow HSO_4^- + SO_4^{2-} + {}^1O_2$ (13)

$HSO_5^{\cdot -} + H_2O \rightarrow HSO_4^- + H_2O_2$ (14)

${}^{\cdot}OH + H_2O_2 \rightarrow HO_2^{\cdot -} + H_2O$ (15)

$HO_2^{\cdot -} \rightarrow H^+ + O_2^{\cdot -}$ (16)

${}^{\cdot}OH + O_2^{\cdot -} \rightarrow {}^1O_2 + OH^-$ (17)

$2H_2O + O_2^{\cdot -} \rightarrow {}^1O_2 + OH^-$ (18)

$Ov + HSO_5^{\cdot -} \rightarrow HSO_4^- + {}^1O_2$ (19)

$ROS\ (SO4^{\cdot -} + {}^1O_2) + NX \rightarrow Intermediates + CO_2 + H_2O$ (20)

Overall in the ZIF@MILs-20/GO/PMS system, the degradation process and contribution of relevant ROS were discovered, indicating that OH had a minor part in NX degradation whereas $O_4^{\cdot -}$ was highly essential. Furthermore, NX degradation was aided by both free radicals and non-radicals, with $SO_4^{\cdot -}$ and ${}^1O_2$ being substantial contributors (Fig. 12a).

8.2. Photo-Fenton catalytic membranes

Intercalating photo-Fenton catalytic Fe-based MOFs into GO nanosheets regulates two-dimensional nanochannels while simultaneously endowing the membrane with photo-Fenton self-cleaning facility. More importantly, the inclusion of GO enhances the photo-Fenton catalytic properties of the membranes by increasing the segregation of photogenerated charge carriers due to its big SSA, better electrical conduction, and excellent charge carrier capacity (Yang et al., 2017a; Liu et al., 2018). As a result, a membrane comprising GO/Fe(III)- intercalating MOF integrated with photo-Fenton activities and membrane separation was developed for better water purification. Likewise, MIL-88A intercalated onto neighboring GO nanosheets as a restricted catalytic membrane in an oil-water separation system

demonstrated a self-cleaning photocatalytic reaction (Xie et al., 2020a). Furthermore, at constant flux, the graphene oxide/MIL-88A(Fe) (GO/M88A) composite membrane maintained an excellent MB separation (97.87%) even after 12 cycles.

Additionally, photo-Fenton catalytic breakdown of pollutants utilizing membranes was 98.81% for MB and 97.27% for BPA (Xie et al., 2020a). The activated GO/M88A membrane release e—h^+ pairs in response to visible light irradiation. Impurities (R) were directly oxides by h^+ while transport of e^- to GO surface enhanced the photoinduced transporter potential for separation and facilitated OH production by H_2O_2 breakdown. Meanwhile, O_2 can collect e^- and convert it to the highly active $O_2^{\cdot -}$ species on GO/M88A surface. Contaminants can be oxidized entirely and degraded by the highly reactive OH and $O_2^{\cdot -}$ species (R). Fe—O clusters can also use Fenton-like reactions to expedite the decomposition of H_2O_2 into OH. Furthermore, the GO nanosheets provide many active catalytic sites, resulting in higher photocatalytic activity (Li et al., 2018). Impurities collected on the membrane's surface may be quickly removed thanks to the strong photo-Fenton catalytic activity, ensuring a better rejection at a high flux (Fig. 12b).

The following is a summary of the reactions that have been proposed (Eqs. 21-26):

$$GO/M88A + hv \rightarrow e^- + h^+ \quad (21)$$

$$H_2O_2 + e^- \rightarrow {}^{\cdot}OH + OH^- \quad (22)$$

$$e- + O_2 \rightarrow {}^{\cdot}O_2^{\cdot -} \quad (23)$$

$$Fe(III) + H_2O_2 \rightarrow Fe(II) + HO_2^{\cdot} + H^+ \quad (24)$$

$$Fe(II) + H_2O_2 \rightarrow Fe(III) + {}^{\cdot}OH + OH^- \quad (25)$$

$${}^{\cdot}OH/{}^{\cdot}O_2^{\cdot -}/h+ + R \rightarrow \text{several steps} \rightarrow \text{by-products} \quad (26)$$

The photo-Fenton degradation of AMX by TiO_2-GO-Fe_3O_4 composites revealed a charge carrier pathway between TiO_2, graphene oxide, and Fe_3O_4, while ${}^{\cdot}OH$ and H^+ dominate the photo-Fenton degradation of AMX. In situ embedding TiO_2 nanoparticles on GO sheets and UV light exposure create surface roughness and wrinkles that facilitate molecular mobility.

A submerged magnetic separation membrane photocatalytic reactor (SMSMPR) using ceramic membranes was created to isolated suspended TiO_2-GO-Fe_3O_4 from waste effluent, and this reactor was integrated with the TiO_2-GO-Fe_3O_4. AMX degradation was improved by raising the H_2O_2 concentration from 0 to 20 mM from 10.0 to 90.1 percent while decreasing it by increasing the pH from 3.0 to 7.0. At pH 3, TOC was removed 90% of the time, while at pH 5, it was only 50%. Furthermore, at pH 3 and pH

5, leaching Fe concentrations were 0.75 and 0.59 mg L^{-1}, respectively, meeting state wastewater release standards (1.0 mg L^{-1}). Backwashing and magnetic separation in the SMSMPR can improve photo-Fenton catalytic activity, persistence, and filtration support to strengthen wastewater treatment applications. The SMSMPR appears well suited for treating acid wastewater because of its better efficiency and less metal leaching under acidic conditions (Li et al., 2019b).

8.3. Photocatalytic Membranes

In previous studies, visible light attributed to TiO_2 activation was enhanced with GO (Li et al., 2019b; Li et al., 2022a). Thus, OH generation and h+/e- pair separation improved photocatalytic functions of GO-TiO_2 obtained (Jiang et al., 2016b; Li et al., 2022a). The photo-Fenton process destroys refractory organic molecules by reducing Fe^{3+} to Fe^{2+} through a photoinduced electron (Li et al., 2019b; Xie et al., 2020a). Several research using TiO_2 and Fe_3O_4 to recover catalysts have been undertaken (Li et al., 2019b; Li et al., 2022a). However, a photocatalytic activity typically degrades due to the weak charge transfer speed between Fe_3O_4 and TiO_2. Thus, the long life of this reusable photocatalyst must be extended. Furthermore, the oxygen functional groups can vide a bonding site to form graphene-supported metal oxide nanocomposites (Zhao et al., 2013). As a result, TiO_2, CuO, CdS, ZnO, and Fe_2O_3 are typically covalently linked using GO (Xu and Wang, 2012; Wang et al., 2013).

To demonstrate photocatalytic degradation of CBZ and DCF Heu et al. (2020) utilized GO in a zirconium-oriented metal-organic framework (UiO-66). They discovered that ultraviolet (UV) photocatalytic activity reduced membrane fouling from 20.7% to 2.4% and enhanced FRR to 98%. After five cycles, the UiO-66 GO/NF-10% composite membrane demonstrated superior physical stability with a comparatively low mass loss of 8.64% compared to those carrying mass of 5 and 15 wt%. In addition, irreversible fouling of UiO-66 GO/NF-10% composite membrane decreased from 20.7 to 2.4% and boosted FFR to 98% with improved photocatalytic activity under ultraviolet (UV) irradiation (bandgap: 3.45 eV).

They previously used $TiOSO_4$ as a Ti source to create a multifunctional GO/TiO_2 membrane for crossflow filtration (Zhu et al., 2017a). The membrane showed significant photocatalytic degradation of Methylene Blue when exposed to UV light. UV light irradiation of 100 min dramatically reduced the membrane fouling, resulting in a 96% flux recovery. Likewise, UV light irradiation of 110 min degraded 92% of MB with a photocatalyst dose of 4 mg. The GO/TiO_2 membrane's exceptional performance revealed its commercial potential in the quality water supply. Similarly, to simultaneously solve TiO2's

catalytic performance, durability, and separation property restrictions, Li and coworkers (Li et al., 2019b) developed a new approach for co-assembling TiO_2 and Fe_3O_4 nanoparticles on GO (Fig. 13).

Fig. 13 about here

The TiO_2-GO-Fe_3O_4 composite membrane showed that (i) doping GO improves catalytic activity and stability by facilitating charge transport, and (ii) on-site growing Fe_3O_4 on the GO surface can increase heterogeneous Fenton degradation of EOMPS and offers photocatalyst affinity for magnetic separation in the water cleaning system. In the presence of Amoxicillin (AMX), the oxidation efficiency of sole TiO_2-GO and Fe_3O_4 was 14.7%, but TiO_2-GO-18wt %$Fe_3O_4$was 18.7%. In the presence of H_2O_2, Fe_3O_4 composites had a 90% oxidation efficiency. On the other hand, the oxidation efficiency of AMX in TiO_2-GO-18wt%Fe_3O_4 is 22.3% due to Fe_3O_4 activation and 15.2% due to visible light irradiation, respectively. However, the performance of the photocatalytic system can still be further enhanced by using appropriate different flow modes, e.g., surface flow, flow-through, cross-flow, and dead-end or statistic mode (Fig. 14a). Gao et al. (2020) demonstrated that the steady increase of solution flow vertical to the membrane surface resulted in an overall increase in degradation efficiency of the photocatalytic system. The membrane degradation efficiency follows an order of FT > CF > SF.

Fig. 14 about here

Ivanković et al. (2021) used adsorption on graphene and functionalized deviations like GO NMs-based photocatalysis to determine the basic characteristics and behavior of the 18 most commonly found PhACs (beta-blockers, lipid regulators, psychotropic drugs, and analgesics) in aquatic environments (Ye et al., 2021b). Metal-organic frameworks (MOFs) were investigated extensively as diverse types of photocatalysts due to their outstanding ligand-metal charge transfer (LMCT) characteristics when exposed to light (Yang et al., 2017b; Gao et al., 2018). Due to their Fe_3-3-oxo clusters and mild toxicity, Fe-based MOFs have a lot of promise as photocatalysts, as they can initiate a heterogeneous photo-Fenton-like response in sewage treatment when activated under light (Liu et al., 2018; Ahmad et al., 2019). In addition, the antifouling potential of the membrane is significantly increased by strengthening the membrane scheme with a photo-Fenton-like system (Xie et al., 2020b).

9. Electrified membranes (EMs)

Different structures of EMs membrane (e.g., flat sheet membrane, hollow-fiber,tubular and spiral membrane) can be formed via free-standing membrane casting, composite membrane assembly process

and membrane modification and used as operated in flow-by and flow-through filtration systems (Fig. 15a). These membranes have been demonstrated to be effective for neutral and low molecular weight EOMPs, exceeding traditional membranes' size- and charge-exclusion separation characteristics (Pollitt et al., 2019). Electrochemical-based redox processes (Fig. 15b), electrooxidation, electro-adsorption, and electrostatic rejection (Tang et al., 2017; Zhu and Jassby, 2019) are just a few of the electro-assisted available technologies, and they overcome fouling and steric hindrance caused by microbes, organic pollutants, and inorganic salts as shown in Fig. 15c (Liu et al., 2020d). As a result, EMs can effectively dissolve and/or modify contaminants during membrane separation operations, enhancing charged species rejection.

Fig. 15 about here

Particular electrode geometry such as nanodots, nanowire, and nanorod arrangement can be used to facilitate the removal of microbes (e.g., virus) in anodic EM (Fig 15d). The process is further improved by (i) optimizing flow convection (Ji et al., 2015), (ii) amplifying the electric field (Zhao et al., 2018), (iii) increasing temperature, and (iv) concentrating reactants (Ji et al., 2019).

Yang et al. (2016) incorporated GO into a ceramic composite tubular membrane and utilized it to eliminate several EOMPs from water. EOMPs includes sulfamethoxazole (SMX), di(2-ethylhexyl) phthalate (DEHP), di-n-butyl phthalate (DnBP), and cephalexin (CLX). They observed that 99% rejection of DEHP and DnBP was achieved in crossflow filtration membrane supported by electrocoagulation and electro-filtration process (EC/EF), whereas those for cephalexin (CLX), sulfamethoxazole (SMX), and caffeine (CAF) varied from 32 to 97%. The predominant removal processes of multifunctional membrane system were (i) size exclusion, (ii) electrostatic repulsion, (iii) adsorption, (iv) electrocoagulation, and (v) electro-filtration (Fig. 15b).

Sulfamethoxazole is an antibiotic that is difficult to remove from wastewater because it produces refractory by-products (Du et al., 2018). The complete separation of SMX from sewage is impossible with the conventional sludge activation method (Ji et al., 2019) because of its resistant and bio-refractory nature. Due to their mild toxicity and high capacity, electrochemical advanced oxidation processes (AOPs) are vital for removing these pharmaceuticals (Moreira et al., 2017). Yu et al. (2020) developed an electrochemically improved carbon nanofibrous anodic membrane (G/SnO_2/CFs) that may be used to oxidize various developing and refractory medicines electrochemically (Fig. 16a).

Due to SnO_2's strong electrooxidation capacity and graphene's excellent electrical conductivity (Kretinin et al., 2014), the electrooxidation performance and conductivity of carbon nanofibers (CFs) can be considerably improved by adding graphene/tin dioxide (G/SnO_2) into them in a unique way. It was discovered that large amounts of anodic membrane and changing the flow-through mode of the PAN-based G/SnO_2/CFs microfiltration improved its degrading efficiency and electrochemical filtration. Furthermore, the composite membrane showed excellent degradation (85%) with promising stability after 10 cycles in 50 h operation, indicating that it can manage dangerous refractory organics in wastewater.

Fig. 16 about here

Electrospinning was utilized by Li et al. (Li et al., 2019a) to create a ZIF-67/polyacrylonitrile (PAN) fibrous membrane that enhanced the simultaneous removal of impurities as a membrane reactor (Wang et al., 2020). However, most catalysts were partially deposited or gathered disorganized in polymers, which obstructs electron movement and necessitates the development of more effective supporting materials in catalytic membrane systems (Zhong et al., 2018). Although GO's mechanical strength and ultra-flexibility make it a strong choice for membrane manufacturing, pollutant buildup on the membrane surface lowers penetration flux (Sun and Li, 2018). Tunable mass transfer channels can separate oil and water while also auto-cleaning photo catalytically by linkers active units into adjoining GO (Cai et al., 2020). However, in PMS stimulation, the utilization of GO stacked frameworks in combination with active catalysts to generate an auto-standing GO-assisted membrane for synchronized screening and catalytic oxidation of EMOPs is unusual.

Recently, an auto-assembly approach was developed for sandwiching active species, lawn-like 2D Fe_2O_3@Co0.08-Fe1.92@nitrogen-doped CNT/reduced GO (rGO) composites, into GO membranes (Ye et al., 2021c). Because of the enhanced interlayer distance of GO nanosheets, the FeCo@GCTs/GO film improved permeability and displayed catalytic auto-cleaning features. The permeation flux of the FeCo@GCTs/GO membrane was enhanced to 487.3 L m^{-2} $h^{-1}bar^{-1}$, which was more than 7.5 times that of the GO membrane (64.6 L m^{-2} $h^{-1}bar^{-1}$), and the antifouling performance of the composite membrane was improved as the interlayer gap of GO nanosheets was increased.

Meanwhile, in the SMX-HA combined setup, their removal efficiencies were 67.5% (by GO membrane), and 99.2% (by a composite membrane) were achieved, suggesting that the FeCo@GCTs/GO membrane can also segregate micro molecules. After 30 minutes, the FeCo@GCTs/GO/PMS system

successfully removed up to 98.4% of SMX. Moreover, following five successive cycles, the FeCo@GCTs/GO membrane sustained above 90% SMX elimination and Cr (VI) removal under 30 min, showing that the FeCo@GCTs/GO membrane was adaptive to repeated use (Fig. 16b). The results revealed that the catalytic membrane/PMS setup could efficiently prevent metal loss.

As per the participation of soluble metal ions, the cleaning rates of Co^{2+} and Fe^{2+} were moderate (< 7%), showing a diverse mechanism for SMX breakdown (Fig. 16b). Additionally, once the catalytic membrane was deployed to a range of contaminants mixture, about 100% degradation rates were achieved for MO, BPA and TC in 15 min, 25 min, and 30 min (Ye et al., 2021c). This self-contained FeCo@GCTs/GO catalytic membrane can be utilized in numerous microchannels membrane substrates in challenging circumstances.

10. Conclusions and outlooks

OMPs have been found in tap water, wastewater, and surface water. Uncontrolled OMPs threaten already constrained water supplies. The conventional strategies used in most WWTP cannot remove OMPs like PPCPs. Therefore, developing efficient and environment-friendly novel supporting technologies is crucial to ensuring water quality and future-proofing potable recovered water use. Membrane filtration has been pragmatic to water treatment contaminated with numerous OMPs. However, owing to cost, fouling control, poor dispersion in aqueous solution, and low sorption affinity, its application on a broad scale remains a challenge.

Furthermore, each membrane technology has its own characteristics that must be considered while deciding on the best treatment. Likewise, the combination of two or more strategies also improved overall performance. For instance, degradation combined with filtration is 2.15 times more effective. GO additive strengthens majorities of available porous polymeric substrates membranes (e.g., PVDF, PC, PAN, and PSF), but the incorporation of GO into inorganic membranes is still limited.

Adsorption is another membrane-based filtration strengthening factor that was improved by incorporating GO nanosheets which provide a hydrophilic layer and increase surface area and adsorption capacity. However, adsorption may accelerate biological fouling and limits water flux. Herein, bactericidal characteristics of GO may promise improved flux recovery (~6 folds) while mixing of other chemical species (e.g., Ag, APTES, SiO_2, ZnO) and incorporation degradation can further enhance (7.5 folds) and make membrane useable for many cycles.

However, chemical and mechanical stability is the most demanding feature of membrane life. For this, hollow metal fibers such as stainless steel (SS) membranes are gaining significant attention. Still, surface passivation is required to prevent oxidation and advanced decoration routes. A similar issue can also be addressed using nanoscale coatings of GO to accelerate electrochemical processes and avoid the early corrosion of bare metal reinforcements during electro-Fenton (EF) reactions.

More studies are warranted to assess the enhancement of GO-assisted photo-Fenton catalytic and Fe-based MOFs catalytic properties. AOPs frequently promote the release of a number of different oxidants, increasing the electrolysis effectiveness of other anode materials. Resultantly make it less effective in less polluted medium with a lower level of pollutants. This can be explained by establishing a limiting phase in the reaction caused by the mass transfer of target contaminants to the anode surface from the liquid. It has been shown that sono-electrolysis increases the mass transfer rate and encourages the destruction of hydroxyl radicals, which are responsible for the production of water, as well as several oxidants produced when these radicals interact with other species found in wastewater (Oturan et al., 2008; Sánchez-Carretero et al., 2011). Likewise, bio-based polymers (used in matrix membranes to improve hydrophilic and permeability) and carboxymethyl cellulose GO may boost tensile strength and Young's modulus by 2 to 3 times. Therefore, GO-based improved mechanical stability in polymeric membranes could appear as a better alternative to ceramic membranes and reduce the operational cost by up to 24-54% (Sagle and Freeman, 2004).

Moreover, the microorganisms and organic matter in wastewater are also limiting factors in the membrane filtration of EOMPs. Improving the operating matrices (washing, conditioning cycles and hydrodynamic optimization) may minimize this issue, and operations and functionality might endure longer.

Achieving a balance between EOMPs, environmental implications, and economic feasibility is essential for constructing an economical and environmentally benign solution. GO mediated gravity-driven membranes for low pressure. Likewise, incorporating GO-ZnO decreases membrane-solute hydrophobic attraction, hinders fouling by sodium alginate, increases rejection rate, and provides high fluxes. The membranes usability at minimal pressure (4 bar) and optimum photocatalytic stand out as ideal technology for low-energy applications in rural parts of developing countries where untreated water is collected and used for various domestic purposes.

GO integration substantially not only facilitate EOPMs removal but also shows an excellent flux recovery ratio in a diverse type of system, which is imperative for long-term performance and reusability. For instance and in the MBR system, 96% atrazine was removed by UF (FRR:98.6%), in photocatalytic degradation, 92% removal of methylene Blue was achieved (FRR:96%), in PVDF membrane, reduced extracellular polymeric substance and removed 97% COD (FRR:98.6%), and along poly (acrylonitrile-methyl acrylate) 99.3% of BSA removed (FRR:98.6%)

GO incorporation has also demonstrated high visible light attributed to TiO2 activation, saving energy. The modified polyvinylidene fluoride GO membrane with Ag_2CO_3 disposition exhibited minimal irreversible fouling ratio (*R*ir) and total fouling ratio (*R*t) readings, indicating excellent antifouling membrane characteristics. This response was attributed to the formation of a hydration layer on the surface of the membrane as a function of mass deposited CO_3^{2-} (hydrophobic group), which protects the membrane surface and inhibits the attachment of pollutants (Qin et al., 2015). As with other photocatalytic materials like TiO_2, Ag_2CO_3 photocatalytic activity under UV or visible irradiations may also be employed to improve the self-cleaning ability of modified membranes.

GO integrated membrane performance can be further optimized by other strategies such as electrocoagulation and electro filtration (phthalate esters, ECs, and PhACs). This approach offers the door for the scalable design of improved combinatorial electro-reactive materials for the oxidation treatment of highly polluted effluents and simultaneous filtration. Instead of screening across the pores, this method permits selectivity across vast pore-sized membranes.

These strategies in conjugation with mixed matrix membrane have enabled the fabrication of GO ultrafiltration membrane, which attains better permeability and excellent selective screening and shows improved antifouling potential and promising mechanical traits. Due to pseudocapacitance properties, MMMs can work as in-situ monitors for membrane fouling which offers long working life, and membranes capable of producing high-efficiency filtration in environmental application separation processes. However, removal rates are often highly variable for target EOMPs (i.e., CAF, SMX, and CLX), particularly in the presence of multiple pollutants, making complexities in applying these membranes. To overcome this shortcoming, further study is needed to figure out how to enhance the removal performance and keep it consistent for various ECs.

More research is needed to ensure the efficient technical transfer of PES-GO membranes in MBR. This additional research could concentrate on (i) exploring the economic level of GO to increase

permeability without jeopardizing membrane antifouling potential; (ii) coupling joint physical and mechanical strategies to remove/reduce the loose cake layer formed on the PES-GO membrane during mixed liquor filtration; and (iii) investigating alternative material for chemical cleaning to cope these challenges.

Finally, although it hasn't been proven that low-level exposure to these compounds is harmful, potable water treatment plants should aim to give pharmaceutical-free water. Water rules ensure water's credibility and safety. More research into the prevalence of these compounds in the biosphere and their impact on quality of life could lead to future legislation.

Acknowledgment

This work is supported by the National Key R&D Program of China (grant Nos. SQ2018YFA030066, SQ2018YFA030143), the National Natural Science Foundation of China (No. 11974169), the Fundamental Research Funds for the Central Universities (Nos. 020414380087, 020414913201), and the Basic Research Program of Jiangsu Province (Grant No. BK20190283). Beenish Mustafa is also thankful to Nanjing University Nanjing, China and the Chinese Government, and the Chinese Scholarship Council for providing her Ph.D. Scholarship. Dr. Abdoulmohammad Gholamzadeh Chofreh is supported by project by the EU project “Sustainable Process Integration Laboratory—SPIL”, project No. CZ.02.1.01/0.0/0.0/15_003/0000456 funded by EU “CZ Operational Programme Research, Development and Education”, Priority 1: Strengthening capacity for quality research .

References

Ahmad, M., Chen, S., Ye, F., Quan, X., Afzal, S., Yu, H., Zhao, X., 2019. Efficient photo-Fenton activity in mesoporous MIL-100 (Fe) decorated with ZnO nanosphere for pollutants degradation. Applied Catalysis B: Environmental 245, 428-438.

Ali, A., Mubashir, M., Abdulrahman, A., Phelan, P.E., 2022. Ultra-permeable intercalated metal-induced microporous polymer nano-dots rooted smart membrane for environmental remediation. Chemosphere 306, 135482.

Alsbaiee, A., Smith, B.J., Xiao, L., Ling, Y., Helbling, D.E., Dichtel, W.R., 2016. Rapid removal of organic micropollutants from water by a porous β-cyclodextrin polymer. nature 529, 190-194.

Attina, T.M., Hauser, R., Sathyanarayana, S., Hunt, P.A., Bourguignon, J.-P., Myers, J.P., DiGangi, J., Zoeller, R.T., Trasande, L., 2016. Exposure to endocrine-disrupting chemicals in the USA: a population-based disease burden and cost analysis. The lancet Diabetes & endocrinology 4, 996-1003.

Ayyaru, S., Ahn, Y.-H., 2017. Application of sulfonic acid group functionalized graphene oxide to improve hydrophilicity, permeability, and antifouling of PVDF nanocomposite ultrafiltration membranes. Journal of Membrane Science 525, 210-219.

Baskoro, F., Wong, C.-B., Kumar, S.R., Chang, C.-W., Chen, C.-H., Chen, D.W., Lue, S.J., 2018. Graphene oxide-cation interaction: Inter-layer spacing and zeta potential changes in response to various salt solutions. Journal of Membrane Science 554, 253-263.

Berger, J., Reist, M., Mayer, J.M., Felt, O., Peppas, N., Gurny, R., 2004. Structure and interactions in covalently and ionically crosslinked chitosan hydrogels for biomedical applications. European journal of pharmaceutics and biopharmaceutics 57, 19-34.

Bhatia, V., Dhir, A., Ray, A.K., 2021. Photocatalytic degradation of atenolol with graphene oxide/zinc oxide composite: optimization of process parameters using statistical method. Journal of Photochemistry and Photobiology A: Chemistry 409, 113136.

Bodzek, M., Konieczny, K., Kwiecińska-Mydlak, A., 2020. Nanotechnology in water and wastewater treatment. Graphene–the nanomaterial for next generation of semipermeable membranes. Critical Reviews in Environmental Science and Technology 50, 1515-1579.

Bolong, N., Ismail, A., Salim, M., Rana, D., Matsuura, T., Tabe-Mohammadi, A., 2010. Negatively charged polyethersulfone hollow fiber nanofiltration membrane for the removal of bisphenol A from wastewater. Separation and Purification Technology 73, 92-99.

Bourassi, M., Kárászová, M., Pasichnyk, M., Zazpe, R., Herciková, J., Fíla, V., Macak, J.M., Gaálová, J., 2021. Removal of Ibuprofen from Water by Different Types Membranes. Polymers 13, 4082.

Bunmahotama, W., Lin, T.F., Yang, X., 2020. Prediction of adsorption capacity for pharmaceuticals, personal care products and endocrine disrupting chemicals onto various adsorbent materials. Chemosphere 238, 124658.

Cai, Y., Chen, D., Li, N., Xu, Q., Li, H., He, J., Lu, J., 2020. A Self-Cleaning Heterostructured Membrane for Efficient Oil-in-Water Emulsion Separation with Stable Flux. Advanced Materials 32, 2001265.

Cao, X., Luo, J., Woodley, J.M., Wan, Y., 2016. Bioinspired multifunctional membrane for aquatic micropollutants removal. ACS applied materials & interfaces 8, 30511-30522.

Cao, X., Luo, J., Woodley, J.M., Wan, Y., 2018. Mussel-inspired co-deposition to enhance bisphenol A removal in a bifacial enzymatic membrane reactor. Chemical Engineering Journal 336, 315-324.

Cetinkaya, A.Y., Ozdemir, O.K., 2018. Phenol removal from synthetic solution using low pressure membranes coated with graphene oxide and carbon. Chemical Papers 72, 327-335.

Cha, M., Boo, C., Song, I.-H., Park, C., 2022. Investigating the potential of ammonium retention by graphene oxide ceramic nanofiltration membranes for the treatment of semiconductor wastewater. Chemosphere 286, 131745.

Chae, J., Lim, T., Cheng, H., Hu, J., Kim, S., Jung, W., 2021. Graphene Oxide and Carbon Nanotubes-Based Polyvinylidene Fluoride Membrane for Highly Increased Water Treatment. Nanomaterials 11, 2498.

Chang, X., Wang, Z., Quan, S., Xu, Y., Jiang, Z., Shao, L., 2014. Exploring the synergetic effects of graphene oxide (GO) and polyvinylpyrrodione (PVP) on poly(vinylylidenefluoride) (PVDF) ultrafiltration membrane performance. Applied Surface Science 316, 537-548.

Chen, L., Li, N., Wen, Z., Zhang, L., Chen, Q., Chen, L., Si, P., Feng, J., Li, Y., Lou, J., 2018a. Graphene oxide based membrane intercalated by nanoparticles for high performance nanofiltration application. Chemical Engineering Journal 347, 12-18.

Chen, W., Liu, P., Min, L., Zhou, Y., Liu, Y., Wang, Q., Duan, W., 2018b. Non-covalently functionalized graphene oxide-based coating to enhance thermal stability and flame retardancy of PVA film. Nano-micro letters 10, 1-13.

Chen, W., Ye, T., Xu, H., Chen, T., Geng, N., Gao, X., 2017. An ultrafiltration membrane with enhanced photocatalytic performance from grafted N–TiO 2/graphene oxide. RSC advances 7, 9880-9887.

Chen, Z.-H., Liu, Z., Hu, J.-Q., Cai, Q.-W., Li, X.-Y., Wang, W., Faraj, Y., Ju, X.-J., Xie, R., Chu, L.-Y., 2020. β-Cyclodextrin-modified graphene oxide membranes with large adsorption capacity and high flux for efficient removal of bisphenol A from water. Journal of Membrane Science 595, 117510.

Cheng, M.-m., Huang, L.-j., Wang, Y.-x., Zhao, Y.-c., Tang, J.-g., Wang, Y., Zhang, Y., Hedayati, M., Kipper, M.J., Wickramasinghe, S.R., 2019. Synthesis of graphene oxide/polyacrylamide composite membranes for organic dyes/water separation in water purification. Journal of Materials Science 54, 252-264.

Cho, K.M., Lee, H.-J., Nam, Y.T., Kim, Y.-J., Kim, C., Kang, K.M., Ruiz Torres, C.A., Kim, D.W., Jung, H.-T., 2019. Ultrafast-selective nanofiltration of an hybrid membrane comprising laminated reduced graphene oxide/graphene oxide nanoribbons. ACS applied materials & interfaces 11, 27004-27010.

Chu, K.H., Fathizadeh, M., Yu, M., Flora, J.R., Jang, A., Jang, M., Park, C.M., Yoo, S.S., Her, N., Yoon, Y., 2017. Evaluation of removal mechanisms in a graphene oxide-coated ceramic ultrafiltration membrane for retention of natural organic matter, pharmaceuticals, and inorganic salts. ACS applied materials & interfaces 9, 40369-40377.

Costa, J.B., Lima, M.J., Sampaio, M.J., Neves, M.C., Faria, J.L., Morales-Torres, S., Tavares, A.P., Silva, C.G., 2019. Enhanced biocatalytic sustainability of laccase by immobilization on functionalized carbon nanotubes/polysulfone membranes. Chemical Engineering Journal 355, 974-985.

Dadvar, E., Kalantary, R.R., Ahmad Panahi, H., Peyravi, M., 2017. Efficiency of polymeric membrane graphene oxide-TiO2 for removal of azo dye. Journal of Chemistry 2017.

Ding, A., Ren, Z., Zhang, Y., Ma, J., Bai, L., Wang, B., Cheng, X., 2021. Evaluations of holey graphene oxide modified ultrafiltration membrane and the performance for water purification. Chemosphere 285, 131459.

Ding, L., Wei, Y., Wang, Y., Chen, H., Caro, J., Wang, H., 2017. A two-dimensional lamellar membrane: MXene nanosheet stacks. Angewandte Chemie International Edition 56, 1825-1829.

Dong, Y., Shao, J., Chen, C., Li, H., Wang, R., Chi, Y., Lin, X., Chen, G., 2012. Blue luminescent graphene quantum dots and graphene oxide prepared by tuning the carbonization degree of citric acid. Carbon 50, 4738-4743.

Du, H., Yang, Z., Tian, Z., Huang, M., Yang, W., Zhang, L., Li, A., 2018. Enhanced removal of trace antibiotics from turbid water in the coexistence of natural organic matters using phenylalanine-modified-chitosan flocculants: effect of flocculants' molecular architectures. Chemical Engineering Journal 333, 310-319.

Dugyala, V.R., Muthukuru, J.S., Mani, E., Basavaraj, M.G., 2016. Role of electrostatic interactions in the adsorption kinetics of nanoparticles at fluid–fluid interfaces. Physical Chemistry Chemical Physics 18, 5499-5508.

Foller, T., Madauss, L., Ji, D., Ren, X., De Silva, K.K.H., Yoshimura, T.M.M., Lebius, H., Benyagoub, A., Kumar, P., Schleberger, M., 2022. Mass transport via in-plane nanopores in graphene oxide membranes. arXiv preprint arXiv:2201.11886.

Fortunato, L., 2017. Biofouling investigation in membrane filtration systems using Optical Coherence Tomography (OCT).

Fryczkowska, B., Machnicka, A., Biniaś, D., Ślusarczyk, C., Fabia, J., 2020. The influence of graphene addition on the properties of composite rGO/PAN membranes and their potential application for water disinfection. Membranes 10, 58.

Gao, S., Cen, W., Li, Q., Li, J., Lu, Y., Wang, H., Wu, Z., 2018. A mild one-step method for enhancing optical absorption of amine-functionalized metal-organic frameworks. Applied Catalysis B: Environmental 227, 190-197.

Gao, Y., Yan, N., Jiang, C., Xu, C., Yu, S., Liang, P., Zhang, X., Liang, S., Huang, X., 2020. Filtration-enhanced highly efficient photocatalytic degradation with a novel electrospun rGO@TiO2 nanofibrous membrane: Implication for improving photocatalytic efficiency. Applied Catalysis B: Environmental 268, 118737.

Ghasemi, S., Nematollahzadeh, A., 2018. Molecularly imprinted ultrafiltration polysulfone membrane with specific nano-cavities for selective separation and enrichment of paclitaxel from plant extract. Reactive and Functional Polymers 126, 9-19.

Guan, K., Shen, J., Liu, G., Zhao, J., Zhou, H., Jin, W., 2017. Spray-evaporation assembled graphene oxide membranes for selective hydrogen transport. Separation and Purification Technology 174, 126-135.

Gupta, I., Chakraborty, J., Roy, S., Farinas, E.T., Mitra, S., 2022. Synergistic Effects of Microwave Radiation and Nanocarbon Immobilized Membranes in the Generation of Bacteria-Free Water via Membrane Distillation. Industrial & Engineering Chemistry Research 61, 1453-1463.

Han, J.-L., Xia, X., Haider, M.R., Jiang, W.-L., Tao, Y., Liu, M.-J., Wang, H.-c., Ding, Y.-C., Hou, Y.-N., Cheng, H.-Y., 2018. Functional graphene oxide membrane preparation for organics/inorganic salts mixture separation aiming at advanced treatment of refractory wastewater. Science of the Total Environment 628, 261-270.

Heo, J., Flora, J.R., Her, N., Park, Y.-G., Cho, J., Son, A., Yoon, Y., 2012. Removal of bisphenol A and 17β-estradiol in single walled carbon nanotubes–ultrafiltration (SWNTs–UF) membrane systems. Separation and Purification Technology 90, 39-52.

Heu, R., Ateia, M., Yoshimura, C., 2020. Photocatalytic Nanofiltration Membrane Using Zr-MOF/GO Nanocomposite with High-Flux and Anti-Fouling Properties. Catalysts 10, 711.

Hu, J., Zeng, X., Wang, G., Qian, B., Liu, Y., Hu, X., He, B., Zhang, L., Zhang, X., 2020. Modulating mesoporous Co3O4 hollow nanospheres with oxygen vacancies for highly efficient peroxymonosulfate activation. Chemical Engineering Journal 400, 125869.

Hu, M., Zheng, S., Mi, B., 2016. Organic fouling of graphene oxide membranes and its implications for membrane fouling control in engineered osmosis. Environmental science & technology 50, 685-693.

Huang, Y., Xiao, C.-f., Huang, Q.-l., Liu, H.-l., Hao, J.-q., Song, L., 2018. Magnetic field induced orderly arrangement of Fe3O4/GO composite particles for preparation of Fe3O4/GO/PVDF membrane. Journal of Membrane Science 548, 184-193.

İlyasoglu, G., Kose-Mutlu, B., Mutlu-Salmanli, O., Koyuncu, I., 2022. Removal of organic micropollutans by adsorptive membrane. Chemosphere, 134775.

Ivanković, K., Kern, M., Rožman, M., 2021. Modelling of the adsorption of pharmaceutically active compounds on carbon-based nanomaterials. Journal of Hazardous Materials 414, 125554.

Ji, Q., Yu, D., Zhang, G., Lan, H., Liu, H., Qu, J., 2015. Microfluidic flow through polyaniline supported by lamellar-structured graphene for mass-transfer-enhanced electrocatalytic reduction of hexavalent chromium. Environmental science & technology 49, 13534-13541.

Ji, Q., Zhang, G., Liu, H., Liu, R., Qu, J., 2019. Field-enhanced nanoconvection accelerated electrocatalytic conversion of water contaminants and electricity generation. Environmental science & technology 53, 2713-2719.

Jia, F., Xiao, X., Nashalian, A., Shen, S., Yang, L., Han, Z., Qu, H., Wang, T., Ye, Z., Zhu, Z., Huang, L., Wang, Y., Tang, J., Chen, J., 2022. Advances in graphene oxide membranes for water treatment. Nano Research 15, 6636-6654.

Jiang, L.-h., Liu, Y.-g., Zeng, G.-m., Xiao, F.-y., Hu, X.-j., Hu, X., Wang, H., Li, T.-t., Zhou, L., Tan, X.-f., 2016a. Removal of 17β-estradiol by few-layered graphene oxide nanosheets from aqueous solutions: External influence and adsorption mechanism. Chemical engineering journal 284, 93-102.

Jiang, Y., Liu, D., Cho, M., Lee, S.S., Zhang, F., Biswas, P., Fortner, J.D., 2016b. In situ photocatalytic synthesis of Ag nanoparticles (nAg) by crumpled graphene oxide composite membranes for filtration and disinfection applications. Environmental Science & Technology 50, 2514-2521.

Jin, Z., Wang, X., Sun, Y., Ai, Y., Wang, X., 2015. Adsorption of 4-n-nonylphenol and bisphenol-A on magnetic reduced graphene oxides: a combined experimental and theoretical studies. Environmental science & technology 49, 9168-9175.

Kanaujiya, D.K., Paul, T., Sinharoy, A., Pakshirajan, K., 2019. Biological treatment processes for the removal of organic micropollutants from wastewater: a review. Current pollution reports 5, 112-128.

Kang, K.M., Kim, D.W., Ren, C.E., Cho, K.M., Kim, S.J., Choi, J.H., Nam, Y.T., Gogotsi, Y., Jung, H.-T., 2017. Selective molecular separation on Ti3C2T x–graphene oxide membranes during pressure-driven Filtration: Comparison with graphene oxide and MXenes. ACS applied materials & interfaces 9, 44687-44694.

Khanzada, N.K., Farid, M.U., Kharraz, J.A., Choi, J., Tang, C.Y., Nghiem, L.D., Jang, A., An, A.K., 2020. Removal of organic micropollutants using advanced membrane-based water and wastewater treatment: A review. Journal of membrane science 598, 117672.

Khorramshokouh, A., Ramezani, H., Sahami, M., SHARIF, M., 2022. Silver Nanoparticles Decorated Graphene Filled PVDF/PMMA Blends with Advanced electrical, mechanical, and thermal properties.

Kim, J.-H., Park, P.-K., Lee, C.-H., Kwon, H.-H., 2008. Surface modification of nanofiltration membranes to improve the removal of organic micro-pollutants (EDCs and PhACs) in drinking water treatment: Graft polymerization and cross-linking followed by functional group substitution. Journal of Membrane Science 321, 190-198.

Kong, F.-x., Yang, Z.-Y., Yue, L.-P., Chen, J.-f., Guo, C.-m., 2021. Nanofiltration membrane with substrate incorporated amine-functionalized graphene oxide for enhanced petrochemical wastewater and shale gas produced water desalination. Desalination 517, 115246.

Kong, S., Lim, M.-y., Shin, H., Baik, J.-H., Lee, J.-C., 2020. High-flux and antifouling polyethersulfone nanocomposite membranes incorporated with zwitterion-functionalized graphene oxide for ultrafiltration applications. Journal of Industrial and Engineering Chemistry 84, 131-140.

Kretinin, A.V., Cao, Y., Tu, J.S., Yu, G.L., Jalil, R., Novoselov, K.S., Haigh, S.J., Gholinia, A., Mishchenko, A., Lozada, M., Georgiou, T., Woods, C.R., Withers, F., Blake, P., Eda, G., Wirsig, A., Hucho, C., Watanabe, K., Taniguchi, T., Geim, A.K., Gorbachev, R.V., 2014. Electronic Properties of Graphene Encapsulated with Different Two-Dimensional Atomic Crystals. Nano Letters 14, 3270-3276.

Kwon, O., Choi, Y., Choi, E., Kim, M., Woo, Y.C., Kim, D.W., 2021. Fabrication techniques for graphene oxide-based molecular separation membranes: Towards industrial application. Nanomaterials 11, 757.

Lapworth, D., Baran, N., Stuart, M., Ward, R., 2012. Emerging organic contaminants in groundwater: a review of sources, fate and occurrence. Environmental pollution 163, 287-303.

Le, T.X.H., Dumée, L.F., Lacour, S., Rivallin, M., Yi, Z., Kong, L., Bechelany, M., Cretin, M., 2019. Hybrid graphene-decorated metal hollow fibre membrane reactors for efficient electro-Fenton-Filtration co-processes. Journal of membrane science 587, 117182.

Lebepe, T.C., Parani, S., Oluwafemi, O.S., 2020. Graphene Oxide-Coated Gold Nanorods: Synthesis and Applications. Nanomaterials 10, 2149.

Lee, J., Chae, H.-R., Won, Y.J., Lee, K., Lee, C.-H., Lee, H.H., Kim, I.-C., Lee, J.-m., 2013. Graphene oxide nanoplatelets composite membrane with hydrophilic and antifouling properties for wastewater treatment. Journal of Membrane Science 448, 223-230.

Lee, J., Kim, I.S., Hwang, M.-H., Chae, K.-J., 2020. Atomic layer deposition and electrospinning as membrane surface engineering methods for water treatment: A short review. Environmental Science: Water Research & Technology 6, 1765-1785.

Lee, T., Min, S.H., Gu, M., Jung, Y.K., Lee, W., Lee, J.U., Seong, D.G., Kim, B.-S., 2015. Layer-by-layer assembly for graphene-based multilayer nanocomposites: synthesis and applications. Chemistry of Materials 27, 3785-3796.

Lemos, H.G., Ragio, R.A., Conceição, A.C.S., Venancio, E.C., Mierzwa, J.C., Subtil, E.L., 2021. Assessment of mixed matrix membranes (MMMs) incorporated with graphene oxide (GO) for co-treatment of wastewater and landfill leachate (LFL) in a membrane bioreactor (MBR). Chemical Engineering Journal 425, 131772.

Li, C., Lu, Z., Ao, X., Sun, W., Huang, X., 2022a. Degradation kinetics and removal efficiencies of pharmaceuticals by photocatalytic ceramic membranes using ultraviolet light-emitting diodes. Chemical Engineering Journal 427, 130828.

Li, C., Yang, Q., Liu, D., Nie, H., Liu, Y., 2021a. Removal of organic phosphonate HEDP by Eu-MOF/GO composite membrane. Journal of Environmental Chemical Engineering 9, 106895.

Li, N., Chen, G., Zhao, J., Yan, B., Cheng, Z., Meng, L., Chen, V., 2019a. Self-cleaning PDA/ZIF-67@ PP membrane for dye wastewater remediation with peroxymonosulfate and visible light activation. Journal of Membrane Science 591, 117341.

Li, Q., Kong, H., Li, P., Shao, J., He, Y., 2019b. Photo-Fenton degradation of amoxicillin via magnetic TiO2-graphene oxide-Fe3O4 composite with a submerged magnetic separation membrane photocatalytic reactor (SMSMPR). Journal of hazardous materials 373, 437-446.

Li, S., Wan, Y., Guo, S., Luo, J., 2021b. Ferric ions mediated defects narrowing of graphene oxide nanofiltration membrane for robust removal of organic micropollutants. Chemical Engineering Journal 411, 128587.

Li, X., Le, Z., Chen, X., Li, Z., Wang, W., Liu, X., Wu, A., Xu, P., Zhang, D., 2018a. Graphene oxide enhanced amine-functionalized titanium metal organic framework for visible-light-driven photocatalytic oxidation of gaseous pollutants. Applied Catalysis B: Environmental 236, 501-508.

Li, X., Liu, L., Yang, F., 2018b. CFC/PVDF/GO-Fe3+ membrane electrode and flow-through system improved E-Fenton performance with a low dosage of aqueous iron. Separation and Purification Technology 193, 220-231.

Li, X., Sotto, A., Li, J., Van der Bruggen, B., 2017. Progress and perspectives for synthesis of sustainable antifouling composite membranes containing in situ generated nanoparticles. Journal of Membrane Science 524, 502-528.

Li, Y., He, Y., Zhuang, J., Shi, H., 2022b. Hierarchical microsphere encapsulated in graphene oxide composite for durable synergetic membrane separation and Fenton-like degradation. Chemical Engineering Journal 430, 133124.

Li, Y., Li, N., Xia, Y., Yuan, S., Zhang, X., 2022c. Tailoring the physicochemical and geometric properties of two-dimensional graphene membranes for aqueous separation. Desalination 530, 115621.

Liang, Z., Wang, J., Zhang, Q., Zhuang, T., Zhao, C., Fu, Y., Zhang, Y., Yang, F., 2021. Composite PVDF ultrafiltration membrane tailored by sandwich-like GO@UiO-66 nanoparticles for breaking the trade-off between permeability and selectivity. Separation and Purification Technology 276, 119308.

Licona, K., Geaquinto, L.d.O., Nicolini, J., Figueiredo, N., Chiapetta, S., Habert, A., Yokoyama, L., 2018. Assessing potential of nanofiltration and reverse osmosis for removal of toxic pharmaceuticals from water. Journal of Water Process Engineering 25, 195-204.

Liu, C., Liu, S., Liu, L., Tian, X., Liu, L., Xia, Y., Liang, X., Wang, Y., Song, Z., Zhang, Y., 2020a. Novel carbon based Fe-Co oxides derived from Prussian blue analogues activating

peroxymonosulfate: Refractory drugs degradation without metal leaching. Chemical Engineering Journal 379, 122274.

Liu, J., Tang, J., Gooding, J.J., 2012. Strategies for chemical modification of graphene and applications of chemically modified graphene. Journal of materials chemistry 22, 12435-12452.

Liu, N., Huang, W., Zhang, X., Tang, L., Wang, L., Wang, Y., Wu, M., 2018. Ultrathin graphene oxide encapsulated in uniform MIL-88A (Fe) for enhanced visible light-driven photodegradation of RhB. Applied Catalysis B: Environmental 221, 119-128.

Liu, T., Liu, X., Graham, N., Yu, W., Sun, K., 2020b. Two-dimensional MXene incorporated graphene oxide composite membrane with enhanced water purification performance. Journal of Membrane Science 593, 117431.

Liu, X., Yuan, H., Wang, C., Zhang, S., Zhang, L., Liu, X., Liu, F., Zhu, X., Rohani, S., Ching, C., Lu, J., 2020c. A novel PVDF/PFSA-g-GO ultrafiltration membrane with enhanced permeation and antifouling performances. Separation and Purification Technology 233, 116038.

Liu, Y., Bai, Z., Lin, G., Wang, L., Xu, X., He, L., Liu, X., 2022. Covalent cross-linking mediated TA-APTES NPs to construct a high-efficiency GO composite membrane for dye/salt separation. Applied Surface Science, 152595.

Liu, Y., Gao, G., Vecitis, C.D., 2020d. Prospects of an electroactive carbon nanotube membrane toward environmental applications. Accounts of Chemical Research 53, 2892-2902.

Liu, Y., Lee, J.H.D., Xia, Q., Ma, Y., Yu, Y., Yung, L.Y.L., Xie, J., Ong, C.N., Vecitis, C.D., Zhou, Z., 2014. A graphene-based electrochemical filter for water purification. Journal of Materials Chemistry A 2, 16554-16562.

Lou, Y., Tan, F.J., Zeng, R., Wang, M., Li, P., Xia, S., 2020. Preparation of cross-linked graphene oxide on polyethersulfone membrane for pharmaceuticals and personal care products removal. Polymers 12, 1921.

Lu, W., Mustafa, B., Wang, Z., Lian, F., Yu, G., 2022. PDMS-Encapsulated MXene@Polyester Fabric Strain Sensor for Multifunctional Sensing Applications. Nanomaterials 12, 871.

Lu, X., Feng, X., Werber, J.R., Chu, C., Zucker, I., Kim, J.-H., Osuji, C.O., Elimelech, M., 2017. Enhanced antibacterial activity through the controlled alignment of graphene oxide nanosheets. Proceedings of the national academy of sciences 114, E9793-E9801.

Luo, J., Cong, J., Fang, R., Fei, X., Liu, X., 2014a. One-pot synthesis of a graphene oxide coated with an imprinted sol–gel for use in electrochemical sensing of paracetamol. Microchimica Acta 181, 1257-1266.

Luo, J., Meyer, A.S., Mateiu, R.V., Kalyani, D., Pinelo, M., 2014b. Functionalization of a membrane sublayer using reverse filtration of enzymes and dopamine coating. ACS applied materials & interfaces 6, 22894-22904.

Luo, Z., Lim, S., Tian, Z., Shang, J., Lai, L., MacDonald, B., Fu, C., Shen, Z., Yu, T., Lin, J., 2011. Pyridinic N doped graphene: synthesis, electronic structure, and electrocatalytic property. Journal of Materials Chemistry 21, 8038-8044.

Ma, C., Hu, J., Sun, W., Ma, Z., Yang, W., Wang, L., Ran, Z., Zhao, B., Zhang, Z., Zhang, H., 2020. Graphene oxide-polyethylene glycol incorporated PVDF nanocomposite ultrafiltration membrane with enhanced hydrophilicity, permeability, and antifouling performance. Chemosphere 253, 126649.

Ma, F., Wu, Y., Guo, Q., Lin, R., Zhang, K., 2022. Double-imprinted mixed matrix membranes with polydopamine-induced nanocomposite for selective recognition and separation applications. Journal of Environmental Chemical Engineering 10, 107069.

Mahlangu, O., Nackaerts, R., Mamba, B., Verliefde, A., 2017. Development of hydrophilic GO-ZnO/PES membranes for treatment of pharmaceutical wastewater. Water Science and Technology 76, 501-514.

Makhetha, T., Moutloali, R., 2018. Antifouling properties of Cu (tpa)@ GO/PES composite membranes and selective dye rejection. Journal of Membrane Science 554, 195-210.

Mansourpanah, Y., Shahebrahimi, H., Kolvari, E., 2015. PEG-modified GO nanosheets, a desired additive to increase the rejection and antifouling characteristics of polyamide thin layer membranes. Chemical Engineering Research and Design 104, 530-540.

Mehmood, T., Gaurav, G.K., Cheng, L., Klemeš, J.J., Usman, M., Bokhari, A., Lu, J., 2021. A review on plant-microbial interactions, functions, mechanisms and emerging trends in bioretention system to improve multi-contaminated stormwater treatment. Journal of Environmental Management 294, 113108.

Mirzaei, M., Mohammadi, T., Kasiri, N., Tofighy, M.A., 2021. Fabrication of magnetic field induced mixed matrix membranes containing GO/Fe3O4 nanohybrids with enhanced antifouling properties for wastewater treatment applications. Journal of Environmental Chemical Engineering 9, 105675.

Mladenov, N., Dodder, N.G., Steinberg, L., Richardot, W., Johnson, J., Martincigh, B.S., Buckley, C., Lawrence, T., Hoh, E., 2022. Persistence and removal of trace organic compounds in centralized and decentralized wastewater treatment systems. Chemosphere 286, 131621.

Mondal, P., Purkait, M.K., 2018. Green synthesized iron nanoparticles supported on pH responsive polymeric membrane for nitrobenzene reduction and fluoride rejection study: optimization approach. Journal of Cleaner Production 170, 1111-1123.

Moreira, F.C., Boaventura, R.A., Brillas, E., Vilar, V.J., 2017. Electrochemical advanced oxidation processes: a review on their application to synthetic and real wastewaters. Applied Catalysis B: Environmental 202, 217-261.

Mubashir, M., Fong, Y.Y., Keong, L.K., Sharrif, M.A.B., 2015. Synthesis and performance of deca-dodecasil 3 rhombohedral (ddr)-type zeolite membrane in CO2 separation–a review. ASEAN Journal of Chemical Engineering 14, 48-57.

Mukherjee, D., Dewanjee, A., Ghosh, S., Majumdar, S., 2018. Development of graphene oxide/chitosan composite membrane on ceramic support for atrazine remediation by MBR process. Environmental Science and Pollution Research 25, 33334-33352.

Nair, R., Sepioni, M., Tsai, I.-L., Lehtinen, O., Keinonen, J., Krasheninnikov, A., Thomson, T., Geim, A., Grigorieva, I., 2012a. Spin-half paramagnetism in graphene induced by point defects. Nature Physics 8, 199-202.

Nair, R., Wu, H., Jayaram, P.N., Grigorieva, I.V., Geim, A., 2012b. Unimpeded permeation of water through helium-leak–tight graphene-based membranes. Science 335, 442-444.

Nanda, S.S., Yi, D.K., Kim, K., 2016. Study of antibacterial mechanism of graphene oxide using Raman spectroscopy. Scientific reports 6, 1-12.

Nebol'sin, V.A., Galstyan, V., Silina, Y.E., 2020. Graphene oxide and its chemical nature: Multi-stage interactions between the oxygen and graphene. Surfaces and Interfaces 21, 100763.

Nguyen, M.N., Weidler, P.G., Schwaiger, R., Schäfer, A.I., 2021. Interactions between carbon-based nanoparticles and steroid hormone micropollutants in water. Journal of Hazardous Materials 402, 122929.

Niedergall, K., Bach, M., Hirth, T., Tovar, G.E., Schiestel, T., 2014. Removal of micropollutants from water by nanocomposite membrane adsorbers. Separation and Purification Technology 131, 60-68.

Ojajuni, O., Saroj, D., Cavalli, G., 2015. Removal of organic micropollutants using membrane-assisted processes: a review of recent progress. Environmental Technology Reviews 4, 17-37.

Oller, I., Malato, S., Sánchez-Pérez, J., 2011. Combination of advanced oxidation processes and biological treatments for wastewater decontamination—a review. Science of the total environment 409, 4141-4166.

Oturan, M.A., Sirés, I., Oturan, N., Pérocheau, S., Laborde, J.-L., Trévin, S., 2008. Sonoelectro-Fenton process: a novel hybrid technique for the destruction of organic pollutants in water. Journal of Electroanalytical Chemistry 624, 329-332.

Palansooriya, K.N., Shaheen, S.M., Chen, S.S., Tsang, D.C., Hashimoto, Y., Hou, D., Bolan, N.S., Rinklebe, J., Ok, Y.S., 2020. Soil amendments for immobilization of potentially toxic elements in contaminated soils: A critical review. Environment international 134, 105046.

Pan, B., Feng, M., McDonald, T.J., Manoli, K., Wang, C., Huang, C.-H., Sharma, V.K., 2020. Enhanced ferrate (VI) oxidation of micropollutants in water by carbonaceous materials: Elucidating surface functionality. Chemical Engineering Journal 398, 125607.

Pedrosa, M., Drazic, G., Tavares, P.B., Figueiredo, J.L., Silva, A.M., 2019. Metal-free graphene-based catalytic membrane for degradation of organic contaminants by persulfate activation. Chemical Engineering Journal 369, 223-232.

Phatthanakittiphong, T., Seo, G.T., 2016. Characteristic evaluation of graphene oxide for bisphenol A adsorption in aqueous solution. Nanomaterials 6, 128.

Polak, D., Zielińska, I., Szwast, M., Kogut, I., Małolepszy, A., 2021. Modification of Ceramic Membranes with Carbon Compounds for Pharmaceutical Substances Removal from Water in a Filtration—Adsorption System. Membranes 11, 481.

Pollitt, K.J.G., Kim, J.-H., Peccia, J., Elimelech, M., Zhang, Y., Charkoftaki, G., Hodges, B., Zucker, I., Huang, H., Deziel, N.C., 2019. 1, 4-Dioxane as an emerging water contaminant: State of the science and evaluation of research needs. Science of the Total Environment 690, 853-866.

Pronk, W., Ding, A., Morgenroth, E., Derlon, N., Desmond, P., Burkhardt, M., Wu, B., Fane, A.G., 2019. Gravity-driven membrane filtration for water and wastewater treatment: a review. Water research 149, 553-565.

Qin, A., Li, X., Zhao, X., Liu, D., He, C., 2015. Preparation and characterization of nano-chitin whisker reinforced PVDF membrane with excellent antifouling property. Journal of Membrane Science 480, 1-10.

Qin, L., Zhang, Y., Xu, Z., Zhang, G., 2018. Advanced membrane bioreactors systems: New materials and hybrid process design. Bioresource Technology 269, 476-488.

Rahman, M., Yanful, E., Jasim, S., 2009. Endocrine disrupting compounds (EDCs) and pharmaceuticals and personal care products (PPCPs) in the aquatic environment: implications for the drinking water industry and global environmental health. Journal of water and health 7, 224-243.

Rashidian, E., Babaeipour, V., Chegeni, A., Khodamoradi, N., Omidi, M., 2021. Synthesis and characterization of bacterial cellulose/graphene oxide nano-biocomposites. Polymer Composites 42, 4698-4706.

Ren, D., Ren, S., Lin, Y., Xu, J., Wang, X., 2021. Recent developments of organic solvent resistant materials for membrane separations. Chemosphere 271, 129425.

Rollings, R.C., Kuan, A.T., Golovchenko, J.A., 2016. Ion selectivity of graphene nanopores. Nature communications 7, 1-7.

Sabir, A., Shafiq, M., Islam, A., Sarwar, A., Dilshad, M.R., Shafeeq, A., Butt, M.T.Z., Jamil, T., 2015. Fabrication of tethered carbon nanotubes in cellulose acetate/polyethylene glycol-400 composite membranes for reverse osmosis. Carbohydrate polymers 132, 589-597.

Sagle, A., Freeman, B., 2004. Fundamentals of membranes for water treatment. The future of desalination in Texas 2, 137.

Sánchez-Carretero, A., Saez, C., Canizares, P., Cotillas, S., Rodrigo, M.A., 2011. Improvements in the electrochemical production of ferrates with conductive diamond anodes using goethite as raw material and ultrasound. Industrial & Engineering Chemistry Research 50, 7073-7076.

Sanchez-Martin, M., Rodriguez-Cruz, M., Andrades, M., Sanchez-Camazano, M., 2006. Efficiency of different clay minerals modified with a cationic surfactant in the adsorption of pesticides: influence of clay type and pesticide hydrophobicity. Applied Clay Science 31, 216-228.

Schrotter, J.C., Bozkaya-Schrotter, B., 2010. Current and emerging membrane processes for water treatment. Membrane Technology: Volume 4: Membranes for Water Treatment 4, 53-91.

Shen, H., Wang, N., Ma, K., Wang, L., Chen, G., Ji, S., 2017. Tuning inter-layer spacing of graphene oxide laminates with solvent green to enhance its nanofiltration performance. Journal of Membrane Science 527, 43-50.

Silvestro, I., Ciarlantini, C., Francolini, I., Tomai, P., Gentili, A., Dal Bosco, C., Piozzi, A., 2021. Chitosan–Graphene Oxide Composite Membranes for Solid-Phase Extraction of Pesticides. International Journal of Molecular Sciences 22, 8374.

Singhal, A.V., George, R., Sharma, A.K., Malwal, D., Lahiri, I., 2020. Development of superhydrophillic tannic acid-crosslinked graphene oxide membranes for efficient treatment of oil contaminated water with enhanced stability. Heliyon 6, e05127.

Somanathan, T., Prasad, K., Ostrikov, K.K., Saravanan, A., Krishna, V.M., 2015. Graphene oxide synthesis from agro waste. Nanomaterials 5, 826-834.

Song, H.-M., Zhu, L.-J., Wang, Y., Wang, G., Zeng, Z.-X., 2022. Fe-based Prussian blue cubes confined in graphene oxide nanosheets for the catalytic degradation of dyes in wastewater. Separation and Purification Technology 288, 120676.

Soroush, A., Ma, W., Cyr, M., Rahaman, M.S., Asadishad, B., Tufenkji, N., 2016. In situ silver decoration on graphene oxide-treated thin film composite forward osmosis membranes: biocidal properties and regeneration potential. Environmental Science & Technology Letters 3, 13-18.

Sun, M., Li, J., 2018. Graphene oxide membranes: Functional structures, preparation and environmental applications. Nano Today 20, 121-137.

Sun, M., Wang, X., Winter, L.R., Zhao, Y., Ma, W., Hedtke, T., Kim, J.-H., Elimelech, M., 2021. Electrified Membranes for Water Treatment Applications. ACS ES&T Engineering 1, 725-752.

Surana, K., Singh, P.K., Bhattacharya, B., Verma, C., Mehra, R., 2015. Synthesis of graphene oxide coated Nafion membrane for actuator application. Ceramics International 41, 5093-5099.

Tang, L., Iddya, A., Zhu, X., Dudchenko, A.V., Duan, W., Turchi, C., Vanneste, J., Cath, T.Y., Jassby, D., 2017. Enhanced flux and electrochemical cleaning of silicate scaling on carbon nanotube-coated membrane distillation membranes treating geothermal brines. ACS applied materials & interfaces 9, 38594-38605.

Thakre, K.G., Barai, D.P., Bhanvase, B.A., 2021. A review of graphene-TiO2 and graphene-ZnO nanocomposite photocatalysts for wastewater treatment. Water Environment Research 93, 2414-2460.

Thambirajoo, M., Maarof, M., Lokanathan, Y., Katas, H., Ghazalli, N.F., Tabata, Y., Fauzi, M.B., 2021. Potential of Nanoparticles Integrated with Antibacterial Properties in Preventing Biofilm and Antibiotic Resistance. Antibiotics 10, 1338.

Thierfelder, C., Witte, M., Blankenburg, S., Rauls, E., Schmidt, W., 2011. Methane adsorption on graphene from first principles including dispersion interaction. Surface Science 605, 746-749.

Tian, Y., Wu, M., Liu, R., Li, Y., Wang, D., Tan, J., Wu, R., Huang, Y., 2011. Electrospun membrane of cellulose acetate for heavy metal ion adsorption in water treatment. Carbohydrate Polymers 83, 743-748.

Trasande, L., Zoeller, R.T., Hass, U., Kortenkamp, A., Grandjean, P., Myers, J.P., DiGangi, J., Bellanger, M., Hauser, R., Legler, J., 2015. Estimating burden and disease costs of exposure to endocrine-disrupting chemicals in the European Union. The Journal of Clinical Endocrinology & Metabolism 100, 1245-1255.

Tsou, C.-H., An, Q.-F., Lo, S.-C., De Guzman, M., Hung, W.-S., Hu, C.-C., Lee, K.-R., Lai, J.-Y., 2015. Effect of microstructure of graphene oxide fabricated through different self-assembly techniques on 1-butanol dehydration. Journal of Membrane Science 477, 93-100.

Vanherck, K., Koeckelberghs, G., Vankelecom, I.F., 2013. Crosslinking polyimides for membrane applications: A review. Progress in polymer science 38, 874-896.

Wang, C., Cheng, P., Yao, Y., Yamauchi, Y., Yan, X., Li, J., Na, J., 2020. In-situ fabrication of nanoarchitectured MOF filter for water purification. Journal of Hazardous Materials 392, 122164.

Wang, H., Wang, W., Wang, L., Zhao, B., Zhang, Z., Xia, X., Yang, H., Xue, Y., Chang, N., 2018. Enhancement of hydrophilicity and the resistance for irreversible fouling of polysulfone (PSF) membrane immobilized with graphene oxide (GO) through chloromethylated and quaternized reaction. Chemical Engineering Journal 334, 2068-2078.

Wang, J., Chen, Z., Chen, B., 2014. Adsorption of polycyclic aromatic hydrocarbons by graphene and graphene oxide nanosheets. Environmental science & technology 48, 4817-4825.

Wang, J., Li, N., Zhao, Y., Xia, S., 2017. Graphene oxide modified semi-aromatic polyamide thin film composite membranes for PPCPs removal. Desalination and Water Treatment 66, 166-175.

Wang, Q., Peng, Y., Ji, X., Hadi, M.K., Zhang, S., Tang, J., Ran, F., 2021a. Conductive 3D networks in a 2D layer for high performance ultrafiltration membrane with high flux-retention and robust cyclic stability. Journal of Membrane Science 640, 119781.

Wang, Q., Yu, Z., Liu, Y., Zhu, X., Long, R., Li, X., 2021b. Electrostatic self-assembly method to prepare intercalated graphene oxide composite membrane to improve hydrophilicity and flux. Diamond and Related Materials, 108492.

Wang, S., Tian, J., Wang, Q., Xiao, F., Gao, S., Shi, W., Cui, F., 2019. Development of CuO coated ceramic hollow fiber membrane for peroxymonosulfate activation: a highly efficient singlet oxygen-dominated oxidation process for bisphenol a degradation. Applied Catalysis B: Environmental 256, 117783.

Wang, X., Meng, G., Zhu, C., Huang, Z., Qian, Y., Sun, K., Zhu, X., 2013. A Generic Synthetic Approach to Large-Scale Pristine-Graphene/Metal-Nanoparticles Hybrids. Advanced Functional Materials 23, 5771-5777.

Wei, X., Huang, J., Cao, S., Chen, Y., Yang, R., Wang, Z., Zhou, Q., Chen, J., Pan, B., 2021. Preparation of graphene oxide/polyamide composite nanofiltration membranes for enhancing stability and separation efficiency. Journal of Applied Polymer Science 138, 50902.

Wu, H., Tang, B., Wu, P., 2014. Development of novel SiO2–GO nanohybrid/polysulfone membrane with enhanced performance. Journal of Membrane Science 451, 94-102.

Wu, L., Liu, Y., Hu, J., Feng, X., Ma, C., Wen, C., 2021a. Preparation of polyvinylidene fluoride composite ultrafiltration membrane for micro-polluted surface water treatment. Chemosphere 284, 131294.

Wu, Q., Xu, Y., Yang, K., Cui, H., Chen, Y., Wang, M., Zhu, Q., Kang, W., Gao, C., 2017. Fabrication of membrane absorbers based on amphiphilic carbonaceous derivatives for selective endotoxin clearance. Journal of Materials Chemistry B 5, 8219-8227.

Wu, S.-H., Bing-zhi, D., Yu, H., 2010. Adsorption of bisphenol A by polysulphone membrane. Desalination 253, 22-29.

Wu, W., Zhang, X., Qin, L., Li, X., Meng, Q., Shen, C., Zhang, G., 2020. Enhanced MPBR with polyvinylpyrrolidone-graphene oxide/PVDF hollow fiber membrane for efficient ammonia nitrogen wastewater treatment and high-density Chlorella cultivation. Chemical Engineering Journal 379, 122368.

Wu, X., Rigby, K., Huang, D., Hedtke, T., Wang, X., Chung, M.W., Weon, S., Stavitski, E., Kim, J.-H., 2022a. Single-Atom Cobalt Incorporated in a 2D Graphene Oxide Membrane for Catalytic Pollutant Degradation. Environmental Science & Technology 56, 1341-1351.

Wu, Y., Lin, R., Ma, F., Yan, J., Sun, Y., Jia, S., Gao, J., 2022b. Dual-imprinted mixed matrix membranes for selective recognition and separation: A synergetic imprinting strategy based on complex initiation system. Journal of Colloid and Interface Science 606, 87-100.

Wu, Y., Zhang, K., Lin, R., Ma, F., Gao, J., 2021b. Dual-imprinted organic/inorganic nanocomposite membranes with highly selective polydopamine-intimated nanostructures for pharmaceutically active compound separation. Journal of Colloid and Interface Science 604, 691-704.

Xie, A., Cui, J., Yang, J., Chen, Y., Lang, J., Li, C., Yan, Y., Dai, J., 2020a. Graphene oxide/Fe (III)-based metal-organic framework membrane for enhanced water purification based on synergistic separation and photo-Fenton processes. Applied Catalysis B: Environmental 264, 118548.

Xie, A., Cui, J., Yang, J., Chen, Y., Lang, J., Li, C., Yan, Y., Dai, J., 2020b. Photo-Fenton self-cleaning PVDF/NH2-MIL-88B (Fe) membranes towards highly-efficient oil/water emulsion separation. Journal of Membrane Science 595, 117499.

Xu, G., Li, M., Wang, Y., Zheng, N., Yang, L., Yu, H., Yu, Y., 2019. A novel Ag-BiOBr-rGO photocatalyst for enhanced ketoprofen degradation: Kinetics and mechanisms. Science of the Total Environment 678, 173-180.

Xu, L., Wang, J., 2012. Magnetic nanoscaled Fe3O4/CeO2 composite as an efficient Fenton-like heterogeneous catalyst for degradation of 4-chlorophenol. Environmental science & technology 46, 10145-10153.

Xu, R., Cui, J., Tang, R., Li, F., Zhang, B., 2017. Removal of 2, 4, 6-trichlorophenol by laccase immobilized on nano-copper incorporated electrospun fibrous membrane-high efficiency, stability and reusability. Chemical Engineering Journal 326, 647-655.

Xu, Z., Wu, T., Shi, J., Wang, W., Teng, K., Qian, X., Shan, M., Deng, H., Tian, X., Li, C., 2016. Manipulating migration behavior of magnetic graphene oxide via magnetic field induced casting and phase separation toward high-performance hybrid ultrafiltration membranes. ACS applied materials & interfaces 8, 18418-18429.

Xu, Z., Ye, X., Hu, P., Yin, M., Lv, B., Zhang, G., Meng, Q., Gao, C., 2022. Azido-group functionalized graphene oxide/polysulfone mixed matrix ultrafiltration membrane with enhanced interfacial compatibility for efficient water and wastewater treatment. Separation and Purification Technology 283, 120162.

Yang, G.C., Chen, Y.-C., Yang, H.-X., Yen, C.-H., 2016. Performance and mechanisms for the removal of phthalates and pharmaceuticals from aqueous solution by graphene-containing ceramic composite tubular membrane coupled with the simultaneous electrocoagulation and electrofiltration process. Chemosphere 155, 274-282.

Yang, G.C., Yen, C.-H., 2013. The use of different materials to form the intermediate layers of tubular carbon nanofibers/carbon/alumina composite membranes for removing pharmaceuticals from aqueous solutions. Journal of membrane science 425, 121-130.

Yang, H., Wang, N., Wang, L., Liu, H.-X., An, Q.-F., Ji, S., 2018. Vacuum-assisted assembly of ZIF-8@GO composite membranes on ceramic tube with enhanced organic solvent nanofiltration performance. Journal of Membrane Science 545, 158-166.

Yang, J., Chen, D., Zhu, Y., Zhang, Y., Zhu, Y., 2017a. 3D-3D porous Bi2WO6/graphene hydrogel composite with excellent synergistic effect of adsorption-enrichment and photocatalytic degradation. Applied Catalysis B: Environmental 205, 228-237.

Yang, S., Zou, Q., Wang, T., Zhang, L., 2019a. Effects of GO and MOF@ GO on the permeation and antifouling properties of cellulose acetate ultrafiltration membrane. Journal of membrane science 569, 48-59.

Yang, Z., Xu, X., Liang, X., Lei, C., Cui, Y., Wu, W., Yang, Y., Zhang, Z., Lei, Z., 2017b. Construction of heterostructured MIL-125/Ag/g-C3N4 nanocomposite as an efficient bifunctional visible light photocatalyst for the organic oxidation and reduction reactions. Applied catalysis B: environmental 205, 42-54.

Yang, Z., Zhou, Y., Feng, Z., Rui, X., Zhang, T., Zhang, Z., 2019b. A review on reverse osmosis and nanofiltration membranes for water purification. Polymers 11, 1252.

Yaya, A., Impellizzeri, A., Massuyeau, F., Duvail, J., Briddon, P., Ewels, C., 2019. Mapping the stacking interaction of triphenyl vinylene oligomers with graphene and carbon nanotubes. Carbon 141, 274-282.

Ye, J., Dai, J., Wang, L., Li, C., Yan, Y., Yang, G., 2021a. Investigation of catalytic self-cleaning process of multiple active species decorated macroporous PVDF membranes through peroxymonosulfate activation. Journal of Colloid and Interface Science 586, 178-189.

Ye, J., Dai, J., Yang, D., Li, C., Yan, Y., 2021b. 1D/2D nanoconfinement FexOy and nitrogen-doped carbon matrix for catalytic self-cleaning membranes removal for pollutants. Journal of Environmental Chemical Engineering 9, 106076.

Ye, J., Wang, Y., Li, Z., Yang, D., Li, C., Yan, Y., Dai, J., 2021c. 2D confinement freestanding graphene oxide composite membranes with enriched oxygen vacancies for enhanced organic contaminants removal via peroxymonosulfate activation. Journal of Hazardous Materials 417, 126028.

Yin, X., Teng, A., Zeng, Z., Meng, H., Wu, W., 2022. Facile and Scalable Preparation of 2d-Mos2/Graphene Oxide Composite for Supercapacitor. Available at SSRN 4049535.

Yu, G.L., Gorbachev, R.V., Tu, J.S., Kretinin, A.V., Cao, Y., Jalil, R., Withers, F., Ponomarenko, L.A., Piot, B.A., Potemski, M., Elias, D.C., Chen, X., Watanabe, K., Taniguchi, T., Grigorieva, I.V., Novoselov, K.S., Fal'ko, V.I., Geim, A.K., Mishchenko, A., 2014. Hierarchy of Hofstadter

states and replica quantum Hall ferromagnetism in graphene superlattices. Nature Physics 10, 525-529.

Yu, L., Zhang, Y., Zhang, B., Liu, J., Zhang, H., Song, C., 2013. Preparation and characterization of HPEI-GO/PES ultrafiltration membrane with antifouling and antibacterial properties. Journal of Membrane Science 447, 452-462.

Yu, S., Gao, Y., Khan, R., Liang, P., Zhang, X., Huang, X., 2020. Electrospun PAN-based graphene/SnO2 carbon nanofibers as anodic electrocatalysis microfiltration membrane for sulfamethoxazole degradation. Journal of Membrane Science 614, 118368.

Yuan, B., Wang, M., Wang, B., Yang, F., Quan, X., Tang, C.Y., Dong, Y., 2020a. Cross-linked Graphene Oxide Framework Membranes with Robust Nano-Channels for Enhanced Sieving Ability. Environmental Science & Technology 54, 15442-15453.

Yuan, X.-T., Xu, C.-X., Geng, H.-Z., Ji, Q., Wang, L., He, B., Jiang, Y., Kong, J., Li, J., 2020b. Multifunctional PVDF/CNT/GO mixed matrix membranes for ultrafiltration and fouling detection. Journal of hazardous materials 384, 120978.

Zambianchi, M., Durso, M., Liscio, A., Treossi, E., Bettini, C., Capobianco, M.L., Aluigi, A., Kovtun, A., Ruani, G., Corticelli, F., 2017. Graphene oxide doped polysulfone membrane adsorbers for the removal of organic contaminants from water. Chemical Engineering Journal 326, 130-140.

Zeng, H., Deng, L., Zhang, H., Zhou, C., Shi, Z., 2020. Development of oxygen vacancies enriched CoAl hydroxide@ hydroxysulfide hollow flowers for peroxymonosulfate activation: A highly efficient singlet oxygen-dominated oxidation process for sulfamethoxazole degradation. Journal of hazardous materials 400, 123297.

Zhang, G., Zhou, M., Xu, Z., Jiang, C., Shen, C., Meng, Q., 2019a. Guanidyl-functionalized graphene/polysulfone mixed matrix ultrafiltration membrane with superior permselective, antifouling and antibacterial properties for water treatment. Journal of colloid and interface science 540, 295-305.

Zhang, H.-C., Gao, S.-X., Sheng, G.-P., 2021. Immobiling enzyme-like ligand in the ultrafiltration membrane to remove the micropollutant for the ultrafast water purification. Journal of Membrane Science 636, 119566.

Zhang, H., Luo, J., Li, S., Woodley, J.M., Wan, Y., 2019b. Can graphene oxide improve the performance of biocatalytic membrane? Chemical Engineering Journal 359, 982-993.

Zhang, W., Cheng, W., Ziemann, E., Be'er, A., Lu, X., Elimelech, M., Bernstein, R., 2018. Functionalization of ultrafiltration membrane with polyampholyte hydrogel and graphene oxide to achieve dual antifouling and antibacterial properties. Journal of Membrane Science 565, 293-302.

Zhang, W., Zhang, Y., Wang, Y., Tian, S., Han, N., Li, W., Wang, W., Liu, H., Yan, X., Zhang, X., 2022a. Fluffy-like amphiphilic graphene oxide (f-GO) and its effects on improving the antifouling of PAN-based composite membranes. Desalination 527, 115575.

Zhang, Y., Yang, H., Cai, Q., Xia, S., 2022b. Graphene oxide modified polypropylene fiber filter membrane for enhanced treatment efficiency of water-based paint wastewater. DESALINATION AND WATER TREATMENT 247, 100-107.

Zhang, Y., Zhang, S., Chung, T.-S., 2015. Nanometric graphene oxide framework membranes with enhanced heavy metal removal via nanofiltration. Environmental science & technology 49, 10235-10242.

Zhao, C., Xu, X., Chen, J., Yang, F., 2013. Effect of graphene oxide concentration on the morphologies and antifouling properties of PVDF ultrafiltration membranes. Journal of Environmental Chemical Engineering 1, 349-354.

Zhao, J., Yang, Y., Jiang, J., Takizawa, S., 2021. Influences of cross-linking agents with different MW on the structure of GO/CNTs layers, membrane performances and fouling mechanisms for dissolved organic matter. Journal of Membrane Science 617, 118616.

Zhao, Y., Lu, D., Cao, Y., Luo, S., Zhao, Q., Yang, M., Xu, C., Ma, J., 2018. Interaction analysis between gravity-driven ceramic membrane and smaller organic matter: implications for retention and

fouling mechanism in ultralow pressure-driven filtration system. Environmental science & technology 52, 13718-13727.

Zheng, X., Jiang, N., Zheng, H., Wu, Y., Heijman, S.G., 2022. Predicting adsorption isotherms of organic micropollutants by high-silica zeolite mixtures. Separation and Purification Technology 282, 120009.

Zhong, Y., Li, T., Lin, H., Zhang, L., Xiong, Z., Fang, Q., Zhang, G., Liu, F., 2018. Meso-/macro-porous microspheres confining Au nanoparticles based on PDLA/PLLA stereo-complex membrane for continuous flowing catalysis and separation. Chemical Engineering Journal 344, 299-310.

Zhu, C., Liu, G., Han, K., Ye, H., Wei, S., Zhou, Y., 2017a. One-step facile synthesis of graphene oxide/TiO2 composite as efficient photocatalytic membrane for water treatment: Crossflow filtration operation and membrane fouling analysis. Chemical Engineering and Processing-Process Intensification 120, 20-26.

Zhu, S., Huang, X., Ma, F., Wang, L., Duan, X., Wang, S., 2018. Catalytic removal of aqueous contaminants on N-doped graphitic biochars: inherent roles of adsorption and nonradical mechanisms. Environmental science & technology 52, 8649-8658.

Zhu, X., Jassby, D., 2019. Electroactive membranes for water treatment: Enhanced treatment functionalities, energy considerations, and future challenges. Accounts of chemical research 52, 1177-1186.

Zhu, Z., Chen, Z., Luo, X., Liang, W., Li, S., He, J., Zhang, W., Hao, T., Yang, Z., 2020a. Biomimetic dynamic membrane (BDM): Fabrication method and roles of carriers and laccase. Chemosphere 240, 124882.

Zhu, Z., Chen, Z., Luo, X., Zhang, W., Meng, S., 2020b. Gravity-driven biomimetic membrane (GDBM): An ecological water treatment technology for water purification in the open natural water system. Chemical Engineering Journal 399, 125650.

Zhu, Z., Jiang, J., Wang, X., Huo, X., Xu, Y., Li, Q., Wang, L., 2017b. Improving the hydrophilic and antifouling properties of polyvinylidene fluoride membrane by incorporation of novel nanohybrid GO@SiO2 particles. Chemical Engineering Journal 314, 266-276.

Zielińska, M., Galik, M., 2017. Use of Ceramic Membranes in a Membrane Filtration Supported by Coagulation for the Treatment of Dairy Wastewater. Water Air Soil Pollut 228, 173-173.

Zinadini, S., Zinatizadeh, A.A., Rahimi, M., Vatanpour, V., Zangeneh, H., 2014. Preparation of a novel antifouling mixed matrix PES membrane by embedding graphene oxide nanoplates. Journal of Membrane Science 453, 292-301.

Figures Captions

Fig. 1 Schematics illustration for different synthesis of graphene oxide (GO) (a-c) Hummers method, pyrolysis of carboxyl compounds method and, pyrolysis of carbon-based waste (Adapted from Ref.(Lebepe et al., 2020) with permission under creative commons CC-BY license, 2020), and (d) GO with functional groups after exfoliate from graphite and acid catalysis.

Fig. 2 Diagram illustrating the various synthesis procedures utilized to manufacture GO membranes. (a) Strategy of vacuum filtration (Baskoro et al., 2018) (b) Pressure-, vacuum-, and evaporation-assisted self-assembly method Adapted from Ref. (Kwon et al., 2021) with permission under creative commons CC-BY license, 2021, (c) spin-coating approach (Nair et al., 2012), (d) LBL assembly method (Zhang et al., 2015) (e) Spray-evaporation assembly methods (Guan et al., 2017) (f) Immersion coating method (Rollings et al., 2016). Reproduced with Elsevier and Royal Society of Chemistry's permission.

Fig. 3 SEM micrographs of surfaces of: tubular ceramic substrate (a), GO membrane (b), SG@GO membrane (c), cross-section of: tubular ceramic substrate (d), GO membrane (e), SG@GO membrane (f), graphical depiction of WCA and SZP of SG@GO laminate with unlike SG levels (Synthesis settings: GO: 0.2 g L^{-1}; immersing time: 0.5 h) (g); Graphic illustration of manufacture of SG@GO membrane on tubular ceramic substrate (h), and, EOMPs retaining of GO membrane and SG@GO composite membrane (i). Reprinted with permission from ref (Shen et al., 2017). Elsevier holds the copyright for 2017.

Fig. 4 SEM micrographs of surface and cross-section morphologies of: Ceramic tube (a), PEI membrane (b), GO/PEI membrane (c), ZIF-8/PEI membrane (d), ZIF-8@GO/PEI composite membrane (ZIF-8@GO:0.005 wt.%) (e), AFM images of GO/PEI membrane, ZIF-8/PEI membrane and ZIF-8@GO/PEI membrane (f), and graphical presentation of vacuum-assisted assembly method based synthesis of crosslinked ZIF-8@GO/PEI composite membrane on tubular ceramic substrate and EOMPs molecules retention (g). Reproduced with permission from ref. (Yang et al., 2018) Copyright 2018, Elsevier.

Fig. 5 Graphical illustration of the two-phase method applied to prepare the GO-functionalized zwitterionic polyampholyte hydrogel PES membrane. WP (b), PEG rejection of the pristine PES, p-PES, and GO-p-PES membranes (values expressed: means ± SD, n = 3) Impact of 3 h surface connection of PES, p-PES, and GO-p-PES membranes to *E. coli* (~ 4 × 104 CFU/1.54 cm^2),the values are stated as means ± SD, n = 8) (c), Biovolume of the live cells, EPS, and dead cells for the three membranes the values are stated as means ± SD, n = 12 arbitrary sites in two repetition experiments (d), time-sensitive reutilizing fluxes of the pristine PES, p-PES, and GO-p-PES membranes in the BSA ultrafiltration test (BSA: 1 g L^{-1} in 10 mM Phosphate-buffered saline solution, initial flux:50 L m^{-2} h^{-1}, transmembrane pressure :0.2–0.7 bar) (e) Reproduced with permission from ref. (Zhang et al., 2018) Copyright 2018, Elsevier.

Fig. 6 (a) Practical GO membrane formulation for EOMPs/salts co-contaminated refractory wastewater treatment, (b) Removal of typical EOMPs. Reproduced with permission from ref. (Han et al., 2018) Copyright 2018, Elsevier, (c) Graphical depiction of PVP-GO nanocomposites and PVP-GO/PVDF hollow fiber membrane synthesis, (d) methodology of MPBR system and (e) flux and EPS study of proteins and polysaccharides using pristine PVDF and PVP-GO/PVDF membrane in the MPBR arrangements. Reproduced with permission from ref. (Wu et al., 2020) Copyright 2020, Elsevier.

Fig. 7 a Time sensitive infiltration of GS-DIMs and NIMs for TC (a), the expected permselectivity action for template molecule by GS-DIMs (values expressed: means ± SD, n = 3) (b), Schematic illustration for the preparation method of GS-DIMs. Real-time filtration fluid curves for GS-DIMs and the corresponding level of different target molecules through the GS-DIMs (values expressed: means ± SD, n = 3). Adopted with permission from ref. (Wu et al., 2021b) Copyright 2021, Elsevier, **b** Time sensitive infiltration of GT-DIMs and NIMs for TC (a), the expected permselectivity action for template molecule by GT-DIMs (values expressed: means ± SD, n = 3) (b), Schematic illustration for the preparation method of GT-DIMs. Real-time filtration fluid curves for GT-DIMs and the corresponding level of TC, OTC, CTX and SMZ through the GT-DIMs (values expressed: means ± SD, n = 3) reproduced with permission (Wu et al., 2022b) Copyright 2022, Elsevier.

Fig. 8 a) Graphical depiction of GO/Co-Al LDH composite membranes synthesis (a), performance of different membranes based on rejection efficiency and flux for 10 ppm MB solution (b), performance of GO/Co-Al-2 based on rejection efficiency and flux for MB solution at different level (10–100 ppm) (c), performance of different membranes based on flux for different EOMPs at 10 ppm level (d), performance of different composite membranes based on rejection efficiency for different EOMPs at 10 ppm (e) reproduced with permission (Wang et al., 2021b) Copyright 2021, Elsevier, and comparison of CS_GLU and CS_GOX_GLU composite membranes for recovery potential of the pesticides (in ascending order of log Kow) (f) reproduced with permission (Silvestro et al., 2021) Copyright 2021.

Fig. 9 Salient features of membrane separation technology. (a) Selective separation of MF, UF, RO, and NF membranes reproduced with permission (Ren et al., 2021), Copyright 2021 Elsevier, (b) Mechanisms involve in

membrane filtration process (b) Reprinted with permission from Khanzada et al. (Khanzada et al., 2020). Copyright 2020 Elsevier.

Fig.10 **a** Graphene design arrangement (a) (E2 molecules denoted estradiol adsorption sites), Routes of steroid hormone absorption by GO dependent on closeness to the hormone (GO is represented symbolically as a GO portion as an marker) (b) reproduced with permission (Nguyen et al., 2021) Copyright 2021 Elsevier; **b** Illustration of the targeted surface change of the GO NF membrane induced by Fe_3^+ (a); Representation of a potential reaction between the mix of APTES and TA and associated contacts with the Fe_3^+- facilitated GO membrane (b), BPA rejection (c) and WP of GO, GO-Zn and GO-Fe membranes coated and noncoated by TA-APTES layer (d) reprinted with permission (Li et al., 2021b) Copyright 2021 Elsevier.; **c** SEM micrographs BDMs: (a) CNT + Lac@UF(a-f): (b) Lac&CNT@UF, (c) CNT&Lac@UF, (d) GO&Lac@UF, (e) Lac&GO@UF and (f) GO&Lac@UF, BDM assembly methods (g), Elimination rate, flux, and laccase activities for diverse BDMs manufactured by various techniques. (h) Elimination rate, flux, and laccase activities at different filtration cycles for CNT/GO&Lac@UF. The experimental conditions were CNT/GO:25 g m^{-2}, laccase dosage:50 g m^{-2}, pollutant concentration:25 g L^{-1}, pressure: 0.1 Mpa, 100 rpm) (i) reprinted with permission (Zhu et al., 2020a) Copyright 2020 Elsevier.

Fig.11 graphical illustration of TAML/GO-PEI/PES working performance in filtration and removal of BPA (a), WF and BPA content in permeate solution in filtration cycles trial of TAML/GO-PEI/PES membrane (b); TAML/GO-PEI/PES membrane adsorption capacity in filtration cycles trial (c); PES, GO-PEI/PES and TAML/GO-PEI/PES membranes performance in EOMPs removal (1 mg L^{-1}) (d), and TAML/GO-PEI/PES membrane filtration attributed degradation pathway of BPA (e) Reproduced with permission from ref. (Zhang et al., 2021) Copyright 2021, Elsevier.

Fig.12 **a** The manufacture method of ZIF@MILs-20/GO catalytic membrane (a), Conceptual depiction of the PMS activation process on the ZIF@MILs-20/GO membrane (b), NX degradation mechanisms in the PMS system, GO membrane, and ZIF@MILs-20 (c), comparative analyses with other catalysts (d), The effects of catalysts (e), WCA (f), catalysts performance at varying system pH (g), catalysts performance at varying reaction temperature (h), the matching activation energy (d), conditions: [catalyst] = 0.01 g L^{-1}, [NX] = 20 mg L^{-1}, [PMS] = 0.3 g L^{-1}, [T] = 25 ˚C, the catalytic membrane's capacity for cleanup following adsorption (i) reprinted with permission from (Ye et al., 2021a) Copyright 2021 Elsevier, **b** Schematic drawing of the assembly of GO/M88A membrane (a). Schematic presentation of photo-Fenton self-cleaning system in GO/M88A membrane-H_2O_2-visible light arrangement (b), the effort of separating BPA from GO/M88A membrane without and using photo-Fenton method (c), curves of BPA degradation by photo-Fenton catalytic (d), digitized images of the color shift of real textile effluent during photo-Fenton/removal operations (e), the elimination of pollutants from true textile effluents using GO/M88A membranes (f) reprinted with permission (Xie et al., 2020) Copyright 2020 Elsevier.,

Fig. 13 (a)Graphical depiction of the SMSMPR, (b) Mineralization mechanism of AMX in water by SMSMPR, (c) Elimination proficiency of AMX in contrasting reaction schemes, (d) diverse light sources' impacts, (e) H_2O_2 dosages and (f) different solution pH on AMX degradation in the TiO_2-GO-18 wt.% Fe_3O_4 & H_2O_2 arrangement by the SMSMPR. Reaction settings: [H_2O_2] = 20 mM (for c, d, f), pH 3 (for c, d, e), [catalysts] = 0.5 g L^{-1} (for c–f), [AMX] = 20 mg L^{-1} (for c–f), and visible light irradiation (for c, e, f) adopted from ref. (Li et al., 2019) with permission, Copyright 2019 Elsevier.

Fig. 14 (a) Diagram illustrating the four functional modes of the photocatalytic filtering reactor, adopted from ref. (Gao et al., 2020) with permission, Copyright 2020 Elsevier (b) Diagram illustrating the suggested methods for eliminating target pollutants via a ceramic composite tubular membrane containing Go combined with the EC/EF process, adopted from ref. (Yang et al., 2016) with permission, Copyright 2016 Elsevier.

Fig. 15 (a) Synthesis of electrified membrane (EM), electrified circuits, and installation Illustration of EM preparation, electrified membrane modules, and cross-flow filtration function, as well as the influence of water convection and diffusion on operating modes, (b) EM filtration for water purification and filtration; (c) various forms of membrane fouling; and (d) improving microbial elimination in anodic EM filtration with improved membrane electrode design. Reprinted with permission from Ref. (Sun et al., 2021). Copyright 2021 American Chemical Society.

Fig. 16 **a** Left: the matching images of electrochemical reactor; middle: complete arrangement of electrochemical membrane device comprises the membrane stacks; right: photos of the unfolded membrane sandwich stacks with three layers from vertically (anode: PAN-based G/SnO_2/CFs membrane maintained by RuO_2 plated titanic (Ti/RuO_2) net, filter: an insulating silicone rubber O-ring separated the electrodes, cathode: RuO_2 plated titanic (Ti/RuO_2) net) (a), Projected conversion pathways for SMX electrocatalytic degradation (b) adopted from ref. (Yu et al., 2020) with permission, Copyright 2020 Elsevier. And **b** FeCo@GCTs/GO membrane reusability in SMX and Cr(VI) solution (a); and the breakdown productivities of metal ions (b) adopted from ref. (Ye et al., 2021b) with permission, Copyright 2021 Elsevier.

Table 1 GO mediated membranes in filtration and adsorption

Compound name	Target pollutant	GO level;	Pollutants removal efficiency and mechanism	Flux/hydrophilicity/ permeability	Major findings and recommendations	Reference
Polyvinylidene fluoride graphene oxide silver carbonate (PGA membranes)	BSA	0.4 wt.%	79%; UF	PWF: PGA-3 (254 LMH) > 2-fold than pristine PVDF membrane (126 LMH); FDR: 83.1	The PG membrane coated three times with Ag_2CO_3 (i.e., PGA-3) showed higher FRR, FDR and antibacterial performance than other membranes and provide best quality of lake water in multi-cycle filtration experiments.	(Wu et al., 2021a)
ZIF-8@GO/PEI	Organic solvents	GO: 0.1-0.4 g L^{-1}	99.1%; NF	3.5 L m^{-2} h^{-1} bar^{-1}	Owing to its exceptional compaction, tubular membrane modules are useful in industry.	(Yang et al., 2018)
PVP-GO/PVDF membrane	extracellular polymeric substance (EPS) COD, NH_4^- N^+ and NO_3^-N	0.5 wt.%	> 97.8, 93.1 and 68.7% removal COD, NO_3-N, NH_4^- and N^+	MP: 1.7 times > PM; WCA: decreased from 97 to 62°), FRR: 96%	PVP-GO function as wipers to remove EPS foulants from membrane surface. PVP-GO/PVDF shown excellent antifouling properties for high-density microbe establishment and ammonia-nitrogen wastewater remediation.	(Wu et al., 2020)
GO additive solvent green (SG)	dye molecules Eriochrome black T	0.2 g L^{-1}	98% similar to PM; NF	330 L m^{-2} h^{-1} bar^{-1} nearly 6- fold more than PM GO (56 L m^{-2} h^{-1} MPa^{-1})	This approach may provide a straightforward technique for optimizing the interlayer spacing of GO laminates for efficient molecular sorting.	(Shen et al., 2017)
GO/Co-Al LDH	RhB, MB, CR, petroleum ether, n-hexane	Al LDH: GO= 4:1	Rejection>90%; VF	718.8 L m^{-2} h^{-1} bar^{-1}	Co-Al LDH may be altered in GO membranes to improve extraction efficiency and wettability.	(Wang et al., 2021b)
HGO	three typical organics in NOM (BSA, SA and HA)	2 mg mL^{-1} GO 0.08 g m^{-2}	NOM 55%; BSA 29%; SA:58–85%; and HA: 72–92%; UF	WP of HGO >26 time than rGO and >2 times to GO; FFR: 96.04%; WCA: reduced from 71° to 35°	Increased HGO dosage may delay the transition from pore blockage to cake layer. Ultimately, HGO coating provides a possible use for the treatment of foulants.	(Ding et al., 2021)
GO/aminated GO (NGO)	petrochemical	GO: 0.05 wt.%	6% more rejection than PM; NF	PWF of PM was > 24.8% increased by 15.6% and 26.9% i.e., 44.93 and 49.30 L m^{-2} h^{-1} with GO and NGO, respectively	The interaction between the amino group of NGOs and TMC lowered the thickness size of TFCNGO. Thin film composite NGO offers a substantially finer layer over TFCGO owing to its larger pore dimensions and increased wettability.	(Kong et al., 2021)
Ceramic-based graphene oxide framework (GOF) membranes	Chloramphenicol (CAP)	0.2 mg mL^{-1}	53.3%; NF	increase in permeability	Cross-linking GOF CM with MPD (m-phenylenediamine) lead in the synchronous rejection of salts and CAP, so overcoming the normal trade-off dilemma.	(Yuan et al., 2020a)

					Involved in the Donnan effect, the molecule/ion screening mechanism were size sieving (steric hindrance), electrostatic interaction, and fractional dehydration.	
GO membrane	Organic matter (COD)	GO:14.4 mg m^{-2}	76%; RO/NF	Flux decrease 7.8 to 3.1 L m^{-2} h^{-1} bar^{-1} at 250 layers of GO	Rejection and flux were optimum up to 100 GO layers, achieve balance for the support membrane, optimum up to 100 Go layers. Negatively charged OM better removed with GO than the electrically neutral polyethylene glycol (PEG).	(Han et al., 2018)
Tannic acid-crosslinked graphene oxide membranes	COD, TDS, TSS and turbidity	0.5 mg mL^{-1}	COD:91.67%; VF		The phenolic hydroxyl segments of tannic acid are plentiful throughout the GO nanosheets, rendering the membrane super oleophobic and ultra-hydrophilic. Low oil adhesion, maximum oil rejection, and high-pressure water filtration.	(Singhal et al., 2020)
Ceramic membrane functionalized with GO (ceramic GO)	NOM (humic acid and tannic acid), pharmaceuticals (ibuprofen and sulfamethoxazole)	1 g	GO improved rejection: 74.6 to 93.5% (NOM); 15.3 to 51.0% (pharmaceuticals); 2.9 to 31.4% (inorganic salts)	MP: 14.4–58.6 vs. 25.1–62.7 L m^{-2} h^{-1} bar^{-1}	Hydrophobic attraction and charge effects by GO removed EOMPs. GO mediated ceramic membrane is effective in removal of multiple pollutant with contrasting nature from water.	(Chu et al., 2017)
GO-TA-APTES-x tannic acid (TA)-aminopropyltriethoxysilane (APTES) nanoparticles	Congo red	0.25 mg mL^{-1}	99.9%; NF	TA-APTES increase 10 times MP; PWF was up to 111. L m^{-2} h^{-1} bar^{-1}, (15 times more to GO)	The crosslinking agent TA-APTES NPs encourage and facilitate resilience in aqueous conditions and is conducive to the transfer of GO nanofiltration membrane from controlled system to industrial use.	(Liu et al., 2022)
fluffy-like poly (acrylonitrile-methyl acrylate) amphiphilic graphene oxide (f-GO/P(AN-MA))	BSA	0.5 wt.%	Increased 70.59% (PM) to 99.33% (MM); UF	PWF 200 to 326 L m^{-2} h^{-1}, while the WCA declined from 92.8° to 68.3°.	FRR: 98.16%. poly (acrylonitrile-methyl acrylate) entangled hudrophobic segment on f-GO f-GO/P(AN-MA) showed long-term resistance to organic matter fouling	(Zhang et al., 2022a)
GO-PEG/PVDF graphene oxide-polyethylene glycol (UF)	BSA	0.5 wt.%	94%; UF	Flux: 93.0 L m^{-2} h^{-1} twice than PM	FRR: 78.0%; MM exhibits superior membrane wettability, porosity, and antifouling ability in commercial systems.	(Ma et al., 2020)
Perfluorosulfonic acid (PFSA) grafted on graphene oxide	BSA	PFSA: GO mass	BSA:93.9%; HA:79.6%; UF	587.4 L m^{-2} h^{-1} 1.5 time higher than PM	FRR: 90.8% Membrane alteration increased hydrophilic nature, limited surface roughness, and	(Liu et al., 2020)

(GO) PFSA-g-GO/PVDF		ratio of 2.5:1			augmented porosity and pore diameter. The mass ratio of PFSA to GO in membrane nanocomposites is the key determinant of pore properties and porosity.	
GO@UiO66/PVDF	BSA	1.0 w.t%	93%; UF	263.3 L m^{-2} h^{-1} WCA: reduced from 78.49 (PVDF) to 63.61 and 58.31 with GO /PVDF and GO@UiO66/PVDF	FRR 81.3% Brilliant structural properties and chemical resistance; Extra hydrophilic active groups of the GO@UiO-66 visibility and PVDF phase transformation from contributed to the formation of a compact hydration sheet on the membrane surface and lowered Zeta potential, thereby enhancing organic invasion and reducing membrane fouling.	(Liang et al., 2021)
PES-HPEI-GO hyperbranched polyethylenimine	BSA	5.0 wt.%	92.0%; UF	153.5 L m^{-2} h^{-1}	FRR 88.7%; WCA 63. Antibiotic efficacy against *Escherichia coli* (*E. coli*) is excellent. The tensile strength and Young's modulus of hybrid membranes were greater.	(Yu et al., 2013)
PVDF/GO	BSA	1.0 wt.%	92.6%; UF	398.7 L m^{-2} h^{-1}	FRR 79.3%; WCA 62.5	(Xu et al., 2016)
PSF-GO	BSA	1.3 wt.%	Rejection was similar to PM-UF	430.0 L m^{-2} h^{-1}	FRR 82.5%; GO nanoplatelets can change the pore dimensions of porous media produced by inversion by up to 20%. Hydrophilicity and electrostatic repulsion boosted anti biofouling, while GO treatment showed higher mechanical strength and water permeability.	(Lee et al., 2013)
PSF-SiO_2/GO	BSA	0.3 wt.%	98.0; UF	185.0 L m^{-2} h^{-1}	FRR 84.4%; WCA 72.0. A spongy and uniform film of silica nanoparticles applied to the surface of the GO as a GO space blanket results in high wettability and dispersibility, as well as an extended in water permeation rate, protein elimination, and antifouling ability.	(Wu et al., 2014)
PVDF/GO	BSA	0.5 wt.%	~ 97%; UF	~ 80 L m^{-2} h^{-1}	FRR ~ 75%; WCA ~ 76. The formation of hydrogen linkages between GO and PVP allows for improved efficiency.	(Chang et al., 2014)
PVDF/GO/PVP	BSA	0.5 wt.%	85; UF	104.3 L m^{-2} h^{-1}	FRR 90.5%; WCA ~ 67. The synergistic impacts of integrated GO and PVP improved surface hydrophilicity and antifouling performance.	(Chang et al., 2014)

PVDF/GO/PVP	BSA	0.3 wt.%	~ 75; UF	~ 800 L m^{-2} h^{-1}	FRR ~ 70%; WCA 65.93 The adhesion forces for BSA was 0.78 mN m^{-1}	(Zhu et al., 2017b)
PVDF/SGO sulfonated graphene oxide (SGO)	BSA	0.12 wt.%	98%; UF	740 L m^{-2} h^{-1} Improvement in PWF 146.6% in P-SGO was for better than 53.3% P-GO blend membranes	FRR 88.7%; WCA 50. SGO has strong hydrogen interaction and electrostatic repulsion towards proteins foulants, together with increased hydrophilicity, water flux, and mechanical performance, pave the way for PVDF ultrafiltration membranes.	(Ayyaru and Ahn, 2017)
graphene oxide immobilized membrane	-	-	-	Improved water vapor flux (30–40%).	Biocidal impacts revealed that fewer energy (20-25 percent) was consumed by thermophilic and mesophilic cells i.e., 90.1% and 59.4%. Both the thermal and nonthermal impacts of microwave irradiation enhanced biocidal efficacy and flux. The ideal temperatures for eliminating thermophilic and mesophilic cells, accordingly, are 80 and 60 ˚C.	(Gupta et al., 2022)
GO-multi-walled carbon nanotubes (MWCNTs)	mineral and ionic species	0.1 wt.%	108.37% improved; VF	GO and MWCNTs decreased 32% contact angles	GO/MWCNT increases PVDF membrane surface characteristics and water purification functionalities.	(Chae et al., 2021)
GO modified polypropylene fiber filter membrane	COD and SS	-	COD: 84.8%; SS: 84.6%	-	Water-based paint wastewater flocculation + GO-PP fiber filter membrane could be a suitable material.	(Zhang et al., 2022b)
Europium-metal organic framework (Eu-MOF)/GO CM	organic phosphine	0.079 mg/cm2	100% rejection; GO based rejection:85.46%; VF	PWF: 1.27 to 16.76 L m^{-2} $h^{-1;}$ PF increased from 0.76 to 5.01 L m^{-2} h^{-1}	The permeability-selectivity computation of molecularly imprinted membrane materials could be addressed if the template molecule has a greater standard of tolerance and penetration.	(Li et al., 2021a)
Diphenyl phosphoryl azido (DPPA) / PSf (DPPA-GO/PSf)	BSA	0.5 wt.%	95.8%; UF	254.1 L h^{-1} m^{-2}	FRR 80.3%. Persistence anti-*E. coli* and S. aureus action. Strong interactions between oxygen-containing AGO nanosheets and polymer matrix eliminate interfacial flaws, resulting in good dispersity and interfacial compliance for PSF membranes.	(Xu et al., 2022)
PES-GO	HA, BSA	0.6 wt.%	>98%, MBR	GO incorporation reduce contact angle reduced from 59.6 to 46.9 and permeability from 288 to 161 L m^{-2} h^{-1} bar^{-1}	PES-GO membranes are effective in removing organic pollutants, but are susceptible to damage from prolonged contact with sodium hypochlorite solution and chlorine.	(Lemos et al., 2021)

GO/PA-NF Polyamide (PA)	Congo red and cationic red X-GTL	0.05 wt.%	Congo red: 100%; cationic red X-GTL: 99.8%; NF	PF:44.2 L m^{-2} h^{-1}, PWF: 15.5 L m^{-2} h^{-1} bar^{-1}	Piperazine (PIP) and trimesoyl chloride (TMC) significantly enhanced the PA NF membrane's wettability and antifouling abilities.	(Wei et al., 2021)
CGO-M/PES cysteine-functionalized GO (CGO)	BSA	0.5 wt.%	99.8%; UF	82.6 L m^{-2} h^{-1} at 0.2 MPa	FRR 92.1% (CGO/PES) > 47.5% (PM) WCA 50.5° at 2.0 wt.% CGO Antifouling polymer-based UF membranes treat protein-rich wastewater.	(Kong et al., 2020)
CA/MOF@GO Cellulose acetate Metal–organic frameworks	BSA	0.03, 0.06, 0.09 and 0.12 g	91.4; UF	183 L m^{-2} h^{-1} at 0.15 MPa	FFR 88.13%; WCA 49.5° HKUST-1 was used as MOF effectively overcome the drawbacks of GO and the properties of GO can be fully utilized.	(Yang et al., 2019)
PVDF/ OMWCNT/GO mixed matrix membranes oxidized multi-walled carbon nanotubes	BSA	0.5 g L^{-1}	85%; UF	125.6 L m^{-2} h^{-1} at 0.1 MPa	WCA and FFR of MM were 67.6° and 60.57% while PM 79.6° and 51.96% Better surface pores, roughness, hydrophilicity, and antifouling. Pollutant layer thickness was proportional to membrane resistance/conductivity, allowing for prompt cleaning and prolonging membrane life.	(Yuan et al., 2020b)
M-GO/CNT-0.5-polyaniline (PANI)	CR	0.00274 g	99.9%; UF	496.4 and 230.4 L m^{-2} h^{-1} at 0.1 and 0 MPa	WCA of M-PES is 74.7° reduce to 46.6° with M-GO/CNT-0.5-PANI which increased permeability, selective separation, antifouling, mechanical strength, and extended life.	(Wang et al., 2021a)
Cu(tpa)@GO/ PES	CR	GO: 0.5 g (Cu(tpa)) 0.9@GO: 0.9:1	90.0%; UF	PWF: 140.0 L m^{-2} h^{-1} at 0.2 MPa	Cu(tpa) was used as MFO. WCA and FFR of (Cu(tpa))0.9@GO were 16° and 70% while PM (PES) was 84°and 43%. The nature of inserted MOFs boosted anionic dyes' selective rejection ratio (CR and MO). Better for wastewater EOMPS.	(Makhetha and Moutloali, 2018)
Guanidyl-functionalized graphene/polysulfone mixed matrix	Antibacterial and antimicrobial0	0.5 wt.%	93.7%; UF	More than 200 L m^{-2} h^{-1}	FRR of PM PSF 73.4% increased to 82.4% with 1 wt.% of GFG. GFG/PSF CM had a porosity of 72.5-72.9%, an average pore width of 30.93-30.97 nm, and a WCA of 86.9-83.3°. Remarkable antimicrobial efficacy and endurance against Escherichia coli and Staphylococcus aureus.	(Zhang et al., 2019a)
Polyamide (PA) + GO	Norfloxacin	0.1 wt.%	53.32%; NF	12.78 L m^{-2} h^{-1} bar^{-1}	GO reduced WCA of PA reduced from 60.82 to 49.3. GO enhanced membrane anti-fouling and norfloxacin and sulfamethoxazole rejection. GO inclusion makes active layer thinner,	(Wang et al., 2017)

					smoother, and denser and increases hydrophilicity and negative surface charge.	
PES/GO	BSA	0.1,0.5 and 1.0 wt.%	96.0; NF	5.1 L m^{-2} h^{-1} bar^{-1}	FRR 90.5%; WCA: 53.2. Irreversible resistance reduced from 66.1% (PM) to 9.5% (MM) PES membranes with magnetic nanoparticles and a magnetic field improve FRR, antifouling, and PWF efficiency.	(Zinadini et al., 2014)
GO/Fe_3O_4/PES mixed matrix membrane	BSA	Fe_3O_4	98.0; UF	175.6 L m^{-2} h^{-1}	FRR 87.9%; Fe_3O_4 Used as hydrophilic additives This membrane reinforcement for elevated NF and RO membranes works successfully.	(Mirzaei et al., 2021)
PVDF/GO-Fe_3O_4	BSA	Fe_3O_4 + magnetic field	92.0; UF	595.0 L m^{-2} h^{-1}	FRR 86.4%; WCA 55.9 Magnetic field driven casting transported Fe_3O_4/GO nanocomposites from the membrane matrix to the surface, creating high-performance hybrid membranes.	(Xu et al., 2016)
M-GO/Fe_3O_4/PES mixed matrix membrane	BSA	Fe_3O_4 + magnetic field	92.0; cross-flow filtration	252.0 L h^{-1} m^{-2}	FRR 80.1%	(Mirzaei et al., 2021)
PVDF/MGO magnetic Fe_3O_4/graphene oxide	BSA	Fe_3O_4 + magnetic field	77.7; UF	484.0 L h^{-1} m^{-2}	FRR 83.0%; WCA 62.0; Outstanding magnetic susceptibility and hydrophobicity	(Huang et al., 2018)
Graphene oxide (GO)-based composite ultrafiltration (UF) membranes	atrazine	0.1 wt.%	95% atrazine elimination, total reduction of TSS, turbidity, and microbes; MBR and UF	At a backwash pressure of 4 kg cm^2 for 1 hour of MBR examination, PF drop was reduced by approximately 5% following back pulsing of different duration and resting period.	FRR:98.6%. Membrane fouling lowers flow, and MLSS induces complete and intermediate blockage mechanisms. Compared to direct membrane filtration or biodegradation, this membrane improves the quality of the permeate.	(Mukherjee et al., 2018)

PWF: pure water flux; WP:water permeability; FRR: flux recovery ratio, FDR: flux decay rate; Rt: reaction time; T: Temperature; SRT: standard room temperature; MP; membrane permeability; PM: pristine membrane; MM: modified membrane; CM: composite membrane, WCA: water contact angle, PF: Permeation flux; RS: rebinding selectivity; SF: suction filtration; CFF: cross-flow filtration; MAC: membrane adsorption capacity

Table 2GO mediated membranes in degradation membranes

Compound name	Target pollutant	Supporting components and removal mechanism	Pollutants removal efficiency	Flux/hydrophilicity/ permeability	Major findings and recommendations	Reference
GO-loaded PDA-TC-SiO_2/AC@PVDF	TC, CEX, SMZ and OTC	Adsorption/filtration/ degradation	106.44 mg g^{-1}	3600 L h^{-1} m^{-2}	DI-MMMs retained 93.5% of initial rebinding capacity after 10 cycles. Improved DI-MMM identification and permeability could help molecularly imprinted membranes overcome the permeability-selectivity compromise.	(Ma et al., 2022)
graphene oxide (GO)/SiO_2-loaded dual-imprinted membranes (GS-DIMs)	antibiotics TC; cefalexin (i.e., sulfamethazine, and oxytetracycline)	0.15 g GO nanosheet	RS: > 3.5; Rejection: (CEX, 98%; SMZ, 99%, and OTC, 97%); SF, adsorption	TC: 4.27, CEX: 3.88 SMZ: 4.11 OTC: remain unchanged in 5 cycles	The CM GO/SiO_2-loaded nano CM worked well in industrial-scale applications and effluent samples. 65.61 mg/g was the total efficiency of elimination (after 20 min)	(Wu et al., 2021b)
GO/CNTs-modified membrane graphene oxide (GO)/carbon nanotubes (CNTs)	DOC	GO/CNTs: 1:4	69%; CFF/ adsorption	DOC water flux of PM and MM was 1280 and 667 kg m^{-2} h^{-1}	MM exhibits good antifouling and rejection rates stability. The wide exterior diameter of CNTs degraded their antifouling efficacy and removal efficiency, whereas small MW cross-linking agents produced total blockage. In the case of HA + Ca^{2+}, the linking effect of Ca^{2+} led to intermediate fouling for all membranes. The WF inhibition increased with increasing CNT mass percent in pure GO, 2:1, 1:2, and 1:4 mixtures.	(Zhao et al., 2021)
PVDF/GO@SiO_2/ PVP	BSA	adsorption	78.5%; adsorption	1232 L h^{-1} m^{-2}	FRR: 77.5%; WCA 63.02; Nanohybrid particle (GO@SiO2) has the best antifouling properties and boosts PVDF membrane performance.	(Zhu et al., 2017b)
chitosan–graphene oxide (CS_GO) CMs	20 types of Pesticides	1% to 20%, *w/w*	95% removal of rifampicin; adsorption	-	The affinity for the most hydrophilic contaminants was decreased by GO, and the R% was enhanced. CS demonstrated Low pollutant extraction with logKow values between 0.8 and 2, and integration of GO at a low level (1%)	(Silvestro et al., 2021)
Ultem + 2.5 wt.% GO	Ibuprofen (IBU)non-steroidal anti-inflammatory drugs	0.5 wt.%	53%; adsorption	-	Through non-covalent π−π contacts between the GO interface and the benzyl ring of IBU, the GO sheet can facilitate faster electron/ion transport.	(Bourassi et al., 2021)

GO-Fe-TA-APTES	endocrine disruptor, BPA, 6-methoxytetralin, naphthalene and pyrene	Fe^{3+}; tannic acid-aminopropyltriethoxysilane (TA-APTES).	PM:26% MM:81%; adsorption	-	GO-Fe-coated membranes can be used in pharmaceuticals, coking, and municipal wastewater treatment. GO-Fe-TA-APTES had no membrane permeability loss after 50 mL filtration, while GO-Fe had 36%. After filtration of 50 mL BPA solution MTHN (70%)	(Li et al., 2021b)
GO-GDBM gravity-driven biomimetic membrane (GO-GDBM)	BPA	CNT/GO dosages (20–65 g m^{-2}) Supported by: biodegradable CA	55~70%; adsorption; Static filtration;	72.1 L h^{-1} m^{-2} at 12 cm of hydrostatic height; After 30 days: 27~42 L h^{-1} m^{-2}	As a GDM, GDBM, specifically CNT-GDBM and GOGDBM, with extraction rate more than 60% and fluxes bigger than 35 Lm^2h can appear as a feasible water purification method in open natural water systems.	(Zhu et al., 2020b)
graphene, graphene oxide, carbon nanotubes and C60	steroid hormones	Supported by: biodegradable CA	GP-AO_2: 6.6 mg/g; adsorption;	-	CNT and GO demonstrated high Biodegradable CA UF membrane screening abilities (over 10 mg g^{-1}) for hormones which remained undetectable in isotherm tests.	(Nguyen et al., 2021)
GO-p-PES membrane (UF)	polyethylene glycol (PEG)	GO:10 mg mL^{-1}; Supported by: biodegradable CA	70% adoption reduce with GO; >90% rejection; adsorption;	Flux decline in PES (65%) was reduce to 25% with GO. FRR in PES (46% while with GO ~ 80%)	In the long run, GO-functionalized polyampholyte hydrogel appears promising for treatment of wastewater. GO loading promoted antibacterial and antibiofouling properties.	(Zhang et al., 2018)
carbon-coated nanofiltration membrane (NF90)	Phenol	Supported by: biodegradable CA	99%; MF, UF, NF; adsorption	36 L h^{-1} m^{-2} 10 bar^{-1}	The NF90 membrane can remove phenol under low pressure 6 bars. GO-coated membranes have a low removal rate due to their high polarity (hydrophilicity).	(Cetinkaya and Ozdemir, 2018)
co-deposition of DA/GO and DA/GO-Zn	bisphenol A (BPA)	Laccase; bio-catalysis; NF	No effect on rejection.	permeate flux coNF-PDA/GO, 7.46 L m^{-2} h^{-1}; coNF-PDA/GO-	GO's enrichment and catalytic characteristics increased laccase activity and stability. The modified membrane showed promising results for removing and detecting EOMPS.	(Zhang et al., 2019b)

				Zn: 29.85 L m^{-2} h^{-1}		
GO&Lac@UF GO additive Biomimetic dynamic membrane (BDM)	MB	Supported by: biodegradable CA	80%; adsorption; UF	≥120 L h^{-1}·m^{-2}	WCA: decreased from 86.43 (PM) to 77.78 (GO&Lac). Laccase activity was higher on GO than CNT. Appropriate production method, GO, and laccase dosage can maximize biomimetic layer and enzyme immobilization, increasing its sustainability.	(Zhu et al., 2020a)
poly(ether sulfone) PES + GO (UF)	Ibuprofen	Supported by: biodegradable CA	44.9%; UF, biodegradable adsorption;	flux 5.27 L h^{-1} m^{-2} bar^{-1}	GO membrane layers gaps affects steric hindrance and elimination rate. GO removed PPCPs in their molecular state using biodegradable CA ultrafiltration and molecular sieving rather than conventional nanofiltration membranes, which rely on electrostatic repulsion.	(Lou et al., 2020)
β-cyclodextrin (β-CD) modified graphene oxide (CDGO) membrane	bisphenol A (BPA)	β-CD molecules; Supported by: biodegradable CA	100%; adsorption, catalytic degradation	water fluxes increase with operating pressure, flux was one or two order of higher than RO and NF	CDGO membrane has stable structures β-CD molecules enhanced surface areas and winding 2D nanochannels and BPA removal. CDGO biodegradable CA ultrafiltration membrane separation capabilities are many times higher than PM, allowing for a larger range of applications in molecular separation and easy regeneration after multiple cycles using ethanol washing.	(Chen et al., 2020)
graphene-containing ceramic composite tubular membrane (TGCCM)	emerging contaminants (ECs) in water, (DnBP, DEHP, CLX, SMX, CAF)	GO nanosheet: 2 g L^{-1}; Electrocoagulation adsorption, Biodegradable CA	DnBP and DEHP removed by 99%; CLX, SMX and CAF by 32-97%; adsorption	140 L h^{-1} m^{-2}	Size exclusion, electrostatic repulsion, Biodegradable CA ultrafiltration membrane separation, electrocoagulation, and electrofiltration are the removal mechanisms	(Yang et al., 2016)

Table 3GO mediated membranes in catalytic and degradation membranes

Compound name	Target pollutant	supporting components/ Experimental condition	Pollutants removal efficiency	Flux/ hydrophilicity/ permeability	Major findings and recommendations	Reference

graphene oxide (GO)	micropollutants DCF (2,6-dichlorophenyl)	K2FeO4	$FeVIO_4^{2-}$:20%; GO-$FeVIO_4^{2-}$: 100%; oxidation	-	The better removal of EOMPs is dictated by their structure (or moieties), which may require a reaction with high-valent iron species (FeIV/FeV) to produce the accelerated action brought about by carbonaceous substances.	(Pan et al., 2020)
G.O and rGO	CBZ	$K2FeO4^{-}$	Removal by $FeVIO_4^{2-}$:30%; GO: <10%; GO-$FeVIO_4^{2-}$: 100%; oxidation	-	GO with $FeVIO_4^{2-}$ showed 60% and 50% more removal of ZBZ compared to rGO and with rGO with $FeVIO_4^{2-}$	(Pan et al., 2020)
graphene oxidepolyethylene imine (GO-PEI)	(Fe(III)-TAML)	H_2O_2	100%; UF; Catalytic oxidation	192 L h^{-1} m^{-2}	GO-PEI boosted porosity and hydrophilicity. H_2O_2 activates enzyme-like ligand, Iron (III)- Tetra-amido macrocyclic ligands to produce high-valence Fe. Five cycles of BPA removal were steady.	(Zhang et al., 2021)
TAML/GO-PEI/PES graphene oxide polyethyleneimine (GO-PEI)	BPA	Iron (III)- Tetra-amido macrocyclic ligand (Fe(III)-TAML) H_2O_2;	100% remove; Catalytic oxidation; UF	192 L h^{-1} m−2	GO-PEI modification in PES membrane enhanced porosity and hydrophilicity and modification increased SSA from 20.03 to 22.36 m2/g, FRR from 34% to 68% while contact angle dropped from 86.5° to 63.4°.	(Zhang et al., 2021)
graphene oxidepolyethylene imine (GO-PEI)	(Fe(III)-TAML)	H_2O_2	100%; UF; Catalytic oxidation	192 L h^{-1} m^{-2}	GO-PEI boosted porosity and hydrophilicity. H_2O_2 activates enzyme-like ligand, Iron (III)- Tetra-amido macrocyclic ligands to produce high-valence Fe. Five cycles of BPA removal were steady.	(Zhang et al., 2021)
N-doped GO	phenol in aqueous solution.	persulfate (PS); catalytic oxidation	0xalic acid (100%) phenol(94%); Catalytic oxidation	-	Negligible elimination by adsorption. The catalytic mechanism is driven by both radical and nonradical degradation of contaminants, however singlet oxygen species were discovered to contribute more significantly.	(Pedrosa et al., 2019)
GO-MWCNTs Co@NCNT-MS membrane (2–2–20)	TC, RhB, and MO		Average: 90% 100%; Filtration/ Fenton degradation	40 L h^{-1} m^{-2} (TC); 70 L h^{-1} m^{-2} (TC, RhB, and MO)	In addition to adsorption sites, radical (SO4-, OH-, and O2-) and nonradical (1O2) species help in degradation. The Co@NCNT-MS cobalt-carbon heterogeneous Fenton-like catalyst eliminates toxins in complex wastewater effluents.	(Li et al., 2022b)

GO nanosheets additive 3D Fe-based metal–organic framework heterostructured membrane	Prussian blue	Fe(III)/Fe(II)	98%; separation and Fenton oxidation	27 L m^{-2} h^{-1}	Sandwich type membrane sheets arrangement provide high flux. In Fenton, GO nanosheets provided enough catalytic reaction time for PB to break down, resulting in excellent oxidation efficiency. Unique isolation and degradation method for EOMPs in wastewater.	(Song et al., 2022)
GO	Octadecyltrichlorosilane (ODTS) Solution Concentration (1%) PPCPs (TC)	0.5 and 1% wt	50%; Fentondegradation/ adsorption	520 L h^{-1} m^{-2} bar^{-1}	GO attributed the membranes' changes increased the efficacy of extracting PPCPs from water.	(Polak et al., 2021)
Co_1-GO membrane	1,4-dioxane (1,4-D)	PMS, vitamin C as a mild reducing agent; membrane filtration and AOPs	GO: 99% Co_1-GO: and Co_1-GO 3 mM PMS: 100%; Catalytic degradation	2.1 ± 0.4 L h^{-1} m^{-2}	The membrane's capacity to reject big organic molecules mitigated their radical-scavenging effects. The kinetics of 1,4-dioxane breakdown were substantially quicker (>640 times)	(Wu et al., 2022a)
Fe_2O_3@Co@nitrogen-doped reduced graphene oxide@carbon nanotube composites	SMX	Peroxymonosulfate	98.5% (0.128 min^{-1}); Catalytic degradation	64.6 and 487.3 L h^{-1} m^{-2} bar^{-1} i.e., 7.5-fold in MM than PM	2D confined catalytic membranes with oxygen vacancies are used to purify sewage. FeCo@GCTs is an ideal electron receiver; turf design and increased oxygen vacancies completely remove SMX and promote Cr (VI) reduction.	(Ye et al., 2021b)
GO-TiO_2	naproxen (NAP), carbamazepine (CBZ) and diclofenac (DCF)	H_2O_2, UV-LED irradiation,	CBZ: 90% DCF: 100% NAP:80%; photodegradation /adsorption	92.6 ± 3.6 L h^{-1} m^{-2} Bar^{-1}	300 nm UV-LEDs showed energy efficiency and optimum removal. UV-LED irradiation, modified membrane eliminated 100% of NAP, DCF, and CBZ in 20 min.Surface flow and dead-end filtering degraded CBZ by 15% and 75% in 120 min. Filtration quadrupled deterioration efficiency. The addition of H_2O_2 to 365 nm/H_2O_2 increased CBZ elimination by 20%.	(Li et al., 2022a)
GO-ZnO/ PES	trace organic compounds (TOrCs) CBZ, metoprolol and theophylline	0.05% GO-ZnO	PM:<40%; PES + 0.05% GO-ZnO: >60%; CFF/photodegradation	>78 L h^{-1} m^{-2}	The introduction of GO-ZnO enhanced trace organic refusal by decreasing membrane-solute hydrophobic affinities; the membranes degraded BB dye; and the modified membranes were less vulnerable to organic fouling by sodium alginate.	(Mahlangu et al., 2017)

N–TiO_2/graphene oxide particles	MB	TiO2	Initial MB 35.8 mg L^{-1} after filtration 12.5 mg L^{-1}, degrade 22.3 mg L^{-1}; photocatalysis, UF	70 L m^{-2} h^{-1}	WCA of is 81° reduce to 64° with GO. The kinetics for NTG-M in sunlight is 4% faster than in UV.	(Chen et al., 2017)
UiO-66_GO/NF photocatalytic Nanofiltration Membrane	CBZ and DCF	photocatalytic activity under ultraviolet (UV) irradiation	CBZ & DCF: 90%/20 min; CBZ (70%) and DCF (93%) after 2 h; photocatalytic degradation	Water flux (up to 63 kg m^{-2} h bar)	FRR: 80%; fouling tolerance:33% In water treatment, the UiO-66 GO nanocomposite is a promising addition to enhanced photocatalytic NF membranes for addressing constrained flow, high energy consumption, and short membrane lifetime.	(Heu et al., 2020)
GO/TiO_2 membrane	Methylene Blue	UV light irradiation, photocatalytic activity under ultraviolet (UV) irradiation	92%; photocatalytic degradation	7.5 L m^{-2} h^{-1}	FRR 96%; UV radiation has the potential to greatly reduce membrane fouling. Adsorption and cake layer were shown to be the main causes of GO/TiO_2 membrane fouling, accounting for 46.3% and 46.0% of membrane resistance, respectively.	(Zhu et al., 2017a)
TiO_2-graphene oxide (GO)-Fe_3O_4	refractory antibiotic amoxicillin organic compounds in aqueous solution	Fe_3O_4/photodegradation	TiO_2-GO and Fe_3O_4:14.7% TiO2-GO-18 wt.% Fe_3O_4:90%; 22.3% oxidation by Fe_3O_4 and 15.2% by photocatalytic degradation	-	GO enhances the catalytic cycle and efficiency. When the concentration of H_2O_2 was increased from 0 to 20 mM, the removal performance climbed from 10% to 90%. SMSMPR CM has excellent photo-Fenton catalytic activity and AMX degradation stability. The AMX intermediates disintegrated into carbon dioxide, water, and inorganic ions.	(Li et al., 2019)
electrochemically modified carbon nanofibrous anodic membrane (G/SnO_2/CFs)	refractory toxic organic - sulfamethoxazole (SMX)	SnO_2; electrooxidation	85%; degradation	PMF is 74 144.9 and 216.4 L h^{-1} m^{-2} at 10, 20 and 30rpm peristaltic pump	Degradation is reduced by increasing the quantity of anodic membrane and using flow-through mode. Nine non-toxic SMX intermediates are discovered using LC-MS/MS. Membrane stability was excellent even at 10 cycles, 50 h reaction. electro oxidative performance and membrane conductivity can be increased by SnO_2 and graphene.	(Yu et al., 2020)

electrochemically active cathodic membrane (CFC/PVDF/GO-Fe^{3+})	Rhodamine B	Fe^{3+}; electrooxidation	10 mg L^{-1} Rhodamine B was ~75% in CSTR; degradation	200 L h^{-1} m^{-2}	In-situ Fe^{2+} regeneration on membrane cathode causes decolorization at pH > 4.0. Only avoiding Fe^{3+}-oxalate complexes improved membrane oxalate oxidation stability.	(Li et al., 2018)
Graphene nanoplatelets: CNT/ PTFE filter	[Fe (CN)6]4-, TC, Phenol, Oxalate, COD, TDS, Nephelometric, Turbidity Unit	electrooxidation and electrochemical filtration	(COD, 91.67%); (TDS, 91.3%), (TSS,98.85%) and (NTU, 96.45%) degradation	52 L h^{-1} m^{-2}	The promise of graphene electrode in flow-through purifiers is demonstrated by a graphene-based electrochemical filter using CNTs as conducting binders.	(Liu et al., 2014)
Hybrid graphene-decorated metal hollow fibre membrane reactors	pharmaceutical pollutant, paracetamol	Electro-Fenton; electrochemical filtration	membrane: 37%; Membrane: 165% wit degradation	High flux and selectivity; comparatively low water flux reduce from 5000 to 4500 L m^{-2} h^{-1} after three cycles	GO cathode performance were highest than all other and showed Tri-cycle stability. Low-cost catalytic membrane reactors with high flux and selectivity from materials reactivity, with promise for mineralizing persistent pollutants.	(Le et al., 2019)
ZIF@MILs-20/GO	norfloxacin (NX)	singlet oxygen ($^1O_2$), electro-Fenton batch experiments,	99.4% degradation	stable flux of 156.3 L m^{-2} h^{-1} bar^{-1} over 10 h	The primary cause of NX degradation is $^1O_2$. Supplemented oxygen vacancies restrict FexOy, and 1D/2D hierarchically porous ZIF@MILs-20 frameworks enhance NX removal via a synergistic "trap-and-zap" method for PMS activation. Catalytic membranes eliminate fouling via filtration and catalytic oxidation of organic compounds.	(Ye et al., 2021a)

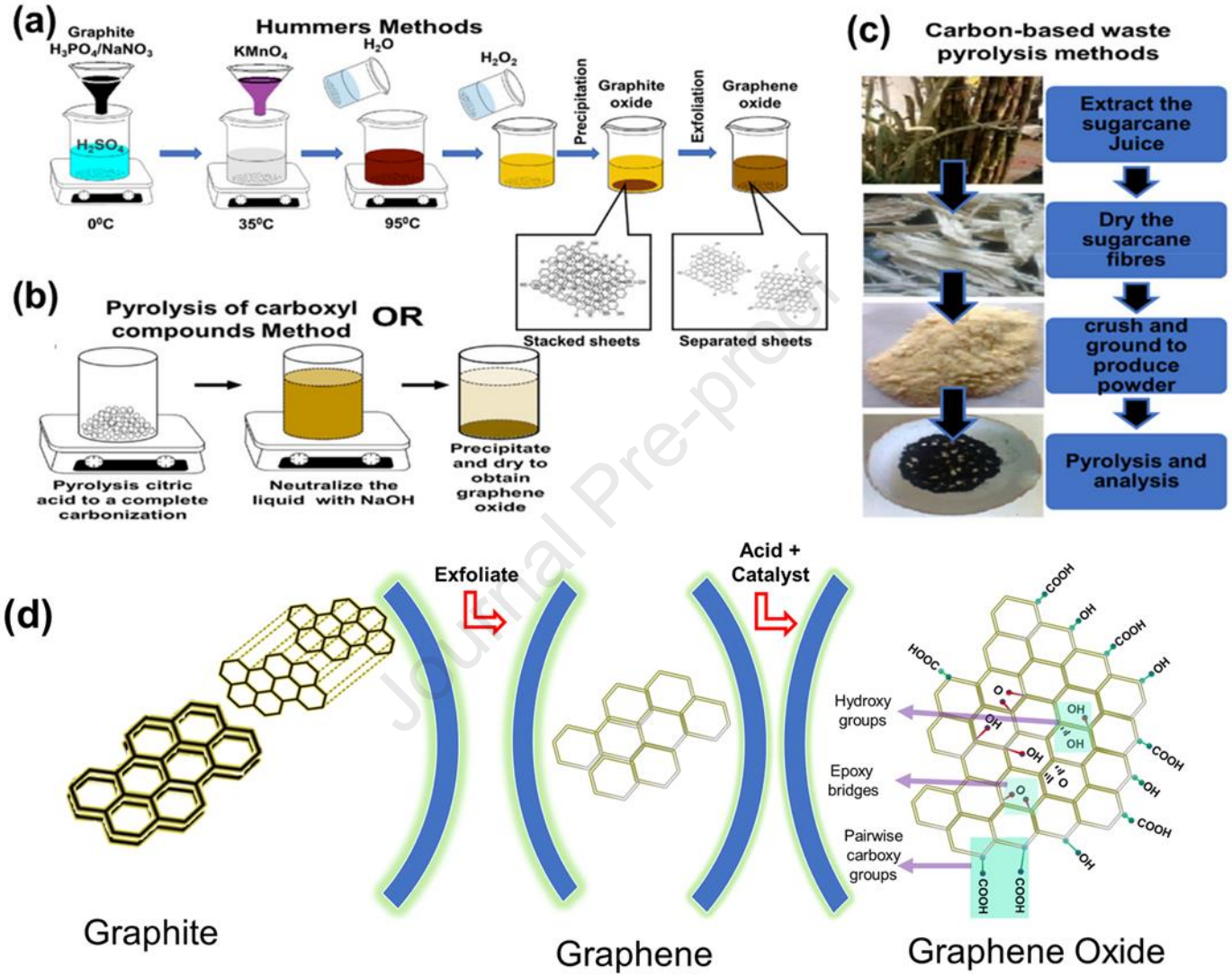
(a)
Graphite
$H_3PO_4/NaNO_3$
H_2SO_4
0°C
Hummers Methods
$KMnO_4$
35°C
H_2O
95°C
H_2O_2
Precipitation
Graphite oxide
Exfoliation
Graphene oxide
Stacked sheets
Separated sheets
(b)
Pyrolysis of carboxyl compounds Method
OR
Pyrolysis citric acid to a complete carbonization
Neutralize the liquid with NaOH
Precipitate and dry to obtain graphene oxide
(c)
Carbon-based waste pyrolysis methods
Extract the sugarcane Juice
Dry the sugarcane fibres
crush and ground to produce powder
Pyrolysis and analysis
(d)
Exfoliate
Acid + Catalyst
Hydroxy groups
Epoxy bridges
Pairwise carboxy groups
Graphite
Graphene
Graphene Oxide

Fig.1

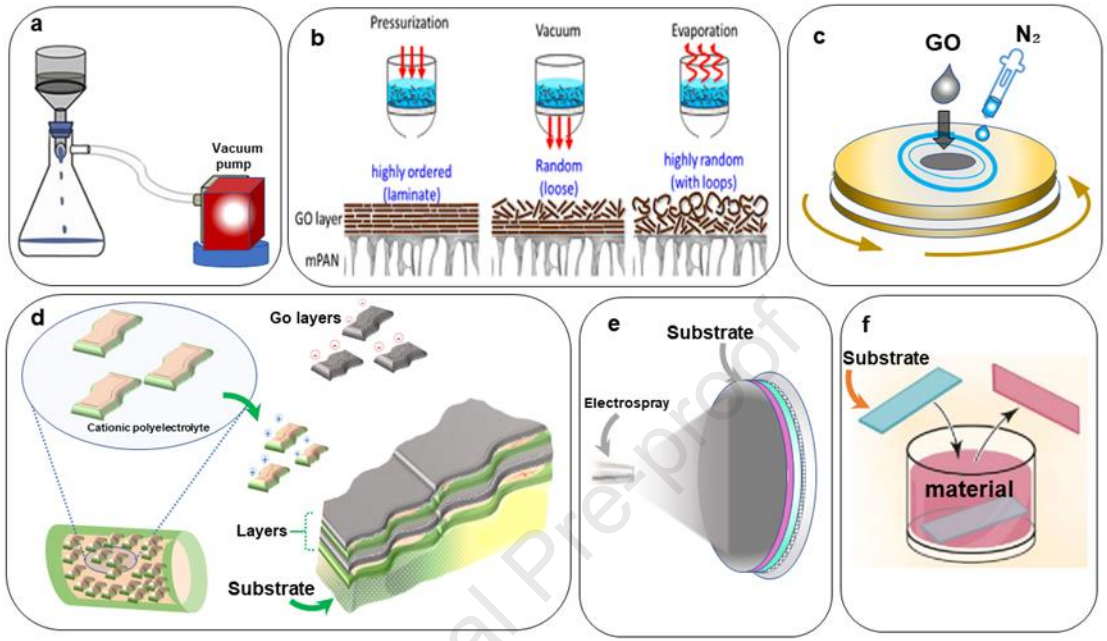

Fig.2

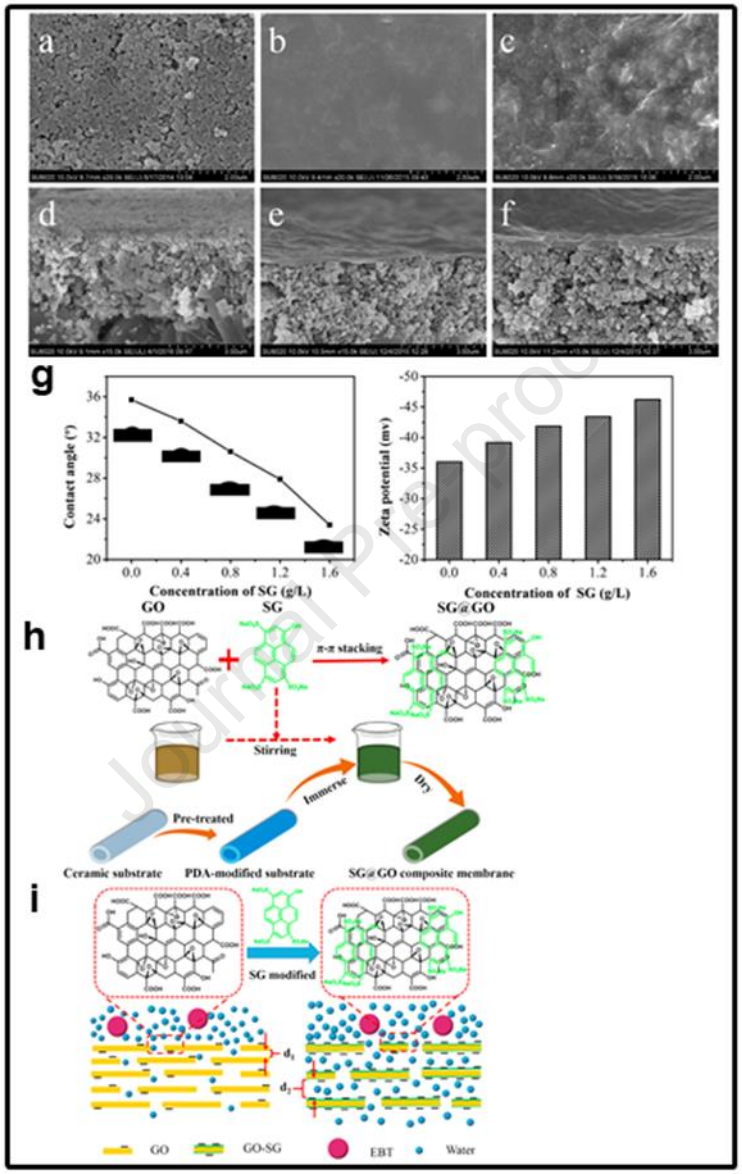
a
b
c
d
e
f
g
Contact angle (°)
Concentration of SG (g/L)
Zeta potential (mv)
Concentration of SG (g/L)
h
GO
SG
SG@GO
π-π stacking
Stirring
Immerse
Dry
Pre-treated
Ceramic substrate
PDA-modified substrate
SG@GO composite membrane
i
SG modified
GO
GO-SG
EBT
Water

Fig.3

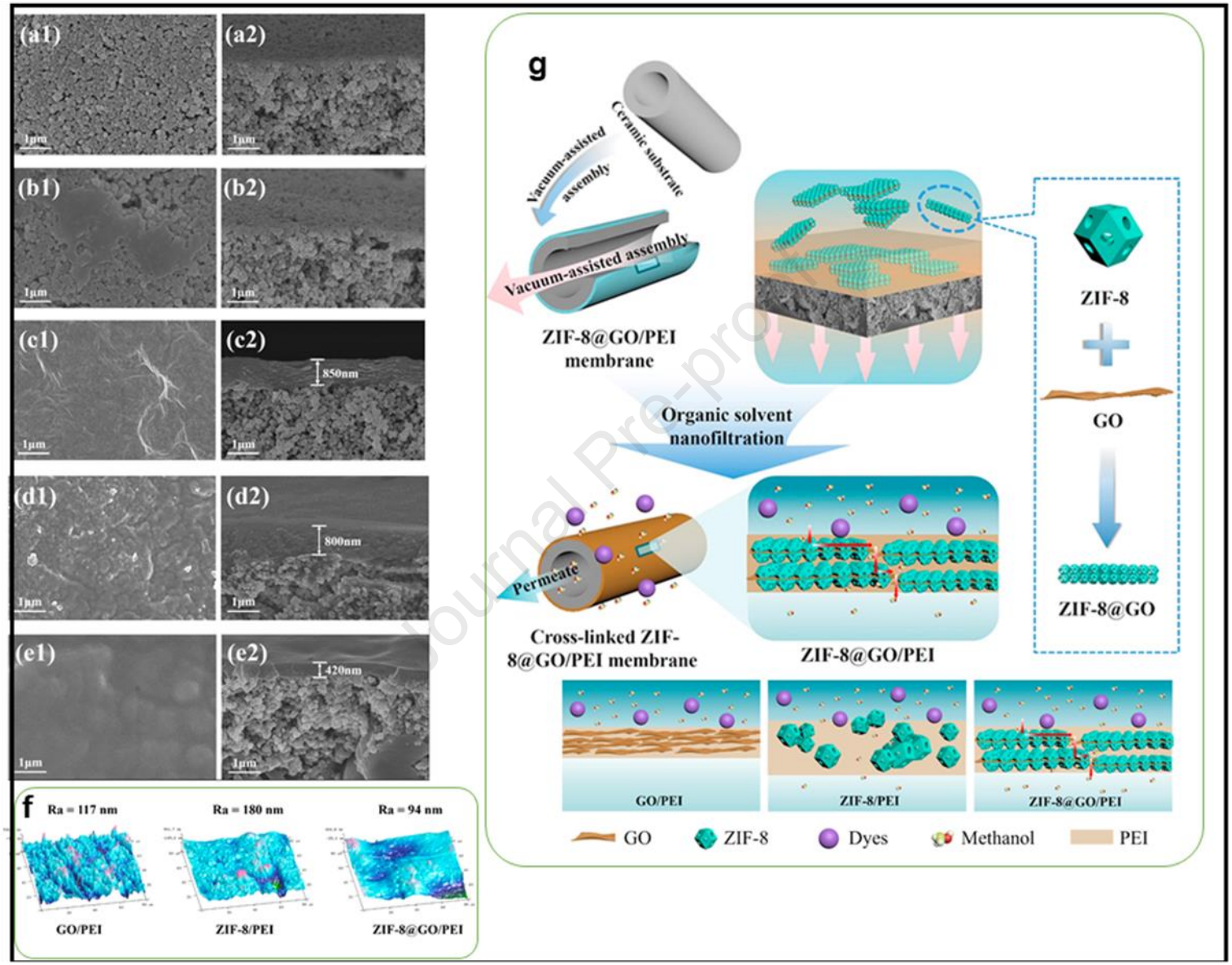
(a1)
(a2)
(b1)
(b2)
(c1)
(c2)
850nm
(d1)
(d2)
800nm
(e1)
(e2)
420nm
1μm
f
Ra = 117 nm
Ra = 180 nm
Ra = 94 nm
GO/PEI
ZIF-8/PEI
ZIF-8@GO/PEI
g
Ceramic substrate
Vacuum-assisted assembly
Vacuum-assisted assembly
ZIF-8@GO/PEI membrane
Organic solvent nanofiltration
Permeate
Cross-linked ZIF-8@GO/PEI membrane
ZIF-8@GO/PEI
ZIF-8
GO
ZIF-8@GO
GO/PEI
ZIF-8/PEI
ZIF-8@GO/PEI
GO
ZIF-8
Dyes
Methanol
PEI

Fig.4

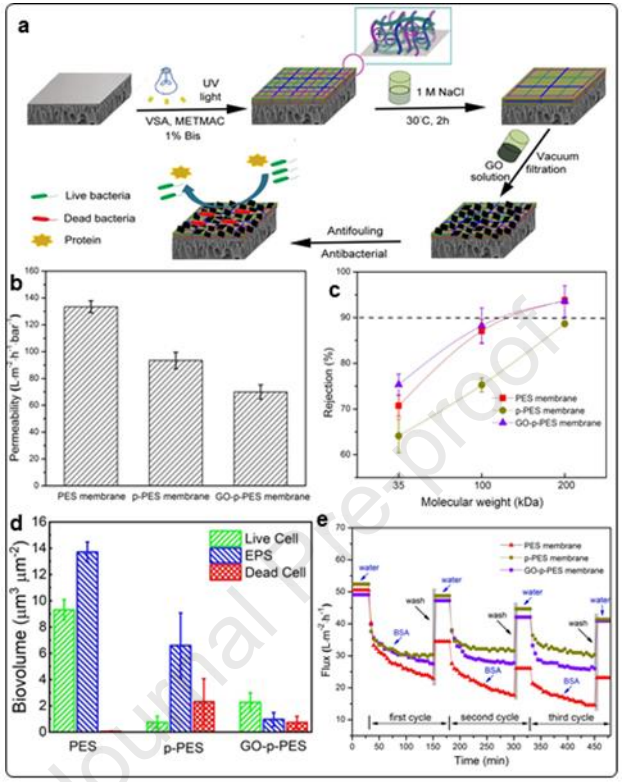

Fig.5

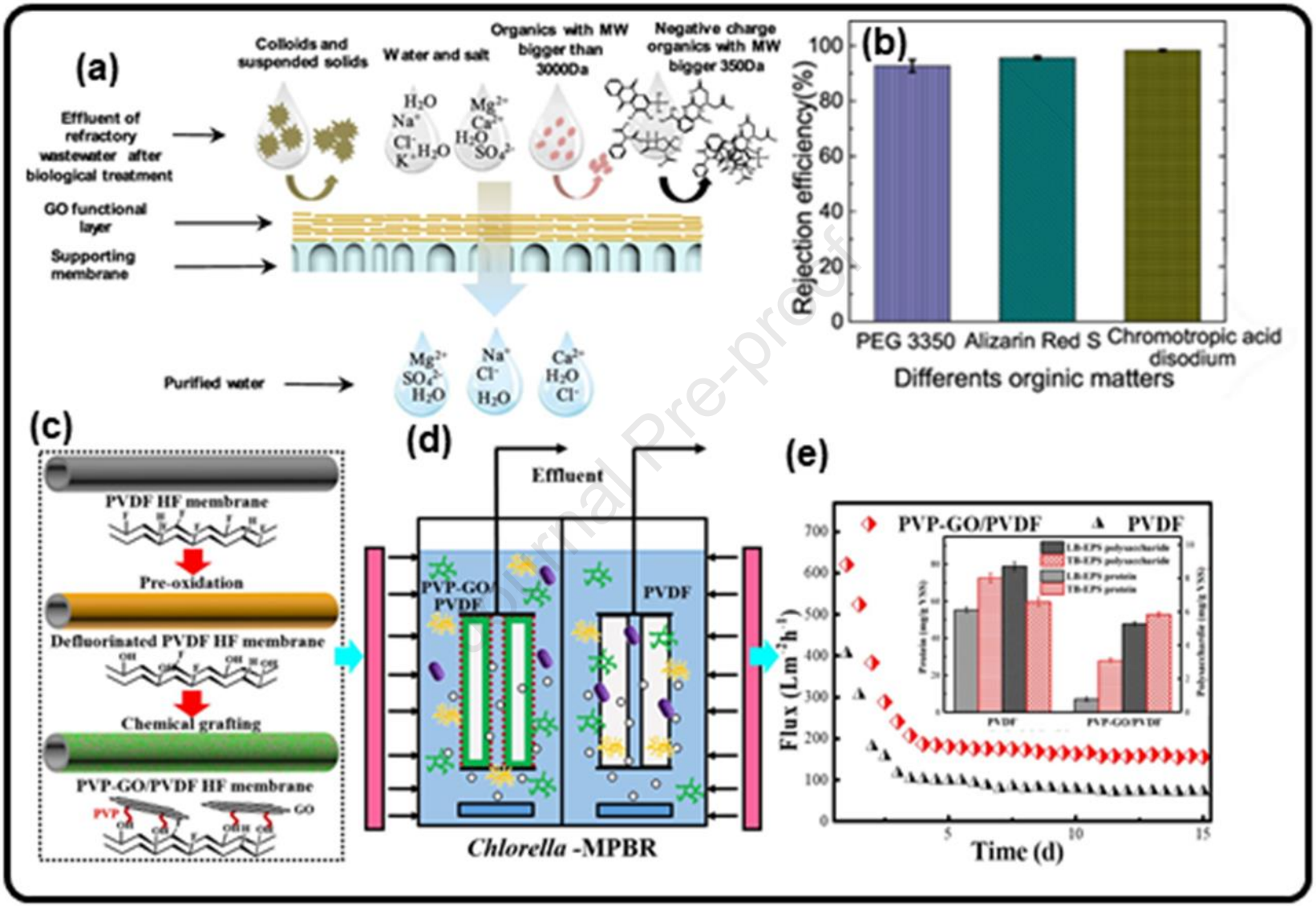
(a)
Colloids and suspended solids
Water and salt
Organics with MW bigger than 3000Da
Negative charge organics with MW bigger 350Da
Effluent of refractory wastewater after biological treatment
GO functional layer
Supporting membrane
Purified water
(b)
Rejection efficiency(%)
PEG 3350
Alizarin Red S
Chromotropic acid disodium
Differents orginic matters
(c)
PVDF HF membrane
Pre-oxidation
Defluorinated PVDF HF membrane
Chemical grafting
PVP-GO/PVDF HF membrane
(d)
Effluent
PVP-GO/PVDF
PVDF
Chlorella -MPBR
(e)
PVP-GO/PVDF
PVDF
Flux (Lm⁻²h⁻¹)
Time (d)

Fig.6

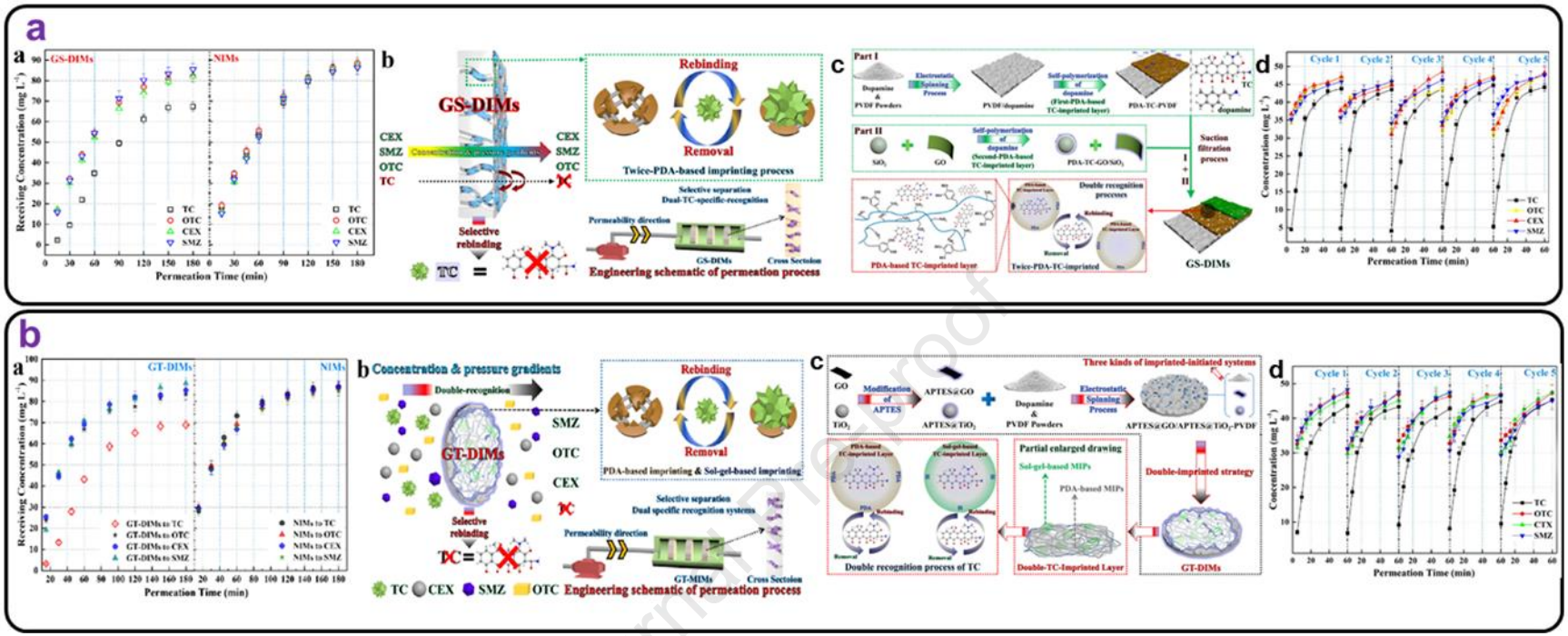

Fig7

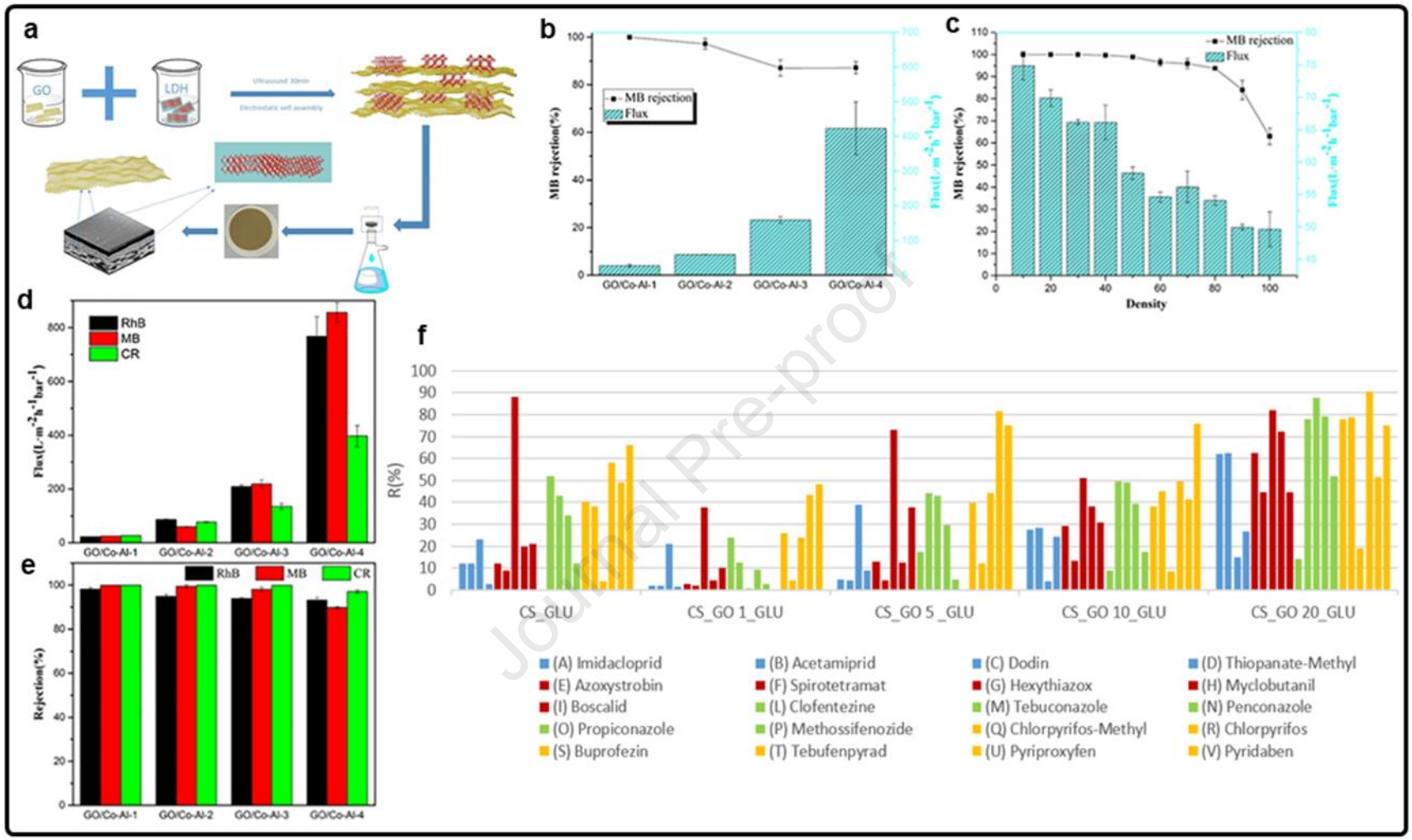

Fig.8

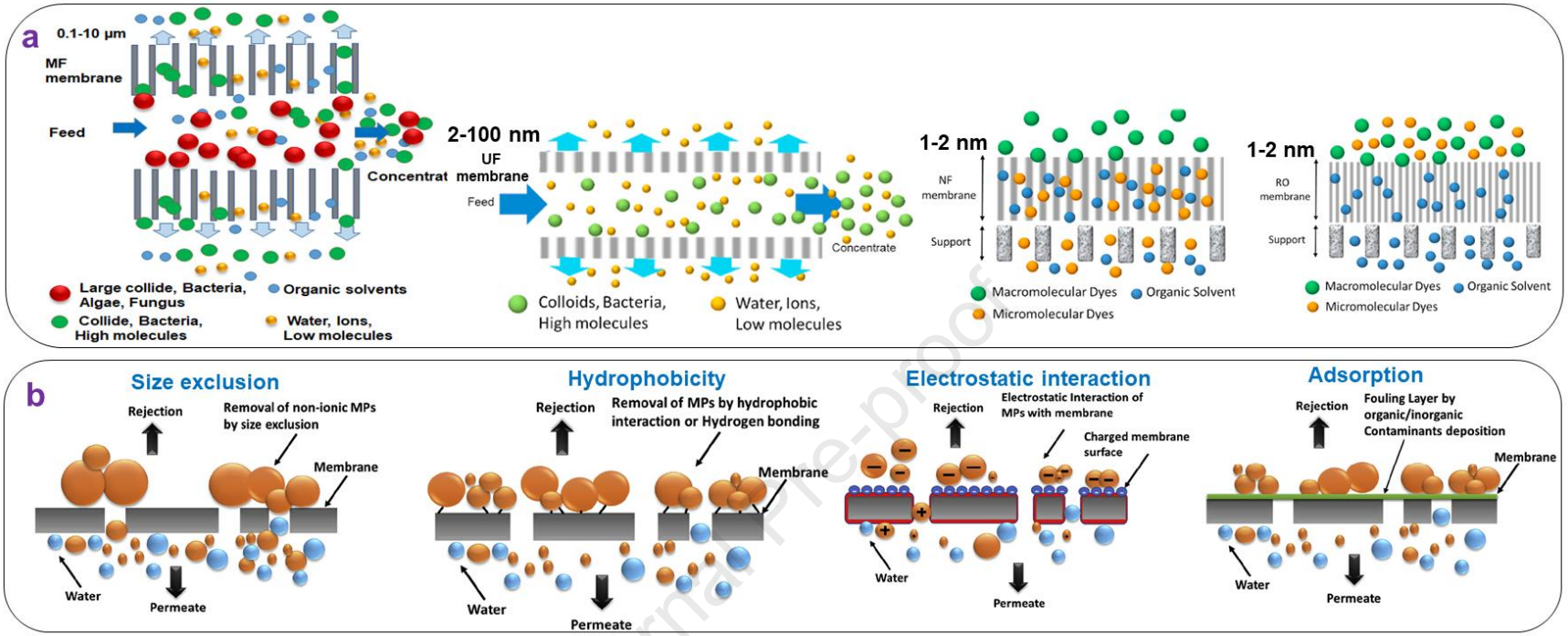

Fig.9

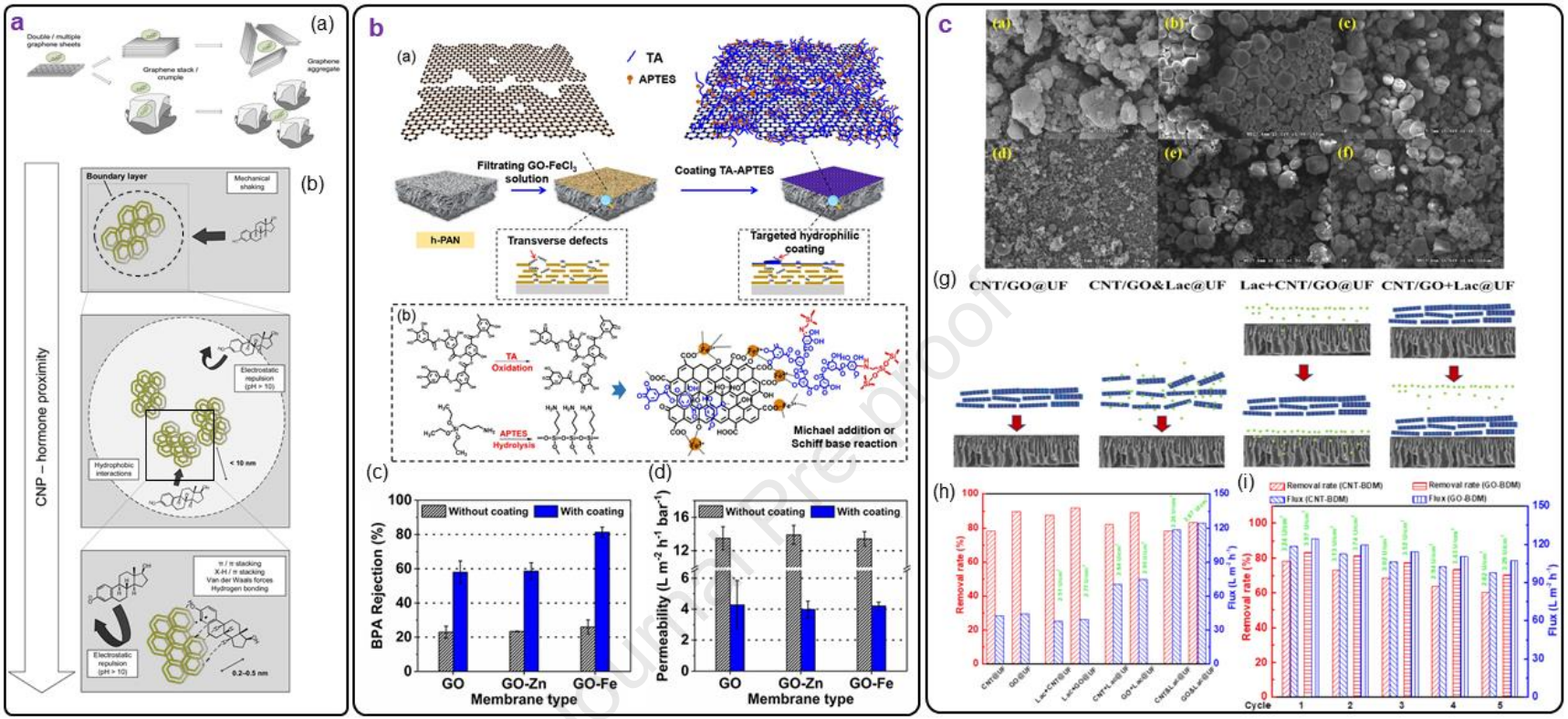
a
(a)
Double / multiple graphene sheets
Graphene stack / crumple
Graphene aggregate
(b)
Boundary layer
Mechanical shaking
CNP – hormone proximity
Electrostatic repulsion (pH > 10)
Hydrophobic interactions
< 10 nm
π / π stacking
X-H / π stacking
Van der Waals forces
Hydrogen bonding
Electrostatic repulsion (pH > 10)
0.2–0.5 nm
b
(a)
TA
APTES
Filtrating GO-FeCl3 solution
Coating TA-APTES
h-PAN
Transverse defects
Targeted hydrophilic coating
(b)
TA Oxidation
APTES Hydrolysis
Michael addition or Schiff base reaction
(c)
Without coating
With coating
BPA Rejection (%)
GO
GO-Zn
GO-Fe
Membrane type
(d)
Permeability (L m-2 h-1 bar-1)
c
(a)
(b)
(c)
(d)
(e)
(f)
(g)
CNT/GO@UF
CNT/GO&Lac@UF
Lac+CNT/GO@UF
CNT/GO+Lac@UF
(h)
Removal rate (%)
Flux (L m-2 h-1)
(i)
Removal rate (CNT-BDM)
Flux (CNT-BDM)
Removal rate (GO-BDM)
Flux (GO-BDM)
Cycle

Fig.10

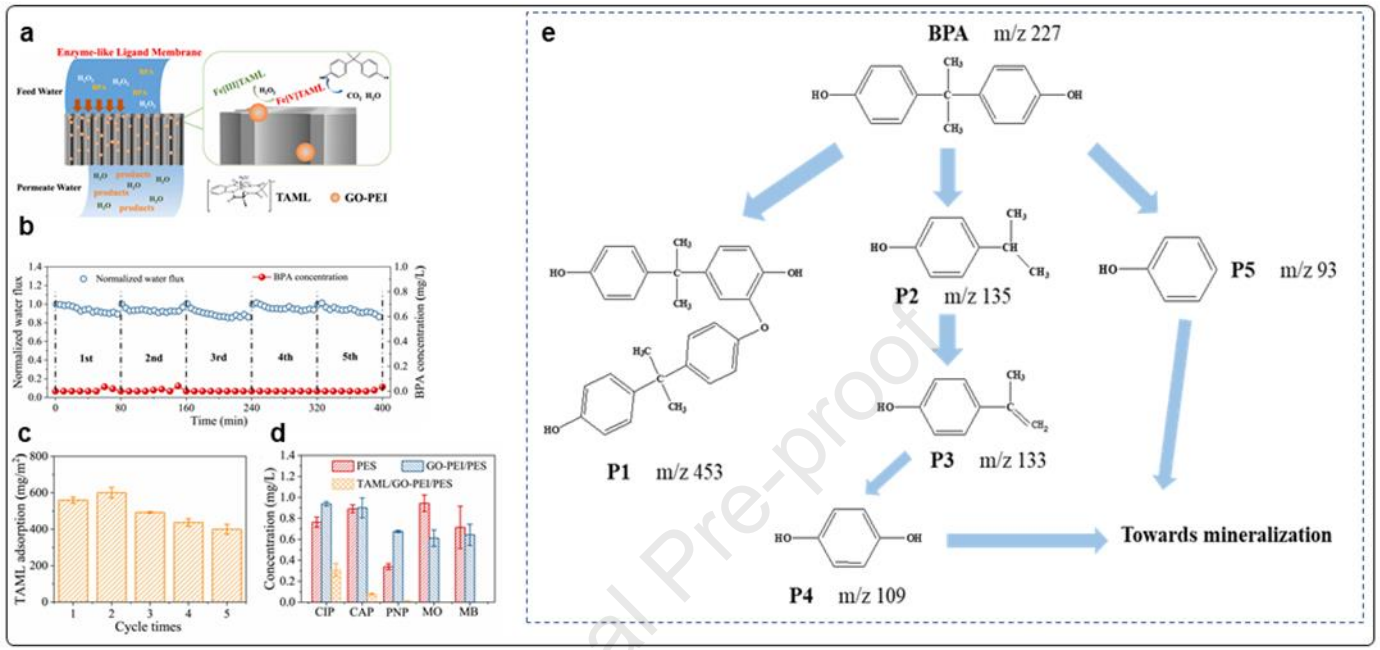

Fig. 11

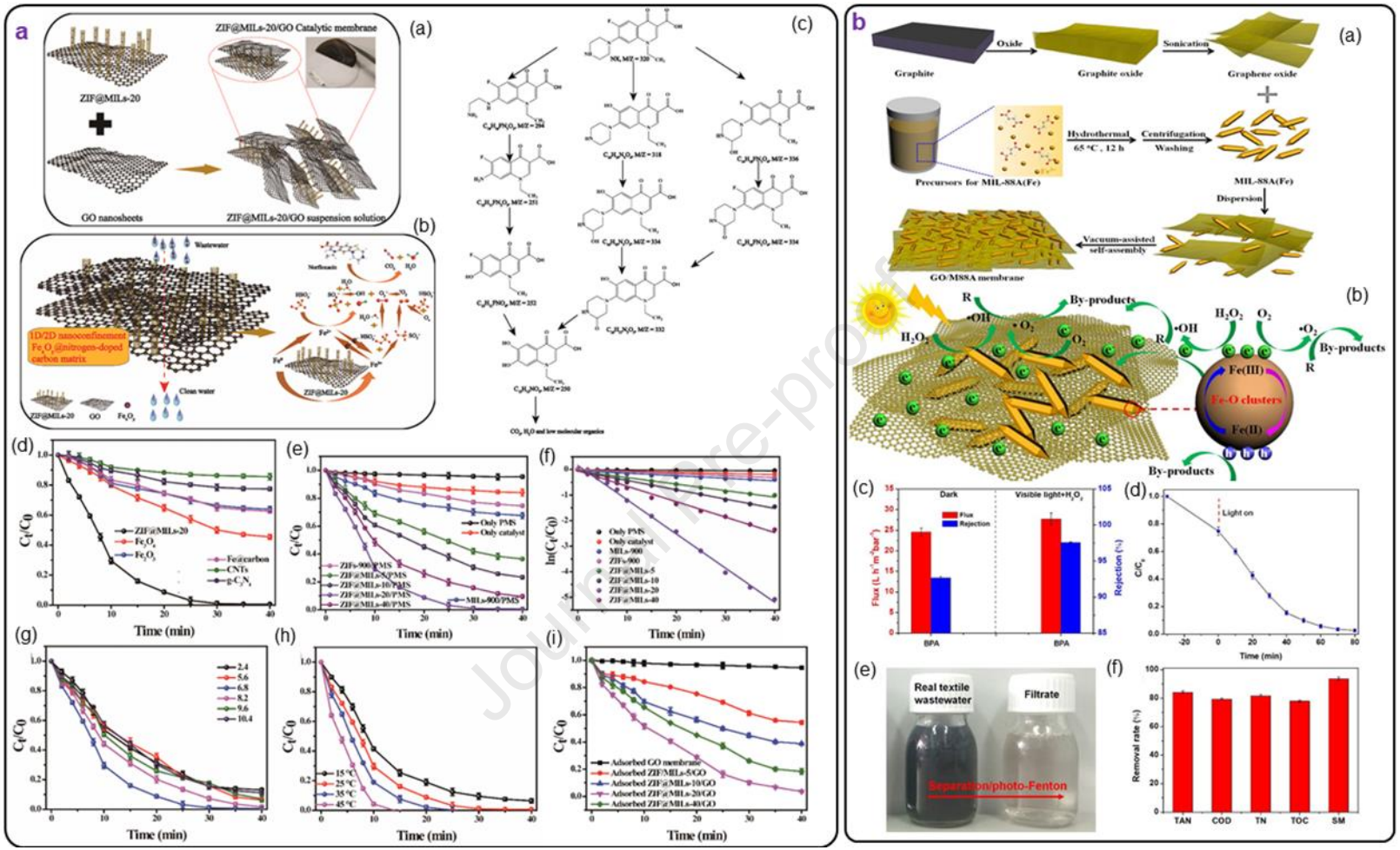
a
ZIF@MILs-20/GO Catalytic membrane
ZIF@MILs-20
GO nanosheets
ZIF@MILs-20/GO suspension solution
Wastewater
Clean water
Time (min)
b
Graphite
Graphite oxide
Graphene oxide
Precursors for MIL-88A(Fe)
MIL-88A(Fe)
GO/MIL88A membrane
By-products
Fe(III)
Fe(II)
Fe-O clusters
Dark
Visible light+H2O2
BPA
Light on
Real textile wastewater
Filtrate
Separation/photo-Fenton
TAN
COD
TN
TOC
SM

Fig.12

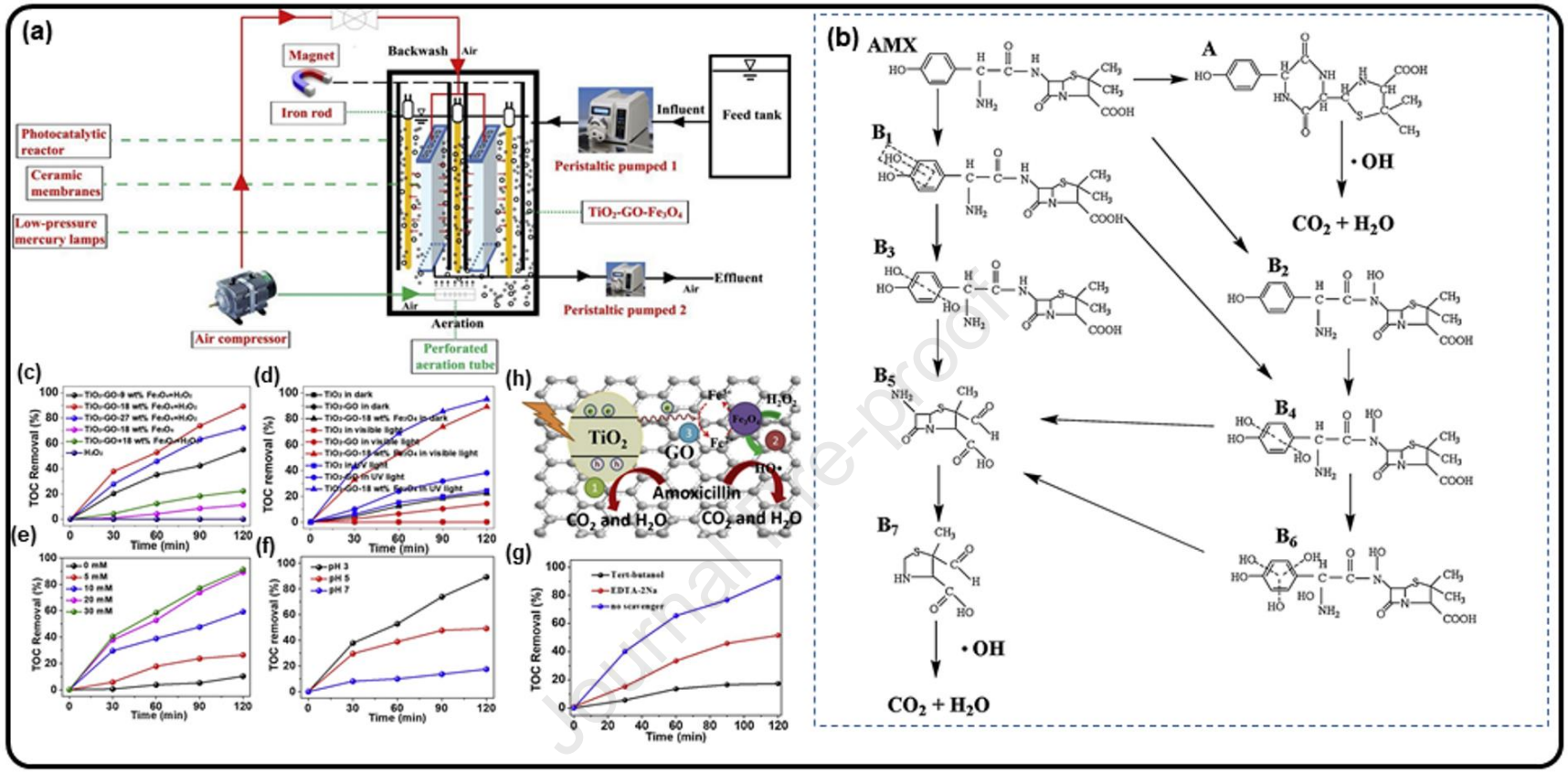
(a)
Magnet
Backwash
Air
Iron rod
Photocatalytic reactor
Ceramic membranes
Low-pressure mercury lamps
Influent
Feed tank
Peristaltic pumped 1
TiO2-GO-Fe3O4
Effluent
Air
Peristaltic pumped 2
Air compressor
Aeration
Perforated aeration tube
(b)
AMX
A
B1
B2
B3
B4
B5
B6
B7
• OH
CO2 + H2O
(c)
(d)
(e)
(f)
(g)
(h)
TiO2
GO
Amoxicillin
CO2 and H2O
TOC Removal (%)
Time (min)
TOC removal (%)
pH 3
pH 5
pH 7
Tert-butanol
EDTA-2Na
no scavenger

Fig.13

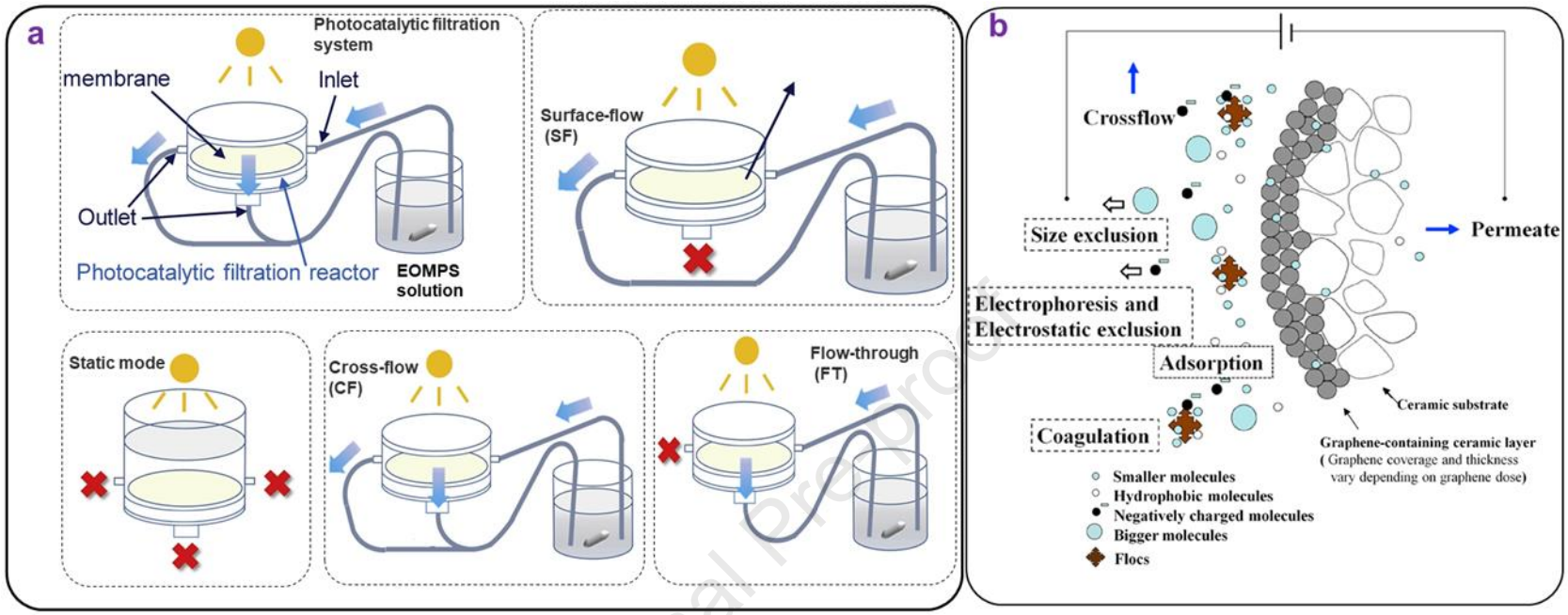

Fig.14

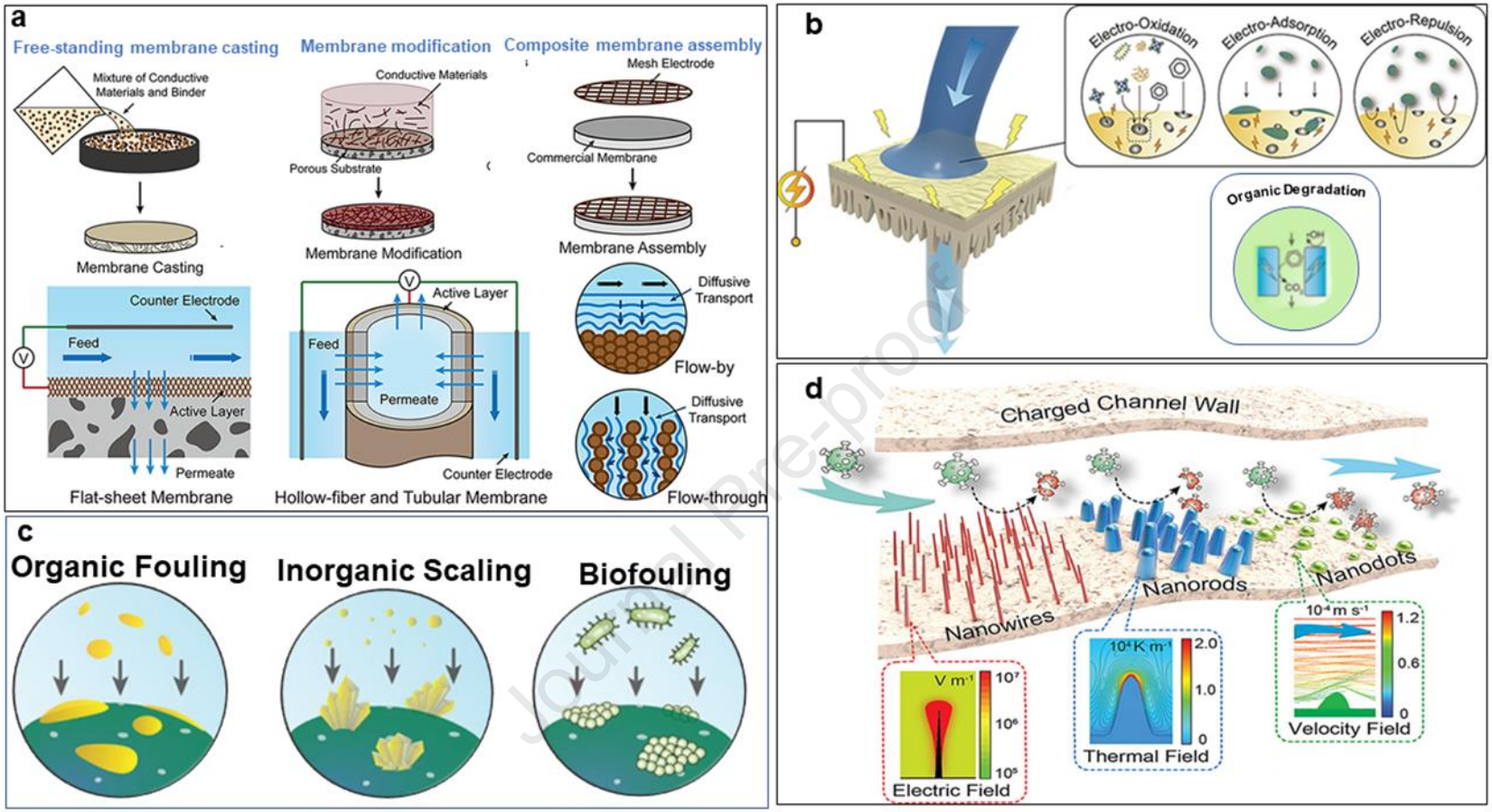
a
Free-standing membrane casting
Membrane modification
Composite membrane assembly
Mixture of Conductive Materials and Binder
Membrane Casting
Conductive Materials
Porous Substrate
Membrane Modification
Mesh Electrode
Commercial Membrane
Membrane Assembly
Counter Electrode
Feed
Active Layer
Permeate
Flat-sheet Membrane
Active Layer
Feed
Permeate
Counter Electrode
Hollow-fiber and Tubular Membrane
Diffusive Transport
Flow-by
Diffusive Transport
Flow-through
b
Electro-Oxidation
Electro-Adsorption
Electro-Repulsion
Organic Degradation
c
Organic Fouling
Inorganic Scaling
Biofouling
d
Charged Channel Wall
Nanowires
Nanorods
Nanodots
Electric Field
Thermal Field
Velocity Field

Fig.15

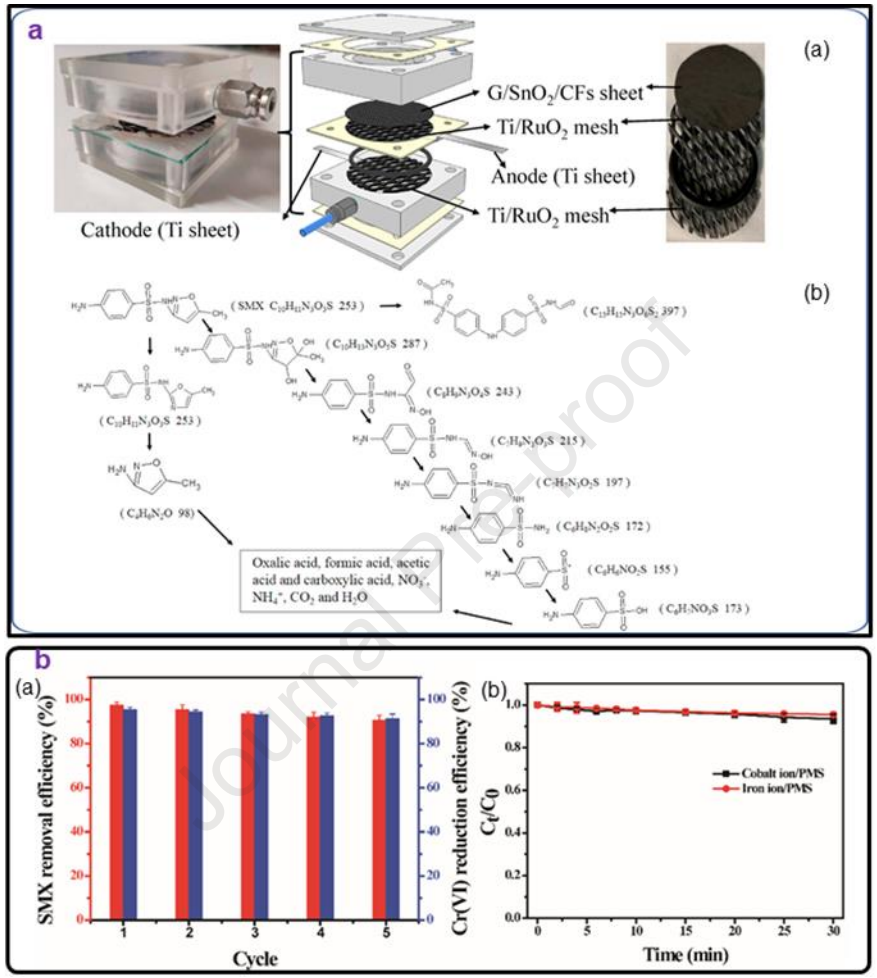

Fig.16

Highlights

- Next-Generation GO membranes showed promising removal of emerging organic micropollutants.
- GO membranes and substrates together act synergistically in water treatment.
- GO can easily accommodate adsorptive, degradative, biomimetic, and filtration membranes.
- Low price and multicycle operational GO membranes have scope for industrial application.
- Present status and future-oriented assessment of GO-based membrane technology are discussed

Declaration of interests

☒ The authors declare that they have no known competing financial interests or personal relationships that could have appeared to influence the work reported in this paper.

☐The authors declare the following financial interests/personal relationships which may be considered as potential competing interests: